

2007/1 vol.4



# ACTA GEO TECHNICA SLOVENICA

2007/1

M. samec et al.

PROBING ION DYNAMICS IN A CLAY-WATER SYSTEM WITH DIELECTRIC SPECTROSCOPY

H. vreč-kojc and s. škrabl

DETERMINATION OF PASSIVE EARTH PRESSURE USING THREE-DIMENSIONAL FAILURE MECHANISM

A. seriani et al.

BEHAVIOUR OF THE SUBWAY TUNNEL IN ALGIERS: PHYSICAL MODEL EXPERIMENTAL STUDY

L. vrankar et al.

THE USE OF THE MESH FREE METHODS (RADIAL BASIS FUNCTIONS) IN THE MODELING OF RADIONUCLIDE MIGRATION AND MOVING BOUNDARY VALUE PROBLEMS

ISSN 1854-0171



**ACTA  
GEOTECHNICA  
SLOVENICA**

ISSN: 1854-0171

**ustanovitelji** **founders**

Univerza v Mariboru, Fakulteta za gradbeništvo  
University of Maribor, Faculty of Civil Engineering



Univerza v Ljubljani, Fakulteta za gradbeništvo in geodezijo  
University of Ljubljana, Faculty of Civil  
and Geodetic Engineering



Univerza v Ljubljani, Naravoslovnotehniška fakulteta  
University of Ljubljana, Faculty of Natural  
Sciences and Engineering



Slovensko geotehniško društvo  
Slovenian Geotechnical Society



Društvo za podzemne in geotehniške konstrukcije  
Society for Underground and Geotechnical  
Constructions



**izdajatelj** **publisher**

Univerza v Mariboru, Fakulteta za gradbeništvo  
University of Maribor, Faculty of Civil Engineering

**odgovorni urednik** **editor-in-chief**

Ludvik Trauner  
Univerza v Mariboru

**urednika** **co-editors**

Stanislav Škrabl  
Univerza v Mariboru  
Bojan Žlender  
Univerza v Mariboru

**tehnična urednika** **desk editors**

Bojana Dolinar  
Univerza v Mariboru  
Borut Macuh  
Univerza v Mariboru

**lektorica** **proof-reader**

Metka Brkan

**naklada** **circulation**

500 izvodov - issues

**tisk** **print**

Tercia tisk d.o.o. Ptuj

Revija redno izhaja dvakrat letno. Članki v reviji so recenzirani s strani priznanih mednarodnih strokovnjakov. Baze podatkov v katerih je revija indeksirana: ICONDA - The international Construction database, GeoRef  
Pri financiranju revije sodeluje Javna agencija za raziskovalno dejavnost republike Slovenije.

**uredniški odbor** **editorial board**

Darinka Battelino  
*Università degli Studi di Trieste*  
József Farkas  
*Budapesti Műszaki és Gazdaságtudományi Egyetem*  
Theodoros Hatzigogos  
*Aristotle University of Thessaloniki*  
Rolf Katzenbach  
*Technische Universität Darmstadt*  
Zlatko Langof  
*Univerzitet u Sarajevu*  
Jakob Likar  
*Univerza v Ljubljani*  
Janko Logar  
*Univerza v Ljubljani*  
Bojan Majes  
*Univerza v Ljubljani*  
Milan Maksimović  
*Univerzitet u Beogradu*  
Borut Petkovšek  
*Zavod za gradbeništvo Slovenije*  
Mihael Ribičič  
*Univerza v Ljubljani*  
César Sagaseta  
*Universidad de Cantabria*  
Stephan Semprich  
*Technische Universität Graz*  
Abdul-Hamid Soubra  
*Université de Nantes*  
Ivan Vaniček  
*České vysoké učení technické v Praze*  
Franjo Verič  
*Sveučilište u Zagrebu*

**naslov uredništva** **address**

ACTA GEOTECHNICA SLOVENICA  
Univerza v Mariboru, Fakulteta za gradbeništvo  
Smetanova ulica 17  
2000 Maribor  
Slovenija  
Telefon / Telephone: +386 (0)2 22 94 300  
Faks / Fax: +386 (0)2 25 24 179  
E-pošta / E-mail: ags@uni-mb.s

**spletni naslov** **web address**

<http://www.fg.uni-mb.si/journal-ags>

The journal is published twice a year. Papers are peer reviewed by renowned international experts. Indexation data bases of the journal: ICONDA - The International Construction Database, GeoRef  
Financially supported also by Slovenian Research Agency.

---

## VSEBINA

---

2 Ludvik Trauner  
UVODNIK

4 marko samec in drugi  
UGOTAVLJANJE ZNAČILNOSTI DINAMIKE  
IONOV V MEŠANICI GLINE IN VODE S  
POMOČJO DIELEKTRIČNE SPEKTROKOPIJE

10 helena vrecl-kojc in stanislav škrabl  
DOLOČITEV PASIVNEGA ZEMELJSKEGA  
PRITISKA Z UPORABO TRIDIMENZIONAL-  
NEGA PORUŠNEGA MEHANIZMA

24 abdelbaki seriani in drugi  
OBNAŠANJE AVTOCESTNEGA TUNELA  
V ALŽIRIJI: EKSPERIMENTALNA  
ŠTUDIJA FIZIKALNEGA MODELA

42 Leopold vrancar in drugi  
UPORABA BREZMREŽNIH METOD  
(RADIALNIH BAZNIH FUNKCIJ) ZA MO-  
DELIRANJE MIGRACIJE RADIONUKLIDOV  
IN PROBLEMOV S PREMIKAJOČO SE MEJO

54 NAVODILA AVTORJEM

---

## CONTENTS

---

Ludvik Trauner 3  
EDITORIAL

marko samec et al. 5  
PROBING ION DYNAMICS IN A  
CLAY-WATER SYSTEM WITH  
DIELECTRIC SPECTROSCOPY

helena vrecl-kojc and stanislav škrabl 11  
DETERMINATION OF PASSIVE EARTH  
PRESSURE USING THREE-DIMENSIONAL  
FAILURE MECHANISM

abdelbaki seriani et al. 25  
BEHAVIOUR OF THE SUBWAY TUNNEL  
IN ALGIERS: PHYSICAL MODEL  
EXPERIMENTAL STUDY

Leopold vrancar et al. 43  
THE USE OF THE MESH FREE METHODS  
(RADIAL BASIS FUNCTIONS) IN THE  
MODELING OF RADIONUCLIDE MIGRATION  
AND MOVING BOUNDARY VALUE PROBLEMS

INSTRUCTIONS FOR AUTHORS 55

---

# UVODNIK

---

Mednarodna revija Acta Geotechnica Slovenica postaja vedno bolj prepoznavna, kar kažejo odzivi tako domače kot tuje strokovne javnosti. Zahvala gre predvsem avtorjem, ki s svojimi prispevki seznanjajo bralce z najnovejšimi znanstvenimi in strokovnimi dosežki s širokega področja geotehnike in številnim tujim in domačim recenzentom, ki skrbijo za kvaliteto izbranih člankov. Kljub velikemu trudu vseh sodelujočih pa revija ne bi mogla izhajati brez finančne podpore številnih sponzorjev, ki se jim zato ob tej priliki tudi lepo zahvaljujem.

Prva številka četrtega letnika prinaša naslednje štiri zelo zanimive prispevke:

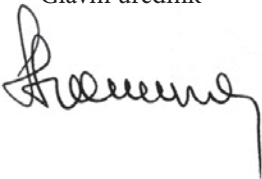
M. Samec, D.Korošak in B. Cvikel predstavljajo karakterizacijo mešanic gline in vode na podlagi dielektrične spektroskopije in analize pridobljenih spektrov. Predlagan je teoretičen model dinamike ionov, ki poleg gibanja ionov v porah elektrolita vključuje tudi njihovo ujetost na površinah mineralov. Časovne konstante, ki določajo dinamiko teh pojavov, so povezane s fizikalnimi lastnostmi snovi. Mikroskopsko gibanje ionov v kompleksnem okolju mešanice gline in vode se lahko opiše z dinamiko delcev, ki vodi do subdifuznega obnašanja.

H. Vredl-Kojc in S. Škrabl v prispevku prikazujeta modificiran prostorski porušni mehanizem za določitev 3D koeficienta pasivnega zemeljskega pritiska ob uporabi teorema zgornje vrednosti metode mejne analize. V analizi je upoštevan translatorski kinematično dopustni porušni mehanizem, ki je generaliziran z globino  $h = 1.0$ . Mehanizem geometrijsko predstavlja prostorski togi blok sestavljen iz osrednjega dela in dveh stranskih togih blokov, ki ju sestavljajo ovojnice bočnih trenjskih stožcev. Rezultati analize predstavljenega modela so prikazani v grafični obliki v odvisnosti od geometrijskih parametrov in lastnosti temeljnih tal. V prispevku sta tudi predstavljena dva v svetovem merilu priznana prostorska porušna mehanizma, ki prav tako temeljita na metodi mejne analize ter primerjava rezultatov med vsemi tremi porušnimi mehanizmi.

A. Seriani, Y. Kismoune Thésard, T. Serradj opisujejo raziskavo, pri kateri so na fizikalnem modelu v razmerju 1:20 eksperimentalno preučili obnašanje avtocestnega tunela v Alžiru ter usipanje okoliških zemljin med izkopavanjem.

L. Vrankar, F. Runovc in G. Turk v članku predstavljajo uporabo radialnih baznih funkcij v geostatistični analizi modeliranja migracije radionuklidov. Migracija radionuklidov je simulirana s pomočjo advekcijske-disperzijske enačbe, in sicer v Eulerjevi in Lagrangeovi obliki. V nadaljevanju so predstavljeni tudi Stefanovi problemi oz. problem primikajočih se meja (površin). Položaji primikajoče meje so simulirani s pomočjo metode primikajočih se centrov in nivojne metode.

Ludvik Trauner  
Glavni urednik



---

# EDITORIAL

---

The international journal *Acta Geotechnica Slovenica* has now attained worldwide renown, which has been proved by both domestic and foreign professionals' response to the journal. Thanks are due especially to the authors whose contributions expose their latest scientific and research achievements in the field of geotechnical engineering, and to numerous foreign and home peer-reviewers who assure a quality selection of articles. All efforts of those participating, however, could not have been realized without a solid financial support of numerous sponsors to whom I would also like to extend my warmest thanks.

Volume 4, issue 1, brings four very interesting articles:

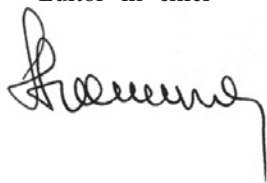
M. Samec, D. Korošak and B. Cvikl present a dielectric spectroscopy characterization of clay-water mixtures and the analysis of the obtained spectra. They propose a theoretical model for ion dynamics in which motion of ions in pore space electrolyte is interrupted by trapping events at the mineral surfaces. Typical time scales for these processes are given in terms of physical properties of the material. It is shown that a microscopic motion of ions in a complex environment of a clay-water system can be described with fractional dynamics leading to sub-diffusive behavior.

H. Vrecl-Kojc and S. Škrabl present a modified three-dimensional (3D) failure mechanism for determining the 3D passive earth pressure coefficient using the upper bound theorem within the framework of the limit analysis theory. The translational kinematically admissible failure mechanism generalized with a depth of  $h = 1.0$  is considered in the analysis. The mechanism geometry presents a volume of rigid blocks composed of the central body and two lateral rigid bodies which are connected by a common velocity field. The results are presented in a graphical form depending on the geometrical parameters and soil properties. A brief description of two world-recognized failure mechanisms based on the limit analysis approach, and the comparison of three failure mechanism results are also presented.

A. Seriani, Y. Kismoune Thésard and T. Serradj describe the behaviour of a subway tunnel in Algiers and the state of transition of the surrounding ground during digging. These phenomena are studied on an experimental basis using a 1/20 physical model scale.

L. Vrankar, F. Runovc and G. Turk have contributed some examples of using RBFs for a geostatistical analysis of modeling radionuclide migration. The migration of radionuclides is simulated using the advection-dispersion equation in Eulerian and Lagrangian forms. Stefan's or moving boundary value problems are also presented. The position of the moving boundary is simulated using the moving data centers method and the level set method.

Ludvik Trauner  
Editor-in-chief



---

# UGOTAVLJANJE ZNAČILNOSTI DINAMIKE IONOV V MEŠANICI GLINE IN VODE S POMOČJO DIELEKTRIČNE SPEKTROSKOPIJE

---

MARKO SAMEC, DEAN KOROŠAK IN BRUNO CVIKL

---

## o avtorjih

Marko Samec

Univerza v Mariboru,

Fakulteta za gradbeništvo

Smetanova ulica 17, 2000 Maribor, Slovenija

E-pošta: marko.samec@uni-mb.si

Dean Korošak

Univerza v Mariboru,

Fakulteta za gradbeništvo

Smetanova ulica 17, 2000 Maribor, Slovenija

E-pošta: dean.korosak@uni-mb.si

Bruno Cvikl

Univerza v Mariboru,

Fakulteta za gradbeništvo

Smetanova ulica 17, 2000 Maribor, Slovenija

E-pošta: cvikl@uni-mb.si

---

## izvleček

*V delu je predstavljena karakterizacija mešanic gline in vode na podlagi dielektrične spektroskopije in analiza pridobljenih spektrov. Predlagan je teoretičen model dinamike ionov, ki poleg gibanja ionov v porah elektrolita vključuje tudi njihovo ujetost na površinah mineralov. Časovne konstante, ki določajo dinamiko teh pojavov, so povezane z fizikalnimi lastnostmi snovi. Mikroskopsko gibanje ionov v kompleksnem okolju mešanice gline in vode lahko opišemo z dinamiko delcev, ki vodi do subdifuznega obnašanja.*

---

## ključne besede

dielektrična spektroskopija, porozna snov, prevodnost, dinamika delca

---

# PROBING ION DYNAMICS IN A CLAY-WATER SYSTEM WITH DIELECTRIC SPECTROSCOPY

---

MARKO SAMEC, DEAN KOROŠAK and BRUNO CVIKL

---

## about the authors

Marko Samec  
University of Maribor,  
Faculty of Civil Engineering  
Smetanova ulica 17, 2000 Maribor, Slovenia  
E-mail: marko.samec@uni-mb.si

Dean Korošak  
University of Maribor,  
Faculty of Civil Engineering  
Smetanova ulica 17, 2000 Maribor, Slovenia  
E-mail: dean.korosak@uni-mb.si

Bruno Cvikl  
University of Maribor,  
Faculty of Civil Engineering  
Smetanova ulica 17, 2000 Maribor, Slovenia  
E-mail: cvikl@uni-mb.si

---

## abstract

*Dielectric spectroscopy characterization of clay-water mixtures is presented and the obtained spectra are analysed. A theoretical model for ion dynamics is proposed in which motion of ions in pore space electrolyte is interrupted by trapping events at the mineral surfaces. The typical time scales for these processes are given in terms of the physical properties of the material. It is shown that the microscopic motion of the ions in a complex environment of clay-water system can be described with fractional dynamics leading to subdiffusive behavior.*

---

## keywords

dielectric spectroscopy, porous media, conductivity, fractional dynamics

---

## 1 INTRODUCTION

Characterization of complex heterogeneous materials such as clay minerals turns out to be a complicated issue experimentally as well as theoretically [1, 2]. One of the reasons for the difficulties is the time scale of the ion dynamic processes which are mostly diffusion governed. The most suitable techniques to probe ion dynamics on these intermediate time scales are NMR and dielectric spectroscopy.

Numerous studies have already demonstrated and analysed the anomalous properties of transport in natural porous media caused by its heterogeneous nature [3]. On the other hand, certain anomalous features of transport were also recently discovered studying random walks [4] and dc electrical conductance [5] on complex networks.

The main consequence of anomalous diffusion of contaminants in geological formations surrounding a potentially contaminated site is the time dependence of the diffusion coefficient [6]. The microscopic properties of diffusion transport of ions in clayey soils [7] present important issues in migration studies of contaminants in moist soil, for soil remediation problems and engineering of natural nuclear waste repository barriers. The effective diffusion constant is sometimes considered [8], while the dependence of the diffusion coefficient on the distance from the clay-water interface was studied by [9] showing as much as a ten times increase in the diffusion coefficient near the interface with respect to its value in the bulk.

With respect to transport through natural porous media (such as soil or rock) the anomalous features stem from the motion of particles owing to the flow of water in saturated soils and the interaction with the solid matrix. The most important property of the porous media has been identified as its surface conductivity [10] and the structure of the electric double layer (EDL) in general. Within the dynamic Stern layer assumption (where counterions in the Stern layer express a

certain mobility), the surface conductivity depends on the contributions from the Stern and the diffusive layer. Recently, a model was proposed for surface electrochemical properties of clay minerals, in which the surface conductivity of the clay was computed based on the dynamic Stern assumption, with the argumentation that the surface conductivity is frequency dependent [11]. However, the analysis of the results of electrical and dielectrical characterization of porous media turns out to be a very complicated issue, specifically in the low frequency region, due to the observed dispersion of the conductivity and the electrode polarization effect [1, 12]. Among the numerous homogenization methods, the Differential Effective Medium (DEM) schemes [13, 14] and the Moment Method (MoM) [15] have shown to be powerful tools for modelling the relationships between microstructural features and electromagnetic parameters (dielectric permittivity and electrical conductivity).

In this paper we present the analysis of a low frequency part of the conductivity spectra of kaolinite clay samples prepared at different water contents approximately covering the range between plastic and liquid limits. We show that the measured spectra exhibit an anomalous part in the low frequency region displayed as a power-law frequency dependence before reaching the plateau. We also show that the conductivity dispersion curves for samples with different water contents follow the same master curve signalling the universality as frequently observed in disordered matter [16]. An attempt to explain experimentally observed features is here presented with a model of ion motion in pore space electrolyte interrupted by trapping events at the mineral surface. The typical time scales for these processes are given in terms of the physical properties of the material. The specific features of measured dielectric spectra can be well described by introducing harmonic restoring potential into the ion equation of motion.

## 2 EXPERIMENTAL DATA

Electrical characteristics of the clay-water system were measured using a low frequency impedance analyser at room temperature. The admittance of the sample placed in the measuring cell between two planparallel electrodes (area  $S=5.5 \text{ cm}^2$ , distance  $L=4.5 - 5 \text{ mm}$ ) was determined from the linear response of the sample to the small oscillating bias on the electrodes of the magnitude of 10 mV. The real (conductance) and imaginary parts (capacitance) of the admittance were measured in the frequency interval of 100 Hz to 100 MHz.

The clay sample used was source clay Kaolin KGa-1b purchased from The Clay Minerals Society with mineral kaolinite as the primary constituent, containing also small amounts of metals (Ca, K, Na, Mg). The plastic and liquid limits of the sample were at 25.9 % and 40.1 % water content, respectively. The specific surface of the clay sample was  $10 \text{ m}^2/\text{g}$  and its solid specific gravity 2.6.

The frequency dependence of the conductance and capacitance was first determined for a dry sample, and then for wet samples, with gravimetric water content ranging from 32 % to 56 %. Wet samples were obtained with the addition of distilled water to the clay.

## 3 RESULTS AND DISCUSSION

The values for real and imaginary parts of frequency dependent conductivity were obtained with recalculating the measured conductance and capacitance. The frequency dependence of the complex conductivity for the samples with different water contents can be well described with the following expression whose physical basis is described below:

$$\sigma(\omega) = \frac{\sigma_0}{1 + i\omega\tau_1 + (i\omega\tau_2)^{-\alpha}} \quad (1)$$

where  $\sigma_0$ ,  $\tau_1$ ,  $\tau_2$  and  $\alpha$  are constants determined from substituting the expressions given by Eq. (1).

The results for conductivity as a function of frequency are presented in Fig. 1 for the real part of the expression given by Eq. (1) and in Fig. 2 for the imaginary part. The results for the samples with 36 % and 56 % water content are only shown. All the samples show qualitatively similar behaviour. The values obtained for the calculated curves shown in Fig. 1 and Fig. 2 are given in Table 1.

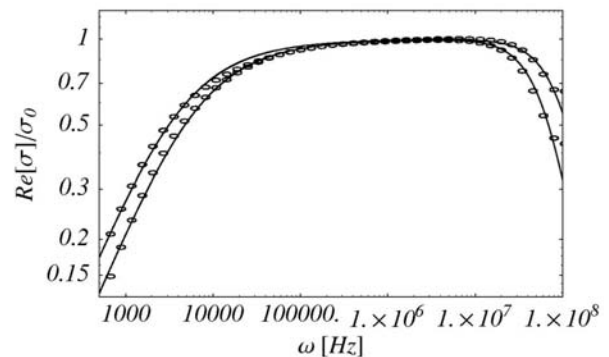


**Figure 1.** Measured (open dots) and calculated (solid lines) real part of frequency dependent conductivity of kaolinite clay samples at 36 % (lower curve) and 56 % (upper curve) water contents.



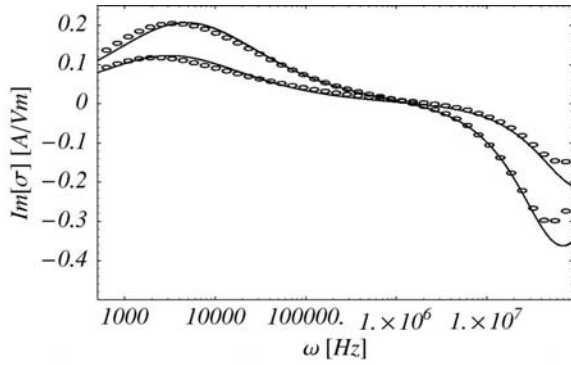


**Figure 2.** Measured (open dots) and calculated (solid lines) imaginary part of frequency dependent conductivity of kaolin-clay samples at 36 % (lower curve) and 56 % (upper curve) water contents.

**Table 1.** Values of the parameters used to calculate the real and imaginary parts of the conductivity shown in Fig. 1 and Fig. 2.

Parametr	Water content	
	36%	56%
$\sigma_0$ [A/Vm]	0,43	0,725
$\tau_1$ [s]	$0,9 \cdot 10^{-8}$	$1,45 \cdot 10^{-8}$
$\tau_2$ [s]	$3,2 \cdot 10^{-4}$	$2,1 \cdot 10^{-4}$
$\alpha$	0,67	0,67

Let us now discuss the physical basis of the Eq. (1) describing the dynamic response of the ions in a clay-water system. In general the ion current can be given by:

$$j(t) = qn_{ion}v(t) \quad (2)$$

where  $q$  is the elementary charge,  $n_{ion}$  is the ion concentration and  $v(t)$  is the ion velocity. Without loss of generality, a simple one-particle one-dimension picture is used here. The ions in the clay-water system move in a complex environment consisting of pore electrolyte. During the motion they also interact with the clay mineral surfaces which are charged. Ions moving in the pore space experience drag force which is proportional to ion velocity:

$$F_d = -m\gamma v \quad (3)$$

Here  $m$  is the mass of the ion, and  $\gamma$  is the drag force coefficient. To describe the electrode-pore electrolyte interface an additional harmonic force is introduced acting on the ion in the double layer near the electrode [1]:

$$F_h = -\frac{q^2 n_{ion}}{\epsilon_s \epsilon_0} x \quad (4)$$

Here, the static dielectric constant is the low frequency limit of the real part of the dielectric function  $\epsilon_s = \epsilon'(\omega \rightarrow 0)$ . The equation of motion for the ion in the external field  $E(t)$  is:

$$\frac{dv(t)}{dt} + \gamma v(t) + \omega_0^2 x(t) = \frac{q}{m} E(t) \quad (5)$$

where the characteristic frequency is defined as:

$$\omega_0^2 = \frac{q^2 n_{ion}}{\epsilon_s \epsilon_0 m} \quad (6)$$

The physical mechanism of the ion dynamics near the mineral particle surface consists of the successive trapping and releasing of the particle. After each such event (at the pore/clay particle surface) the particles undergo the Brownian motion in the pore space electrolyte. The time scale for this motion between trapping events is  $\tau_r = 1/\gamma$ , while  $\tau_t$  is set for the intrinsic time scale for the trapping event. We can estimate the characteristic trapping time by considering the linear dimension of the clay particle  $a$  (i.e. radius) and thermal velocity of the particle  $v_{th} = \sqrt{kT/m}$ , where  $T$  is the temperature and  $k$  is the Boltzmann constant:

$$\tau_t = \frac{a}{v_{th}} \quad (7)$$

The characteristic time for the motion in the pore space depends on the mean free path of the ion and its thermal velocity. For an unsaturated clay-water system we can estimate the mean free path with the average distance between the two adjacent clay particles:

$$\tau_r = \frac{\langle l \rangle}{v_{th}} \approx \frac{1}{a^2 n_{clay} v_{th}} \quad (8)$$

In this simplified picture the relation between the characteristic times of ion dynamics can be written as:

$$\tau_r = p\tau_t, \quad (9)$$

where the details of the clay structure, relative orientation of clay particles and the topology is simply collected within a single parameter  $p$ , usually of order one.

It was shown [17, 18] that the stochastic motion of the particle experiencing trapping events lead to a memory relation between the mean position and the mean velocity of the particle expressed with a fractional derivative of velocity:

$$\phi \frac{dx(t)}{dt} = {}_{-\infty} D_t^{1-\alpha} v(t) \quad (10)$$

where  $\phi = \tau_i^\alpha / \tau_r$ . The Fourier transform of the velocity leads to:

$$v(\omega) = \phi (i\omega)^\alpha x(\omega) \quad (11)$$

After the Fourier transformation of the equation of motion (10) and using  $j(\omega) = \sigma(\omega)E(\omega)$  the frequency dependent conductivity is:

$$\sigma(\omega) = \frac{\sigma_0}{1 + (\omega_0 \tau_r)^2 (i\omega \tau_t)^{-\alpha} + i\omega \tau_r} \quad (12)$$

where

$$\sigma_0 = \frac{q^2 n_{ion} \tau_r}{m} = \varepsilon_s \varepsilon_0 \omega_0^2 \tau_r \quad (13)$$

By rewriting the derived expression for the conductivity (13) we can obtain the forms of Eq. (1). Here the notations  $\tau_2 = \tau_t (\omega_0 \tau_r)^{-2/\alpha}$ , and  $\tau_1 = \tau_r$  were introduced.  $\tau_2$  is the effective low frequency relaxation time as detected in the dielectric spectra, determining the peak of the imaginary component of conductivity  $\sigma_2^* = \text{Im}[\sigma(\omega = 1/\tau_2)]$ . The value of the static dielectric constant can thus be estimated as:

$$\varepsilon_s = \sigma_2^* \tau_2 / \varepsilon_0 \quad (14)$$

Since  $\tau_1$  and  $\tau_2$  are usually several orders of magnitude apart (see Table 1) we also have:

$$\varepsilon_s = \frac{\sigma_0 \tau_2 \sin(\pi\alpha/2)}{2\varepsilon_0 (1 + \cos(\pi\alpha/2))} \quad (15)$$

All the parameters of the model are (Eqs. (13)-(15)) expressed in this way with two free parameters  $p$  and  $\alpha$ , while all other quantities are material dependent (ion density, temperature, clay particle radius (i.e. specific surface), ion mass). Further investigation into the properties of the ion-surface interaction is necessary to determine the exact values of the remaining parameters.

In the low frequency limit, the frequency dependence of the conductivity follows the power-law behaviour:

$\sigma \propto \omega^\alpha$ . The properties of the diffusive motion of the ions near the clay particle-water interface are contained in the frequency dependent diffusion constant  $D(\omega)$  to which the conductivity is connected via the generalized Einstein relation [19]:

$$\sigma(\omega) = \frac{q^2 n_{ion}}{kT} D(\omega) . \quad (16)$$

Recently Revil and Linde [20] have studied the transport of ions and water in charged, deformable porous media, and showed that the relationship between the diffusion coefficient and conductivity was much more complex than the one given in Eq. (16). Since the focus here is on the motion of ions near the clay particle – water interface we consider Eq. (16) as an operational model in which the couplings to other transport mechanisms (such as chemico-osmotic effect) are neglected [21].

The frequency dependent diffusion coefficient is given by [19]:

$$D(\omega) = -\frac{1}{6} \omega^2 \int_0^\infty e^{-i\omega t} \langle x^2 \rangle dt , \quad (17)$$

where  $\langle x^2 \rangle$  is the mean-square displacement of the ion. Normal diffusion is characterized by the mean-square displacement that is linear in time  $\langle x^2 \rangle \propto t$ , while anomalously diffusing particles display the mean-square displacement of the  $\langle x^2 \rangle \propto t^\beta$ , where  $\beta \neq 1$ . For  $\beta = 1 - \alpha$  in Eqs. (3) and (4) we obtain the expression for the low frequency limit of the ion conductivity in the clay-water mixture  $\sigma \propto \omega^\alpha$ . The ion surface diffusion transport is therefore subdiffusive, and could be characterized with the time-dependent diffusion coefficient  $D(t) \propto t^{-\alpha}$ . This indicates that the experimentally observed dielectric properties result from anomalous ion transport in a clay-water system characterized with the time-dependent diffusion coefficient often observed in complex systems [22, 23]. Recently Dudko et al. have considered the time-dependent diffusion coefficient in periodic porous materials and showed that the diffusion coefficient decreases with time from its value in a free solvent to its effective value which is much smaller [24].

## 4 CONCLUSIONS

The conductivity spectra as obtained by dielectric spectroscopy measurements of the clay-water mixtures at different water content levels are analysed. It is shown that the origin for the anomalous conductivity dispersion can be attributed to the motion of the ions near the clay particle-water interface. The ion dynamics is described with the Brownian motion interrupted with trapping events at clay surfaces. The transport of the ions near the clay particle surface is found to be subdiffusive with the effective time-dependent diffusion constant.

We have shown that the analysis of the low-frequency part of the dielectric spectra can yield an important insight into certain properties of the diffusion processes of ions in porous media. With respect to contaminant transport it contributes to better understanding and prediction of the long time migration of contaminants in complex environments.

## REFERENCES

- [1] Sanabria, H., and Miller, J. H. (2006). Relaxation processes due to electrode-electrolyte interface in ionic solutions. *Phys. Rev. E*, Vol. 74, 051505.
- [2] Rotenberg, B. et al. (2005). An analytical model for probing ion dynamics in clays with broadband dielectric spectroscopy. *J. Phys. Chem. B*, 109, 15548.
- [3] Hunt, A. G. (2005). Basic transport properties in natural porous media. *Complexity*, Vol.10, 22, 22 - 37.
- [4] Gallos, L. K. (2004). Random walk and trapping processes on scale-free networks. *Phys. Rev. E*, Vol. 70, 046116.
- [5] Lopez, E., Buldyrev, S. V., Havlin, S. and Stanley, H. E. (2005). Anomalous transport in scale-free networks. *Phys. Rev. Lett.*, Vol. 94, 248701.
- [6] Guerrini, I. A., and Swartzendruber, D. (1997). Fractal concepts in relation to soil water diffusivity. *Soil Sci.* 162, 778.
- [7] Kozaki T., Inada K., Sato S. and Ohashi, H. (2001). Diffusion mechanisms of chloride ions in sodium montmorillonite. *J. Cont. Hyd.*, Vol. 47, 159-170.
- [8] Maes, N., Moors, M., Dierckx A., De Canniere, P. and Put, M. (1999). The assessment of electromigration as a new technique to study diffusion of radionuclides in clayey soils. *J. Cont. Hyd.*, Vol. 36, 231-247.
- [9] Yukhnovskii, I. R., Tokarchuk, M. V., Omelyan, I. P. and Zhelem, R. I. (2000). Statistical theory for diffusion of radionuclides in ground and subterranean water. *Rad. Phys. Chem.*, Vol. 59, 361-375.
- [10] Revil, A., and Glover, P. W. J. (1997). Theory of ionic-surface electrical conduction in porous media. *Phys. Rev. B*, 55, 1757.
- [11] Leroy, P., and Revil, A. (2004). A triple-layer model of the surface electrochemical properties of clay minerals. *Journal of Colloid and Interface Science*, 270, 371-380.
- [12] Hilfer, R. (1991). Geometric and dielectric characterization of porous media. *Phys. Rev. B*, Vol 44.
- [13] Cosenza, Ph., Camerlynck, C. and Tabbagh, A. (2003a). Differential effective medium schemes for investigating the relationship between high frequency relative dielectric permittivity and water content of soils. *Water Resources Research*, Vol. 39, n°9, 1230 doi:10.1029/2002WR001774.
- [14] Cosenza, P., Guérin R. and Tabbagh A., (2003b). Relationship between thermal conductivity and water content of soils using numerical modelling. *European Journal of Soil Science*, Vol. 54, 581-587.
- [15] Cosenza, P., and Tabbagh, A. (2004). Electromagnetic determination of clay water content: role of the microporosity. *Applied Clay Science*, Vol. 26, Issues 1-4, 21-36.
- [16] Dyre, J. C., and Schroeder, T. B. (2000). Universality of ac conduction in disordered solids. *Rev. Mod. Phys.*, Vol. 72, 873-892.
- [17] Metzler, R., and Klafter, J. (2000). Subdiffusive transport close to thermal equilibrium: From the Langevin equation to fractional diffusion. *Phys. Rev. E*, Vol. 61, 6308.
- [18] Metzler, R., Barkai, E. and Klafter J. (1999). Anomalous Diffusion and Relaxation Close to Thermal Equilibrium: A Fractional Fokker-Planck Equation Approach. *Phys. Rev. Lett.* 82, 3563.
- [19] Scher, H., and Lax, M. (1973). Stochastic transport in a disordered solid. I. Theory, *Phys. Rev. B*, 7, 4491-4502.
- [20] Revil, A., and Linde, N. (2006). Chemico-electromechanical coupling in microporous media. *J. Coll. Int. Sci.*, Vol. 302, 682-694.
- [21] Revil, A., Leroy, P. and Titov, K. (2005). Characterization of transport properties of argillaceous sediments. Application to the Callovo-Oxfordian Argillite. *J. Geophys. Res.*, Vol. 110, B06202.
- [22] Fa, K. S., and Lenzi, E. K. (2005). Time-fractional diffusion equation with time dependent diffusion coefficient. *Phys. Rev. E*, Vol 72, 011107.
- [23] Campos, D., Mendez, V. and Fort, J., Description of diffusive and propagative behavior on fractals. *Phys. Rev. E*, Vol. 69, 2004, 031115.
- [24] Dudko, O. K., Berezhkovski, A. M. and Weiss, G. H. (2005). Time dependent diffusion coefficients in periodic porous materials. *J. Phys. Chem.*, Vol. 109, 21296-21299.

---

# DOLOČITEV PASIVNEGA ZEMELJSKEGA PRITISKA Z UPORABO TRIDIMENZIONALNEGA PORUŠNEGA MEHANIZMA

---

HELENA VRECL-KOJC IN STANISLAV ŠKRABL

---

## o avtorjih

Helena Vrecl-Kojc  
Univerza v Mariboru,  
Fakulteta za gradbeništvo  
Smetanova ulica 17, 2000 Maribor, Slovenija  
E-pošta: helena.vrecl@uni-mb.si

Stanislav Škrabl  
Univerza v Mariboru,  
Fakulteta za gradbeništvo  
Smetanova ulica 17, 2000 Maribor, Slovenija  
E-pošta: stanislav.skrabl@uni-mb.si

---

## izvleček

*Prispevek prikazuje modificiran prostorski porušni mehanizem za določitev 3D koeficienta pasivnega zemeljskega pritiska ob uporabi teorema zgornje vrednosti metode mejne analize.*

*V analizi je upoštevan translatorski kinematično dopustni porušni mehanizem, ki je generaliziran z globino  $h = 1.0$ . Mehanizem geometrijsko predstavlja prostorski togi blok sestavljen iz osrednjega dela in dveh stranskih togih blokov, ki ju sestavljajo ovojnice bočnih trenjskih stožcev.*

*Sprednja ploskev osrednjega dela mehanizma je v interakciji s podporno konstrukcijo, medtem, ko je zgornja ploskev lahko obremenjena z dodatno obtežbo. Bočni segmenti predstavljajo štiri ali tristrani mnogokotnik v prerezni ravnini z osrednjim delom, zaradi tega definirajo poligonalno drsino osrednjega dela. Na zunanji strani je vsak segment sestavljen iz infinitizimalno oddaljenih togih polstožcev, ki tvorijo ovojnico.*

*Numerični rezultati mejnih vrednosti tridimenzionalnega (3D) pasivnega zemeljskega pritiska so predstavljeni v obliki brezdimenzijskega koeficienta  $K_{py}$  kot posledica lastne teže zemljine ter  $K_{pq}$  zaradi dodatne površinske obtežbe. Namen raziskave je bil izboljšanje do sedaj najnižjih vrednosti rešitev pridobljenih po teoriji mejne analize.*

*Rezultati analize predstavljenega modela so prikazani v grafični obliki v odvisnosti od geometrijskih parametrov in lastnosti temeljnih tal. V prispevku sta tudi predstavljena dva v svetovem merilu priznana prostorska porušna mehanizma, ki prav tako temeljita na metodi mejne analize ter primerjava rezultatov med vsemi tremi porušnimi mehanizmi.*

---

## ključne besede

teorem zgornje vrednosti, optimiranje, pasivni pritisk, tridimenzijski porušni mehanizem

---

# DETERMINATION OF PASSIVE EARTH PRESSURE USING THREE-DIMENSIONAL FAILURE MECHANISM

---

HELENA VRECL-KOJC and STANISLAV ŠKRABL

---

## about the authors

Helena Vrecl-Kojc  
University of Maribor,  
Faculty of Civil Engineering  
Smetanova ulica 17, 2000 Maribor, Slovenia  
E-mail: helena.vrecl@uni-mb.si

Stanislav Škrabl  
University of Maribor,  
Faculty of Civil Engineering  
Smetanova ulica 17, 2000 Maribor, Slovenia  
E-mail: stanislav.skrabl@uni-mb.si

---

## abstract

*This paper presents a modified three-dimensional (3D) failure mechanism for determining the 3D passive earth pressure coefficient using the upper bound theorem within the framework of the limit analysis theory. The translational kinematically admissible failure mechanism generalized with a depth of  $h = 1.0$  is considered in the analysis. The mechanism geometry presents a volume of rigid blocks composed of the central body and two lateral rigid bodies, which are connected by a common velocity field. The front surface of the central body interacts with the retaining wall, while the upper surface can be loaded by surcharge loading. The lateral body segments represent four- and three-sided polygons in the cross section of the central body; therefore, they define the polygonal failure surface of the central part. At the outer side, each segment of the lateral body is bounded by infinitesimally spaced rigid half-cones that describe the envelope of a family of half-cones. The numerical results of 3D passive earth pressure limit values are presented by non-dimensional coefficients of passive earth pressure influenced by the soil weight  $K_{py}$  and a coefficient of passive earth pressure influenced by the surcharge  $K_{pq}$ . This research was intended to improve the lowest values obtained until now using the limit analysis theory.*

*The results are presented in a graphical form depending on the geometrical parameters and soil properties. A brief description of two world-recognized failure mechanisms based on the limit analysis approach, and the comparison of three failure mechanism results are also presented.*

---

## keywords

upper-bound theorem, optimization, passive pressure, three-dimensional failure mechanism

---

## 1 INTRODUCTION

Passive earth pressure acting on the rigid retaining wall has been widely studied in the past with a stress on refining a 2D analysis. The calculations are based either on the limit-equilibrium method ([3], [13], [14], [16]), the slip line method ([5], [9]), or the limit analysis method ([2], [6], [11]). Three-dimensional (3D) problems of the passive earth pressure were presented by Blum [1] to a restricted extent, by Soubra and Regenass [10] with a multi-block translation failure mechanism using the limit analysis, and by Škrabl and Macuh [12] with a rotational hyperbolic failure mechanism.

This paper presents a new modified 3D translational kinematically admissible failure mechanism for determining the passive earth pressure coefficients within the framework of the upper-bound theorem of the limit analysis.

The limit analysis theory determines the limit pressures that provide strict lower or upper bounds to the true limit load ([2], [7]). The upper-bound theorem ensures that the rate of work due to the external forces of kinematical systems in equilibrium is smaller than or equal to the rate of dissipated internal energy for all kinematically admissible velocity fields that obey strain



velocity compatibility conditions and velocity boundary conditions, as well as the flow rule of the considered materials.

This analysis considers a general case of frictional and cohesive soils ( $\phi$  and  $c$ ) with the eventual surcharge loading  $q$  on the ground surface. The numerical results of the 3D passive earth pressure are presented in the form of dimensionless coefficients  $K_{p\gamma}$  and  $K_{pq}$ , representing the effects of the soil weight and surcharge loading.

The coefficient  $K_{pc}$ , which represents the effects of cohesion, can be determined using the coefficient of passive earth pressure due to the surcharge  $K_{pq}$  [5].

In conclusion a brief description of two world-recognized failure mechanisms based on the approach of limit analysis is presented ([10], [12]). The lowest upper-bound solutions of the 3D passive earth pressure coefficient given by a new failure mechanism are compared with the results relating geometrical parameters and soil properties.

## 2 FAILURE MECHANISM

A new modified translational three-dimensional failure mechanism within the framework of the upper-bound theorem of the limit analysis has been developed in order to optimize the 3D passive earth pressure coefficient [15].

The 3D coefficient is distinguished from the two-dimensional one, by its growing difference, depending on soil properties and geometrical data. Therefore, these coefficients are very useful when analysing different kinds of geotechnical problems, where a 3D state gives more exact and realistic results. For example, it can be applied to retaining pile walls in the case of axially spaced piles, when the resistance of piles along the embedment depth is analysed [15].

### 2.1 SUPPOSITIONS AND LIMITATIONS

The following suppositions and limitations are applied:

- Soil characteristics present a homogeneous, isotropic Coulomb material using the associative flow rule obeying Hill's maximal work principle [4].
- The translational failure mechanism is bounded by a polygonal sliding surface in the  $x$ - $y$  plane, a rigid block of the dimensions  $b \cdot h$  ( $b$  = width,  $h$  = height)

in the  $y$ - $z$  plane, and the envelope of a family of half-cones at both lateral sides, with a horizontal backfill.

- The redistribution of the contact pressures over the entire height  $h = 1$  for the passive pressure due to the soil weight is triangular and is assumed to be inclined at the constant friction angle  $\delta$  at the soil-structure interface.
- The velocity at the soil-structure interface is assumed to be inclined at  $\delta$  to the wall in order to respect normality conditions [8].
- The work equation is obtained by equating the rate of external work done by external forces to the rate of internal energy dissipation along different velocity discontinuities.
- The resulting value of passive earth pressure is defined by:

$$P_p = K_{p\gamma} \cdot \gamma \cdot \frac{h^2}{2} b + K_{pq} \cdot q \cdot hb + K_{pc} \cdot c \cdot hb \quad (1)$$

where  $\gamma$  is the unit weight of the soil,  $q$  is surcharge loading, and  $c$  is cohesion.

### 2.2 VELOCITY FIELD FORMULATION

The new translational three-dimensional kinematically admissible failure mechanism is shown in Fig. 1, where the cross-section and plane view of the lateral part of the failure mechanism are schematically presented. The Cartesian co-ordinate system is selected with the  $y$ -axis along the wall. The optimal polygonal sliding surface in the  $x$ - $y$  plane consists of a final number of rigid segments, the mechanism is dimensionless with a height of  $h' = 1$  (see Fig. 2).

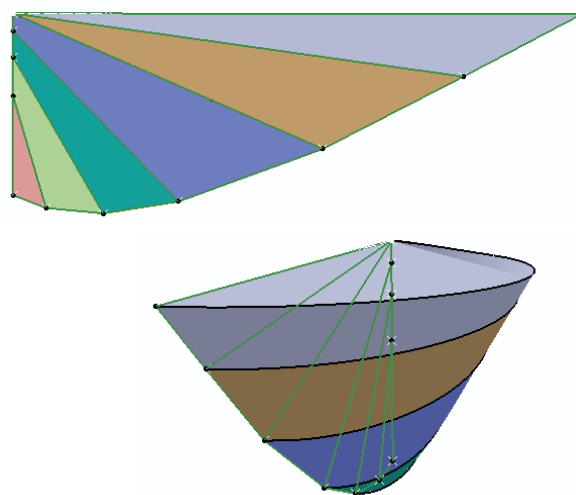


Figure 1. The scheme of the cross-section and plane view of the three-dimensional failure mechanism lateral plane.

A cross-section of the proposed failure mechanism with the velocity field is presented in Fig. 2. The individual segment  $j$  has a starting point  $(x_{opt}, y_{opt})_j$  and a final point  $(0, Y_{opt})_j$ , where the variables are calculated during the optimization procedure (see Fig. 2a).

The kinematically-admissible velocity field (see Fig. 2b) is composed of  $j = 7$  rigid segments bounded by the embedment point  $O(0, -1)$ , and the final point  $(X_{opt}, 0)$ . In general, the number of segments can be varied. The kinematics of the segments velocities  $V_i$  are inclined at an angle of  $\alpha_j + \phi$  to the horizontal axis, and the inter-segment velocities  $V_{j,j+1}$  are inclined at an angle of  $\beta_{j,j+1} - \phi$  to the horizontal axis. The mechanism is defined by  $2n-1$  angular parameters  $\alpha_j$  ( $j = 1, \dots, n-1$ ) and  $\beta_{j,j+1}$  ( $j = 1, \dots, n$ ). The movement of each of the  $n$  rigid segments accommodates the movement of the whole failure mechanism soil mass, and its movement accommodates the movement of the retaining structure.

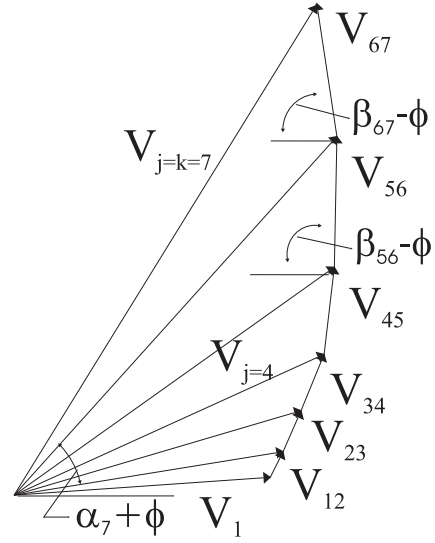


Figure 2b. The velocity field of the failure mechanism.

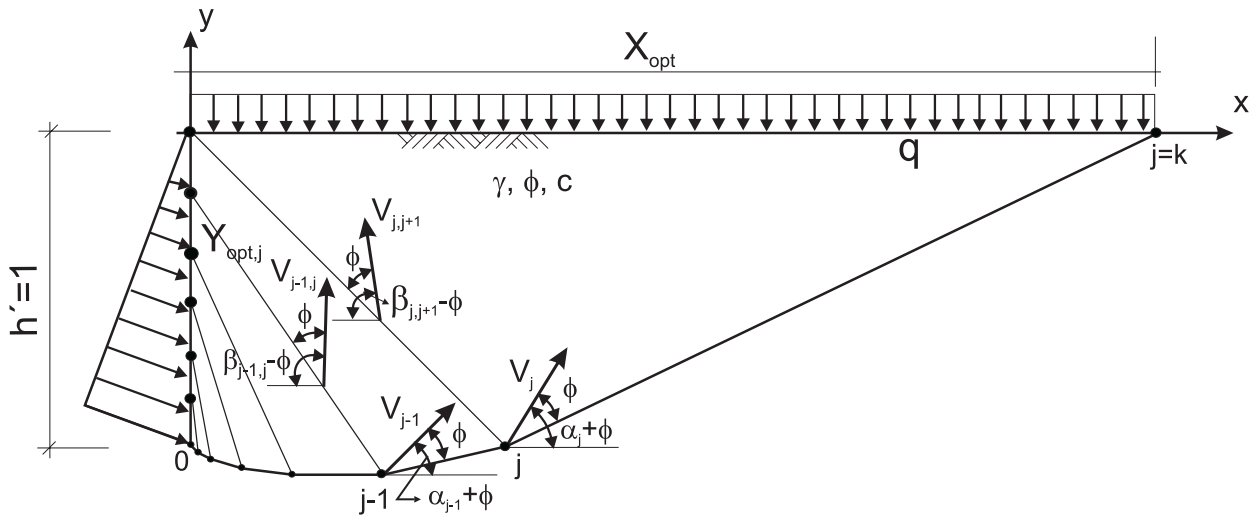


Figure 2a. The cross-section of the failure mechanism.

The segment velocities  $V_i$  and the inter-segment velocities  $V_{i,i+1}$  are given by

$$V_{j+1} = V_j \frac{\sin(\beta_{j,j+1} - 2\phi - \alpha_j)}{\sin(\pi - \beta_{j,j+1} - \alpha_{j+1})} \quad (2)$$

$$V_{j,j+1} = V_j \frac{\sin(\alpha_{j+1} - \alpha_j)}{\sin(\beta_{j,j+1} - \alpha_j - 2\phi)} \quad (3)$$

The kinematically admissible velocity field is consistent with the normality condition (at the angle  $\phi$  to the sliding surface) not only in the  $x$ - $y$  plane of the interface between rigid segments (as shown in Fig. 2) but also on the interfaces perpendicular to this plane.

### 2.3 GEOMETRY OF RIGID LATERAL BODIES

The geometry of the failure mechanism presents rigid space-segments consisting of a central part and two lateral rigid bodies constituted of the family of half-cone envelopes.

Fig. 3a presents the envelope of a family of cones of the first segment of the lateral body where the  $s$ - $t$  is the local coordinate system and  $x$ - $y$  the global system.

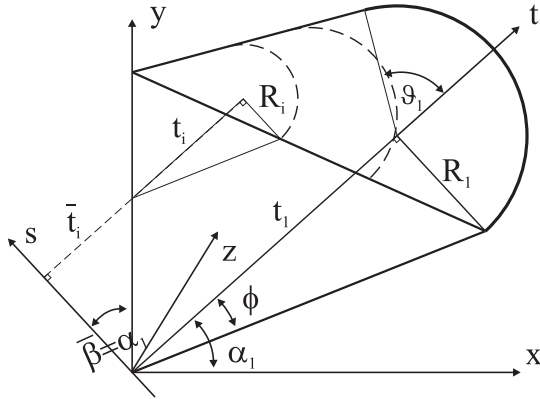


Figure 3a. Geometry of the first segment.

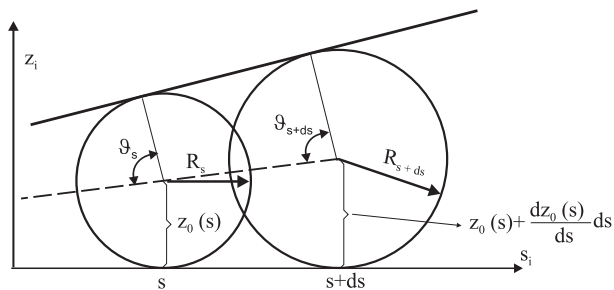


Figure 3b. The envelope of a family of half-cones.

The parametrical equation of a circle in the coordinate system  $(z, s)$  is:

$$z_i = R_i \cdot \cos \vartheta_i \quad (4)$$

$$s_i = R_i \cdot \sin \vartheta_i \quad (5)$$

where  $R_i$  is the radius of the cone, and  $\vartheta_i$  is the angle of deflection of a tangent to a curve, as a consequence of the differential  $dR/ds$ .

The radius of the cone  $R_i$  in the local coordinate system  $(t, s)$  is obtained with:

$$R_{i(s-t)} = (t_i - \bar{t}_i) \cdot \text{tg } \phi = (t_i - s_i \cdot \text{tg } \bar{\beta}) \cdot \text{tg } \phi \quad (6)$$

where  $\bar{\beta}$  is the angle between the global  $(x, y)$  and the local  $(t, s)$  coordinate systems.

The point on the envelope of a family of cones is defined by  $dR/ds$  and  $\vartheta$  (see Fig. 3b):

$$\frac{dR_i}{ds_i} = -\text{tg } \bar{\beta} \cdot \text{tg } \phi \equiv \sin \vartheta_i \Rightarrow \vartheta_i = a \sin(\text{tg } \bar{\beta} \cdot \text{tg } \phi) \quad (7)$$

Each point coordinate of the envelope of a family of half-cones in the local coordinate system is defined by:

$$s_i = k \cdot t_i + n \Rightarrow k = \frac{s_k - s_0}{t_k - t_0} \wedge n = s_k - k \cdot t_k \quad (8)$$

$$t_i = \frac{n}{\text{tg } \phi \cdot \sin \vartheta_i - k} \quad (9)$$

Transformation from the local to the global coordinate system leads to:

$$\begin{aligned} x_i &= x_{0,j} + t_i \cdot \cos \alpha_j - s_i \cdot \sin \alpha_j \\ y_i &= y_{0,j} + t_i \cdot \sin \alpha_j + s_i \cdot \cos \alpha_j \end{aligned} \quad (10)$$

where  $x_{0,j}; y_{0,j}$  is the distance from the origin of the global coordinate system to the first point on the segment  $j = 1$ .

The envelope of a family of cones for the first segment ( $j = 1$ ) is defined by the equations (4) to (10), while for other blocks ( $j = 2, M$ ) it is based upon the equation:

$$\vartheta_{i,j} = a \sin(\text{tg } \bar{\beta}_j \cdot \text{tg } \phi) + a \text{tg} \left[ \frac{\left( \frac{dz}{dn} \right)_{i,j}}{\cos \bar{\beta}_j} \right] \quad (11)$$

where  $\vartheta_{i,j}$  is the deflection angle on the envelope at point  $i$  of segment  $j$ .

Fig. 4 presents the scheme of the envelope of the third segment and its surface plane.

After the angle  $\vartheta_{i,j}$  is known at each of the analysed cones, the envelope of a family of cones can be uniformly defined by Eqs. (8) - (10). Fig. 5 presents the ground plane along the  $x$ -axis of the last segment.



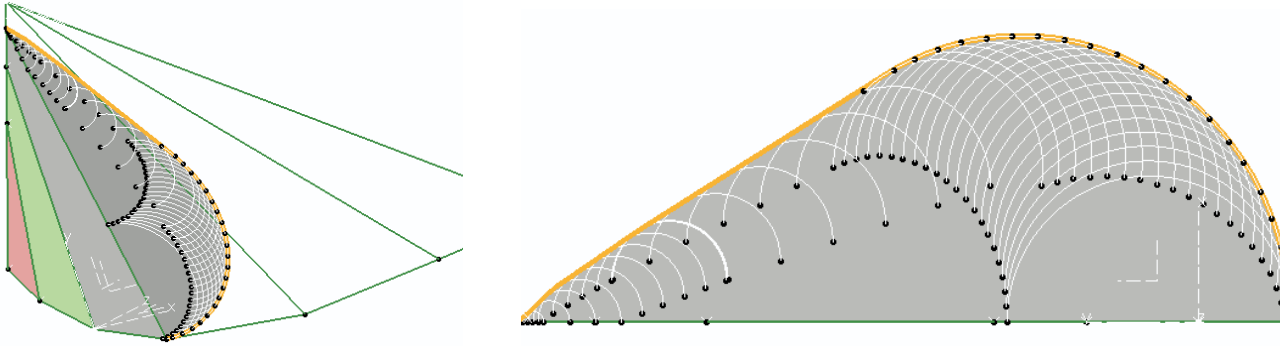


Figure 4. The scheme and the surface plane of the failure mechanisms third segment.

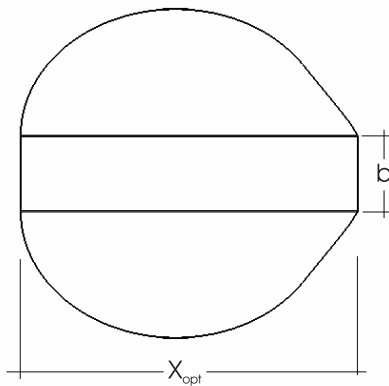


Figure 5. The ground plane of the failure mechanism along the  $x$ -axis.

On the basis of these results, the volume of the separate block  $j$  and finally the volume of the whole failure mechanism needed in the work equation of the upper-bound theorem of the limit analysis can be calculated. The work equation and the background of the limit analysis has been explained in detail ([7], [10], [12]), therefore no attention will be paid to the background of the theory in this paper.

Considering the work equation for the condition of equality between the external rate of work and internal rate of dissipation along the velocity interface for no cohesive rigid-plastic material, the coefficients can be written by:

$$K_{p\gamma} = \frac{g_\gamma}{f_\gamma} ; K_{pq} = \frac{g_q}{f_q} \quad (12)$$

where  $f_\gamma$  and  $g_\gamma$  denote the reduced values of the rate of work due to the passive earth pressure and the rate of work due to the unit weight of the ground at  $K_{p\gamma} = 1$ , and

$f_q$  and  $g_q$  denote the reduced values of the rate of work due to the passive earth pressure and the rate of work due to the surcharge loading on the backfill surface at  $K_{pq} = 1$ .

The coefficient  $K_{pc}$ , which represents the effects of cohesion, can be determined using the coefficient of passive earth pressure due to the surcharge  $K_{pq}$  [5]:

$$K_{pc} = \frac{K_{pq} - 1/\cos\delta}{\tan\phi} \quad (13)$$

### 3 NUMERICAL RESULTS

With the numerical analysis, the most critical non-dimensional three-dimensional passive earth pressure coefficient is obtained, where all variables are calculated by considering the scalars and the rigorous system of equality and inequality constraints. The Solver optimization tool of Microsoft Excel, together with the generalized-reduced-gradient method, was used during the numerical process.

The scalars, constraints and variables:

- geometry scalars are points (0,0) and (0,-1), ratio  $b/h$ ,
- material scalars are soil properties  $\phi, \delta$ ,  
 $\gamma' = 1.0, q' = c' = 0$ ,
- variable points on  $x$ -axis  $(X_{opt}, 0)_{j=7}$  and on the  $y$ -axis  $(0, Y_{opt})_j$ ,
- variable points on sliding surface  $(x_{opt}, y_{opt})_{j=1, M}$ ,
- inequality equation of the angles  $\alpha_j \leq \alpha_{j+1} - 0.01$  and  $\beta_j \leq \pi/2 - \phi$ ,
- inequality equation of points on the  $y$ -axis  $y_j \geq y_{j+1} + 0.001$ .

The results of three-dimensional passive earth pressures are presented in the form of dimensionless coefficients  $K_{py}$  and  $K_{pq}$  representing the effects of soil weight and surcharge loading, respectively. They are calculated for different soil characteristics for  $\phi$  ranging from  $15^\circ$  to  $45^\circ$ , for three values of  $\delta/\phi$  ( $\delta/\phi = 0, 0.50$  and  $1.00$ ), and for three values of  $b/h$  ( $b/h = 0.25, 1$  and  $10$ ).

Fig. 6 presents the critical failure mechanism in the  $x-y$  plane for different soil characteristics. The following conclusion has been re-established from these results: any increase of the soil friction angle  $\phi$  influences the failure mechanism; and while the volume of the failure mechanism increases, the shape of the sliding surface becomes more curved and the length of the last segment on the  $x$ -axis increases continuously.

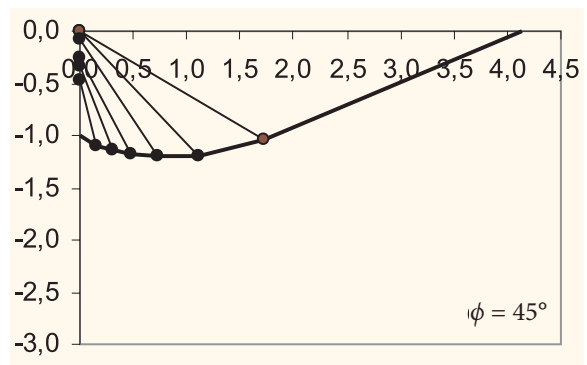
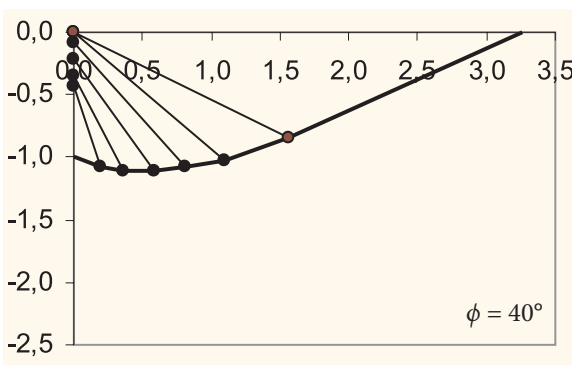
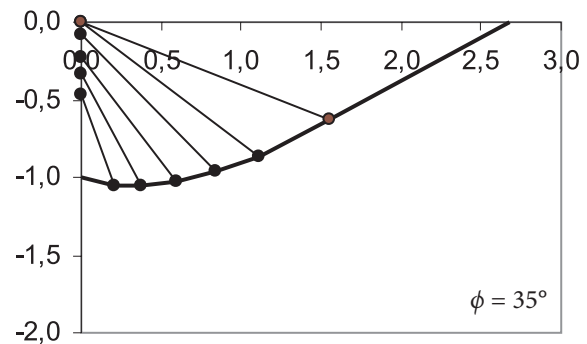
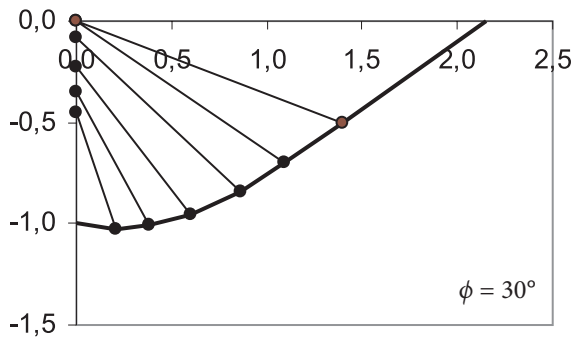
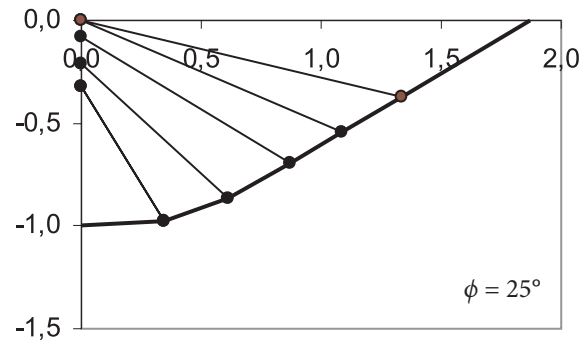
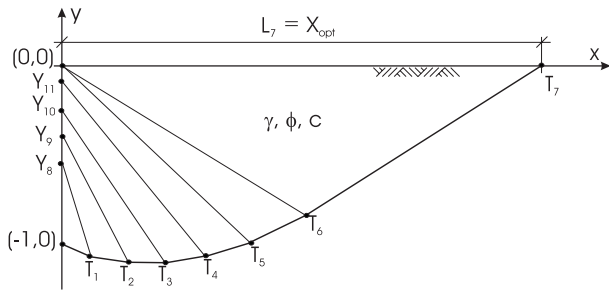


Figure 6. Critical failure mechanism in the  $x-y$  plane for  $\gamma' = 1.0, q' = c' = 0, b/h = 0.25$  and  $\phi = 25 \div 45^\circ$ .

From Fig. 7, it can be established that the length  $X_{opt} = L_7$  and, consequently, the volume of the failure mechanism is maximal at  $\phi = 45^\circ$  and  $\delta = \phi$ ; these values decrease by lowering the soil friction angle. The friction angle at the soil-structure interface  $\delta$  essentially influences the

results, and the geometrical factor  $b/h$  has the largest influence at the minimum soil friction angle  $\phi = 25^\circ$  in the region  $b/h = 0.25$  to  $b/h = 1$ ; however, at  $b/h > 1$  the influence of the geometry parameters declines.

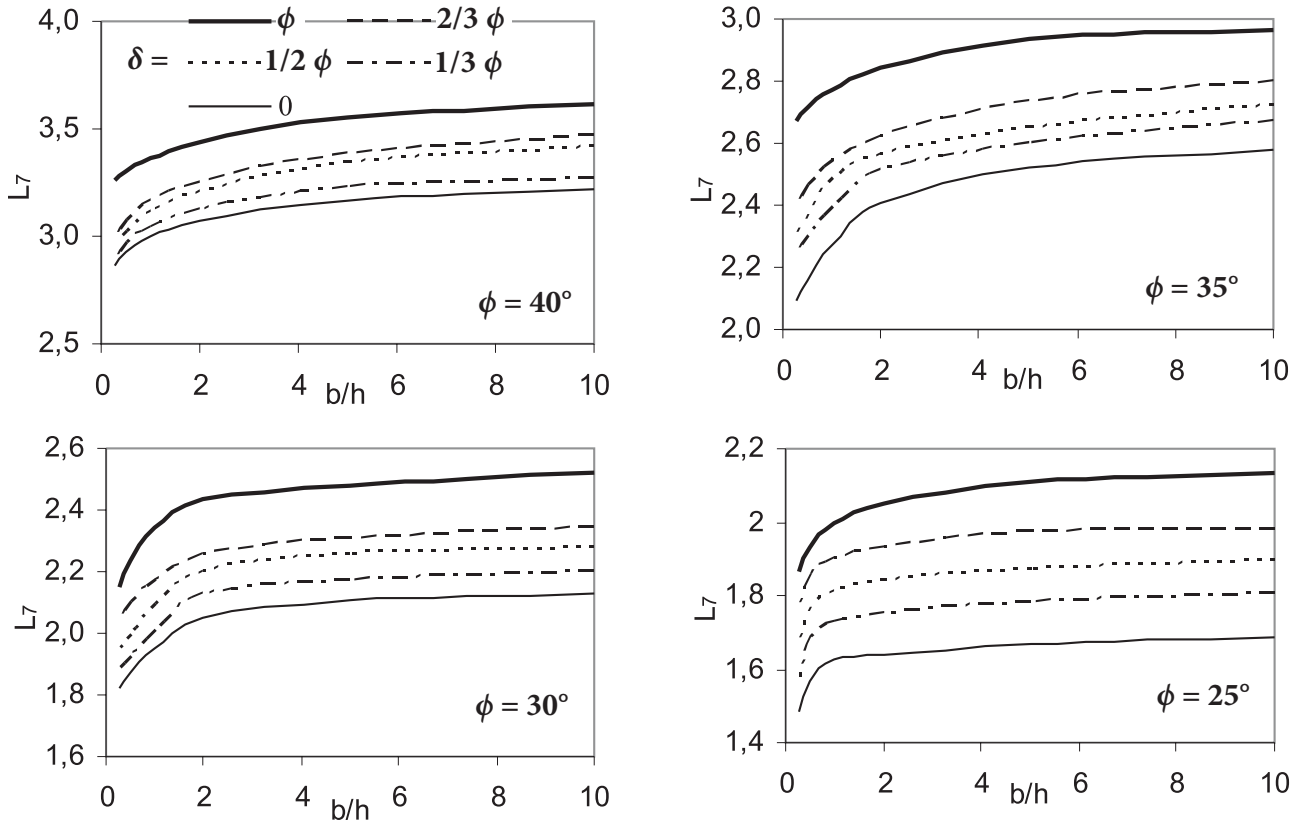
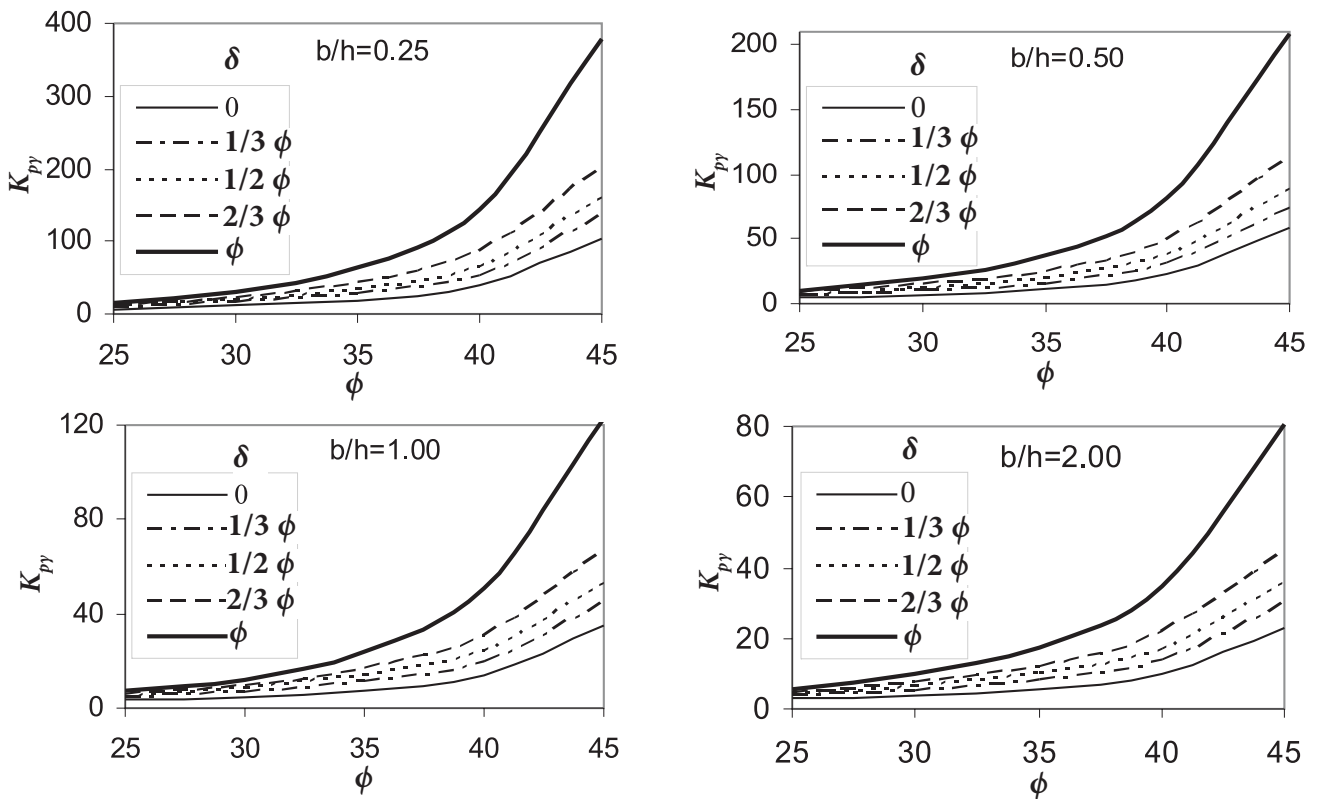


Figure 7. The last segment length along the  $x$ -axis  $X_{opt} = L_7$  against  $b/h$  for different  $\delta$  and  $\phi$ .



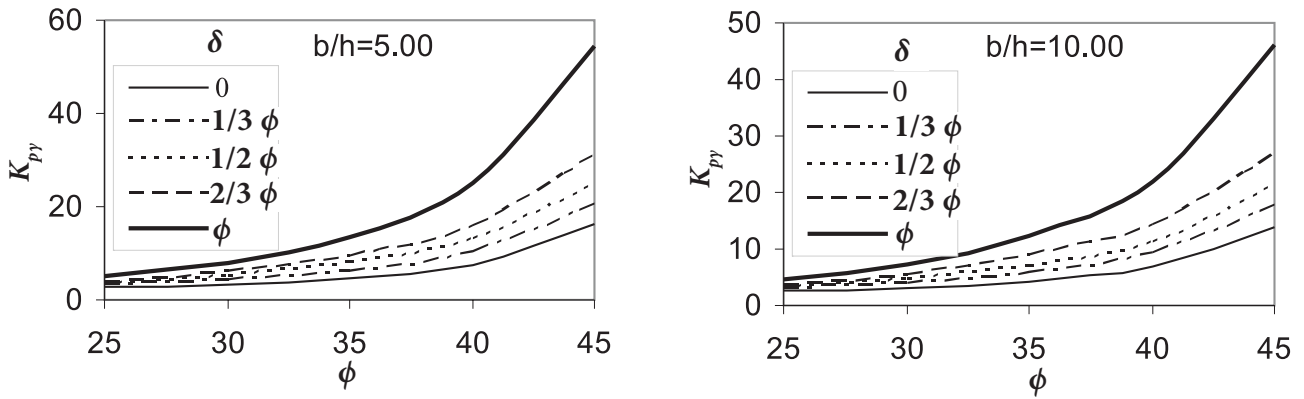


Figure 8 (also on previous page). Non-dimensional coefficients of  $K_{py}$  against  $\phi$ ,  $\delta$  and  $b/h$ .

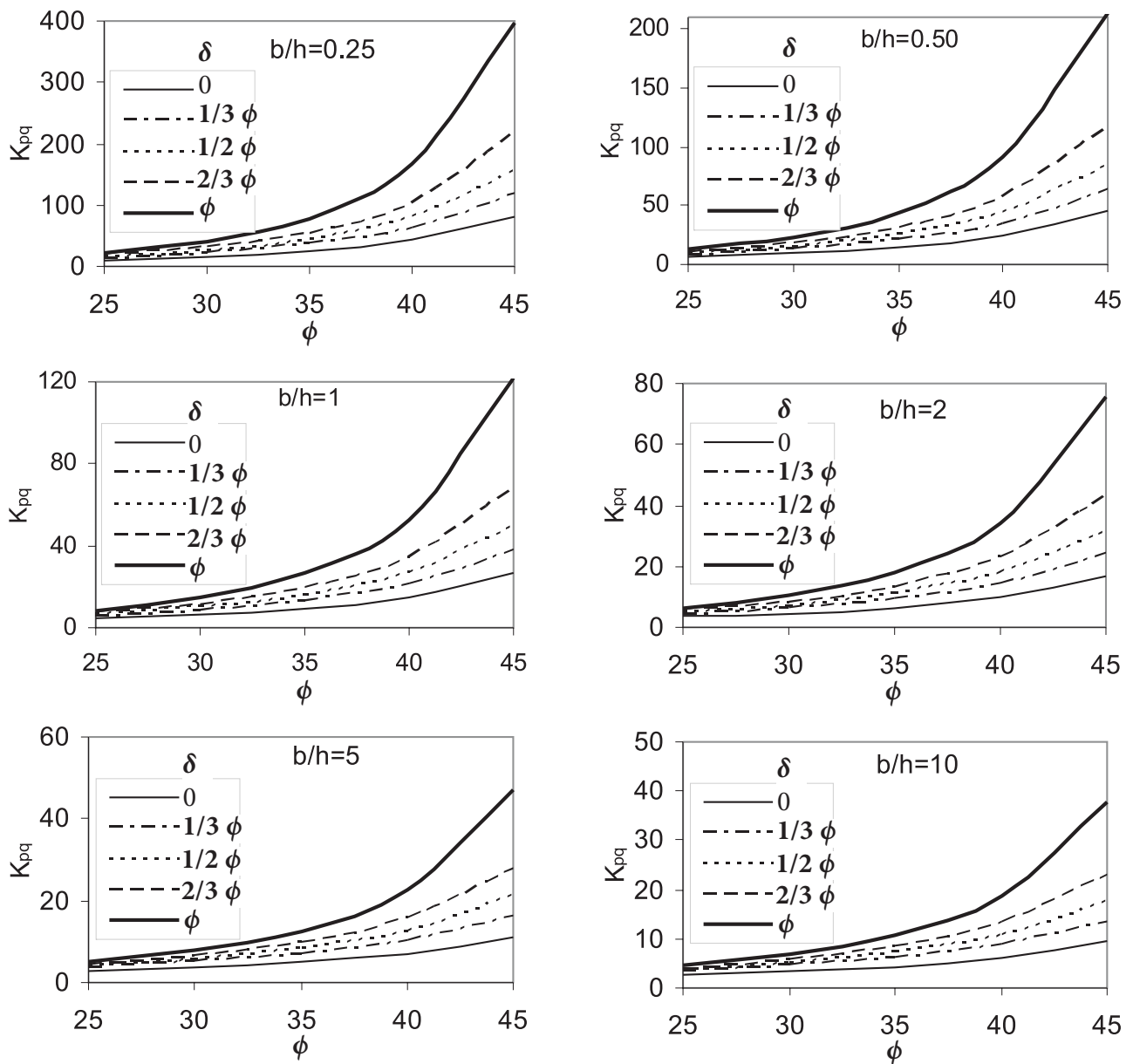


Figure 9. Non-dimensional coefficients of  $K_{pq}$  against  $\phi$ ,  $\delta$  and  $b/h$ .

Figs. 8 to 9 represent the values of the coefficients  $K_{py}$  and  $K_{pq}$  for different values of  $b/h$ , different shear angles and friction quotients between the retaining structure and the backfill soil.

The analysis results show that for the values of  $K_{py}$  and  $K_{pq}$ , which decrease essentially by increasing the ratio of  $b/h$ , the coefficients resemble the value in the 2D state at  $b/h = 10$ ; likewise, the failure mechanisms of 2D and  $b/h = 10$  have similar shapes [5]. Also the friction angle at the soil–structure interface  $\delta$  plays an important role, as by increasing the ratio of  $\delta/\phi$  the coefficients  $K_{py}$  and  $K_{pq}$  increase essentially. The results from Figs. 8 to 9 can be used in geotechnical practice.

#### 4 COMPARISON WITH THE EXISTING SOLUTIONS

The three-dimensional passive earth pressure acting on a rigid retaining wall has been re-established using a simplified translational failure mechanism [10] and a rotational log spiral failure mechanism [12]. Follows a

brief presentation of these two world-recognized failure mechanisms.

##### 4.1 MULTI-BLOCK FAILURE MECHANISM $M_{nt}$

Soubra and Regenass [10] published a truncated multi-block translational failure mechanism referred to as  $M_{nt}$ , which has been improved from his two previously proposed mechanisms, i.e. the one-block mechanism  $M_1$  and the multi-block mechanism  $M_n$ . The improvement from  $M_n$  has been obtained by a volume reduction of the final block, and from  $M_1$  by increasing the number of blocks from one to  $n$ .

Fig. 10 presents the cross-section and the plan view of the  $M_{nt}$  mechanism. In this improved mechanism, the lower plane and the lateral planes of the last block of the  $M_n$  mechanism are truncated by two portions of right circular cones with vertices at  $D_{n-1}$  and  $D'_{n-1}$ , respectively. The right (left) cone is tangential to the lateral plane  $BD_{n-1}D_n$  ( $B'D'_{n-1}D'_n$ ) and the lower plane  $D_nD'_{n-1}$  ( $D_{n-1}D'_{n-1}$ ).

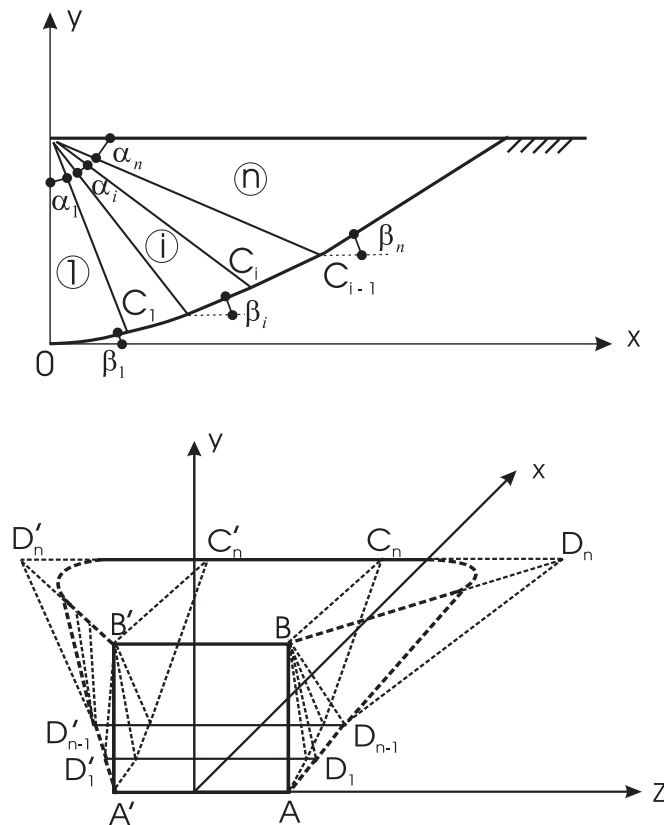


Figure 10. The cross-section and the plane view of the  $M_{nt}$  translational failure mechanism by Soubra and Regenass [10].

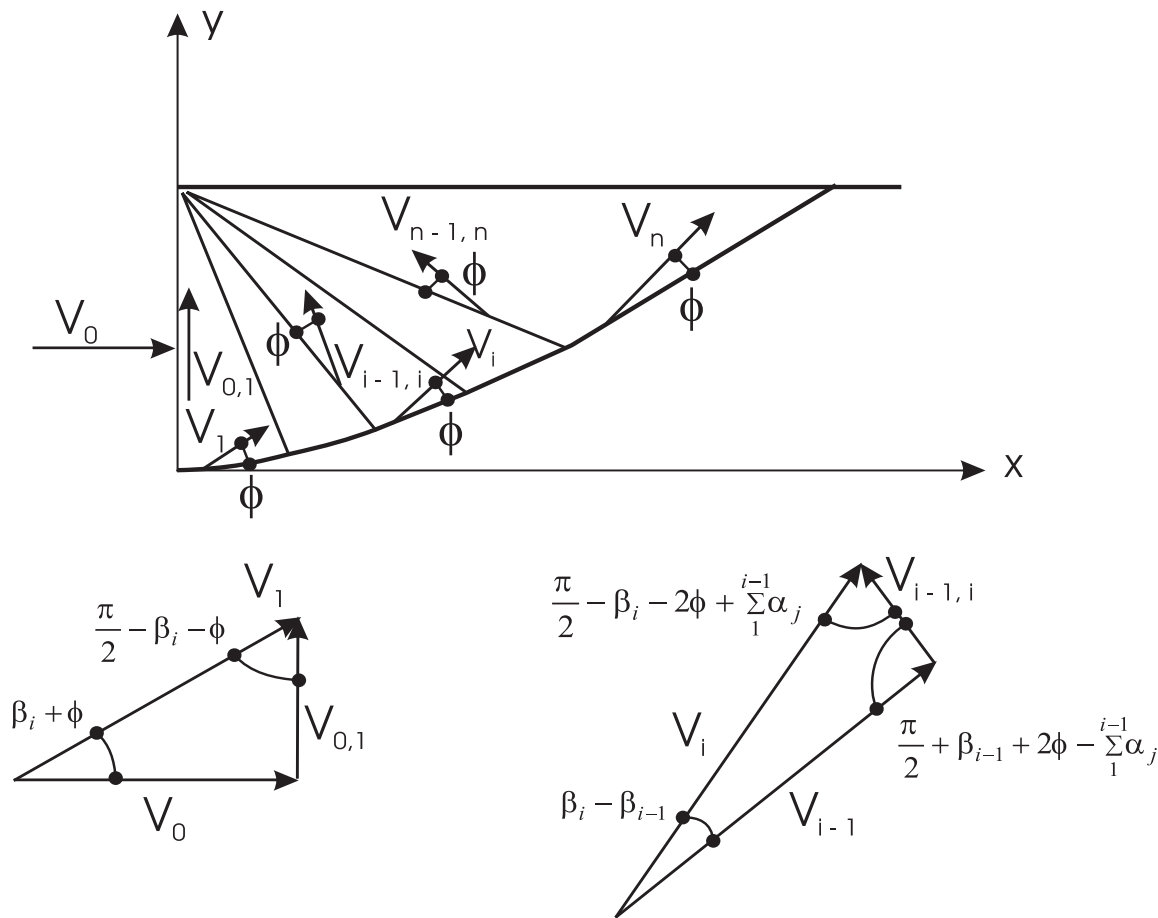


Figure 11. The velocity field of the  $M_{nt}$  mechanism.

Fig. 11 presents the velocity field of the  $M_{nt}$  mechanism. The soil mass of each block moves with the velocity  $V_i$  inclined at an angle of  $\beta_i + \phi$  to the horizontal direction. The inner-block velocity  $V_{i-1,i}$  is inclined to the inner planes of  $\phi$ , and to the outer velocities, as shown in Fig. 11. The wall moves with the velocities  $V_o$  and  $V_{o,i}$  representing the relative velocities at the soil-structure interface. All of these velocities are parallel to the vertical symmetrical plane  $xOy$ .

A comparison between this failure mechanism and the one presented in this paper can be made while both models are translational, using the same suppositions. The difference from the presented failure mechanism in this paper can be seen from Figs. 2 and 9. The  $M_{nt}$  mechanism of Soubra and Regenass [10] has two major differences from the presented modified failure mechanism, i.e. all blocks have the same starting point, which is the origin of the  $x-y$  coordinate system, and just one portion of the right circular cones is used on each side in the lateral plane.

#### 4.2 3D ROTATIONAL HYPERBOLICAL FAILURE MECHANISM

Škrabl and Macuh [12] developed this approach within the framework of the limit analysis theory. Similar to the mechanism described before, it is based on a three-dimensional rotational hyperbolic failure mechanism (see Fig. 12). This failure mechanism represents the extension of the plane slip surface in the shape of a log spiral (Fig. 13).

The outer sides are laterally bounded by a curved and kinematically-admissible hyperbolic surface, which is defined by enveloping the hyperbolic half cones and part of the case surface of the leading half cone. Every point along the retaining wall height (1-0, see Fig. 12) has an exactly defined hyperbolic friction cone. A common velocity field connects all the bodies. The difference from this mechanism and the presented modified failure mechanism can be seen in Fig. 2 and Figs. 12 to 13.

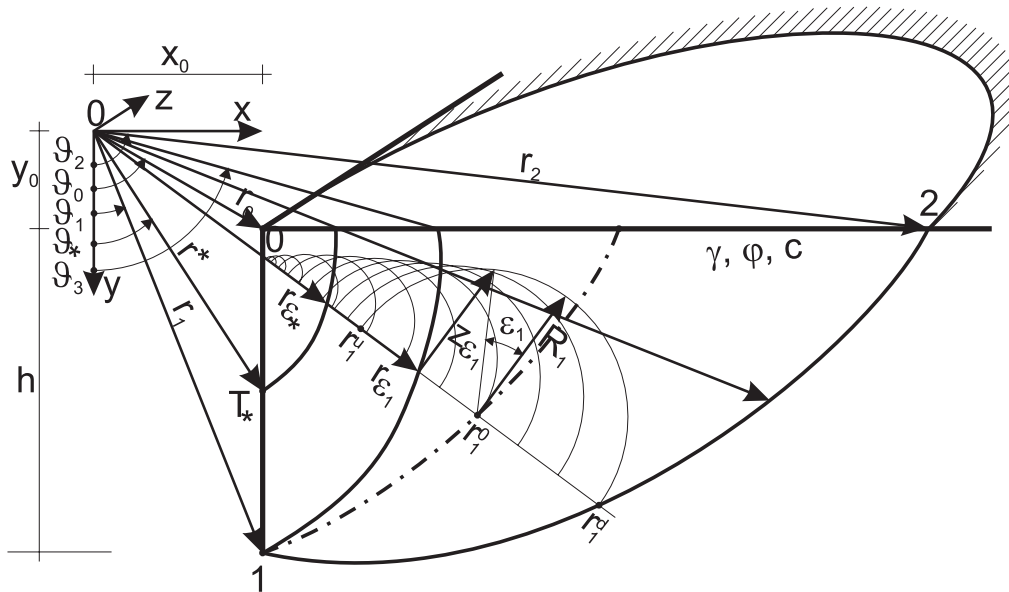


Figure 12. Scheme of the rotational hyperbolic failure mechanism.

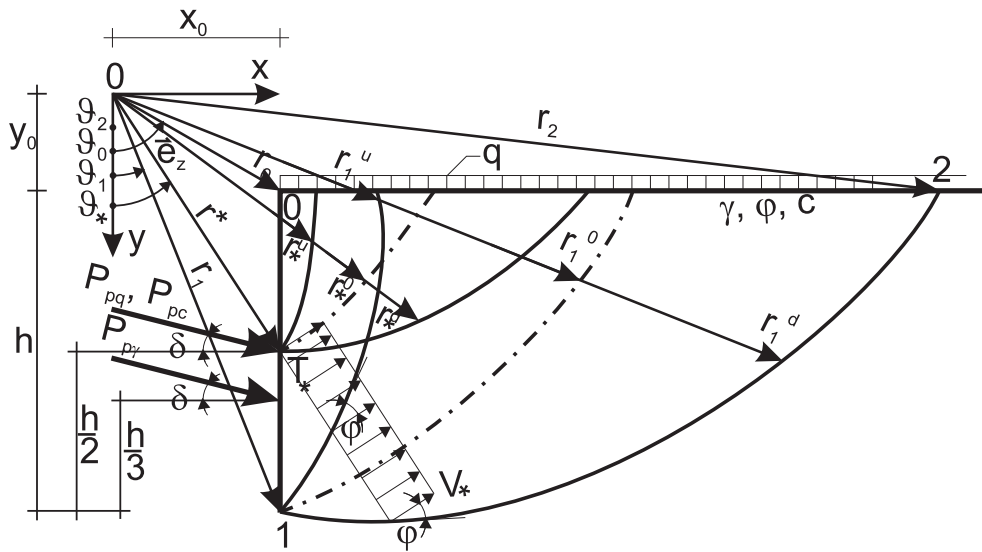


Figure 13. Log spiral slip surface of the mechanism.

### 4.3 COMPARISON OF THE RESULTS

The results for the dimensionless 3D passive earth pressure coefficients were compared to the results for other types of failure mechanism using the upper-bound theorem ([10], [12]). Table 1 shows the results for  $K_{py}$ ,

and Table 2 the results for  $K_{pq}$  for different values of  $\phi$ ,  $\delta$  and  $b/h$ . The highest differences are at  $\phi = 45^\circ$  and  $b/h = 0.25$ ; by lowering the friction angle  $\phi$  and increasing the value  $b/h$  the differences decrease, the smallest value being at  $\phi = 25^\circ$  and  $b/h = 10$ .

**Table 1.** Comparison of  $K_{py}$  results depending on parameters  $\phi$ ,  $\delta$  and  $b/h$ .

$\phi$ (°)	$b/h$	$K_{py}$ (Soubra and Regenass)			$K_{py}$ (Škrabl and Macuh)			$K_{py}$ (proposed model)		
		0.5	1.0	10.0	0.5	1.0	10.0	0.5	1.0	10.0
25	0.5	7.963	5.779	3.770	7.360	5.539	3.625	7.296	5.027	3.253
	1.0	12.776	8.798	5.004	10.985	7.809	4.885	10.431	7.360	4.579
35	0.5	22.855	15.150	8.150	20.779	13.709	7.320	19.847	13.533	7.079
	1.0	54.064	33.202	13.730	40.135	25.839	12.857	37.509	24.229	12.131
45	0.5	178.689	99.555	26.684	104.658	61.825	23.293	88.334	53.074	20.652
	1.0	379.494	212.364	59.215	239.688	140.857	51.747	207.888	122.938	45.991

**Table 2.** Comparison of  $K_{pq}$  results depending on parameters  $\phi$ ,  $\delta$  and  $b/h$ .

$\phi$ (°)	$b/h$	$K_{pq}$ (Soubra and Regenass)			$K_{pq}$ (Škrabl and Macuh)			$K_{pq}$ (proposed model)		
		0.5	1.0	10.0	0.5	1.0	10.0	0.5	1.0	10.0
25	0.5	10.135	6.873	3.748	9.733	6.579	3.687	9.368	6.346	3.627
	1.0	14.599	9.445	4.620	13.699	9.058	4.782	12.598	8.394	4.495
35	0.5	30.545	19.006	7.951	26.859	16.699	7.426	25.356	15.844	7.209
	1.0	57.371	33.627	11.708	49.308	29.814	12.044	43.675	26.561	10.860
45	0.5	176.444	96.248	23.101	107.038	60.919	19.397	86.218	50.080	17.420
	1.0	338.705	184.474	43.854	249.114	140.401	42.041	215.048	121.667	36.648

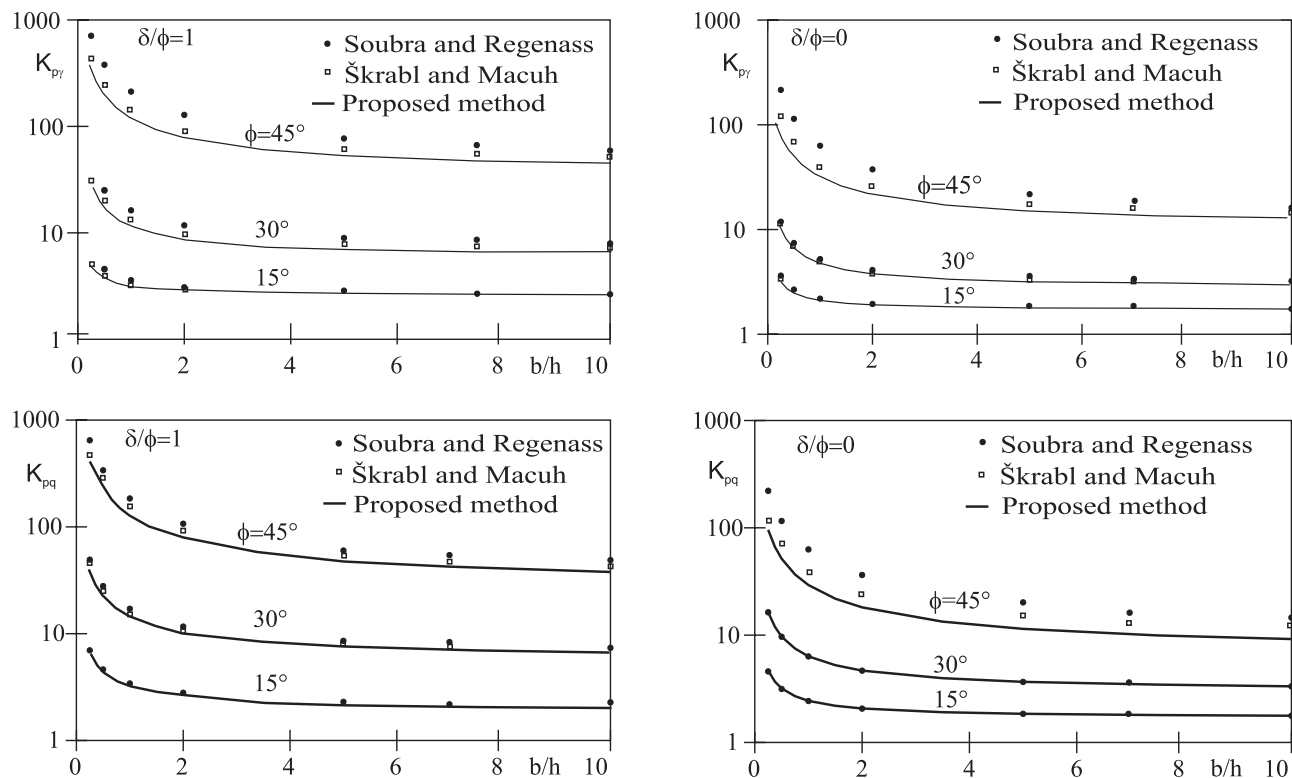


**Figure 14.** Comparison of the results for  $K_{py}$  and  $K_{pq}$  against  $b/h$  for  $\delta/\phi = 1$  and  $\delta/\phi = 0$ ,  $\phi = 15^\circ, 30^\circ, 45^\circ$ .



Fig. 14 presents a comparison of the coefficients  $K_{py}$  and  $K_{pq}$  for  $\phi = 15^\circ, 30^\circ$  and  $45^\circ$ ,  $\delta/\phi = 1$  and  $\delta/\phi = 0$  against the ratio  $b/h$ .

The comparison of these results shows that the difference in the coefficient is the greatest at  $\phi = 45^\circ$ , at low ratio  $b/h = 0.25$ , and  $\delta/\phi = 0$ .

## 5 CONCLUSIONS

The modified translational failure mechanism presented in this paper was developed for the improvement of the 3D passive earth pressure coefficients. The approach used is based on a new translational three-dimensional failure mechanism within the framework of the upper-bound theorem of the limit analysis. The geometry of the kinematically-admissible failure mechanism presents a rigid space-block consisting of a central part and two lateral rigid parts of a family of cone envelopes.

In the past the three-dimensional passive earth pressure was determined by a translational failure mechanism [10] and a rotational hyperbolic failure mechanism [12]. A description of these two failure mechanisms is briefly presented in this paper for a better understanding of differences between all three failure mechanisms.

The numerical results for a limit value of 3D passive earth pressure are presented graphically by a non-dimensional coefficient of passive earth pressure influenced by the soil weight  $K_{py}$  and a coefficient of passive earth pressure influenced by the surcharge  $K_{pq}$ .

A comparison of the results for all three mechanisms shows that the difference in the coefficient increases with any improvement in soil properties and lowering the ratio  $b/h$ .

## REFERENCES

- [1] Blum, H. (1932). Wirtschaftliche Dalbenformen und den Berechnung. *Bautechnik*, 10(5), 122-135.
- [2] Chen, W.F. and Liu, X.L. (1990). Limit analysis in Soil Mechanics. Elsevier, Amsterdam.
- [3] Coulomb, C.A. (1776). Essai sur une application des règles de maximis et minimis à quelques problèmes de statique relatifs à l'architecture. *ACAD. r.Sci. Mém. Math. Phys. par divers savants*, 7, 343-382.
- [4] Hill, R. (1950). The Mathematical Theory of Plasticity. Clarendon Press, Oxford.
- [5] Kèrisel, J. and Absi, E. (1990). Tables for the calculation of passive pressure, active pressure and bearing capacity of foundations. Gauthier-Villard, Paris.
- [6] Lysmer, J. (1970). Limit analysis of plane problems in soil mechanics. *Journal for Soil Mechanics and Foundation*, 96, No. 4, 1311-1334.
- [7] Michalowski, R.L. (2001). Upper-bound load estimates on square and rectangular footings. *Geotechnique*, 51, No. 9, 787-798.
- [8] Mroz, Z. and Drescher, A. (1969). Limit plasticity approach to some cases of flow of bulk solids. *Journal of Engineering for Industry*, ASME, 91, 357-364.
- [9] Sokolovski, V.V. (1965). Static of granular media. Pergamon Press, New York.
- [10] Soubra, A.H. and Regenass, P. (2000). Three-dimensional passive earth pressures by kinematical approach. *Journal of Geotechnical and Geoenvironmental Engineering*, ASCE, 2, No.2, 969-978.
- [11] Soubra, A.H. and Macuh, B. (2002). Active and passive earth pressure coefficients by a kinematical approach. *Proceedings of the Institution of Civil Engineers-Geotechnical Engineering*, 155, No. 2, str. 119-131.
- [12] Škrabl, S. and Macuh, B. (2005). Upper-bound solutions of three-dimensional passive earth pressures. *Canadian Geotechnical Journal*, 42, No.5, 1449-1460.
- [13] Škrabl, S. (2006). Interactional approach of cantilever pile walls analysis. *Acta Geotechnica Slovenica*, 3, No. 1, 46-59.
- [14] Terzaghi, K. (1943). Theoretical soil mechanics. Wiley, New York.
- [15] Vrecl-Kojc, H. (2006). Upper-bound theorem used for optimizing a geomechanical model of a cantilever retaining structure. *PhD thesis*, University of Maribor.
- [16] Zakerzadeh, N., Fredlund, D.G., and Pufahl, D. E. (1999). Interslice force functions for computing active and passive earth force. *Can. Geotech. J.*, Ottawa, 36(6), 1015-1029.

---

# OBNAŠANJE AVTOCEŠTNEGA TUNELA V ALŽIRIJI: EKSPERIMENTALNA ŠTUDIJA FIZIKALNEGA MODELA

---

ABDELBAKI SERIANI, Y. KISMOUNE THÉSARD IN TAYEB SERRADJ

---

## o avtorjih

Abdelbaki Seriani  
Genius University Badji Mokhtar,  
Faculty of Science of the Ground  
BP 12, 23000 Annaba, Alžirija  
E-pošta: seriani7@yahoo.fr

Y. Kismoune Thésard  
Genius University Badji Mokhtar,  
Faculty of Science of the Ground  
BP 12, 23000 Annaba, Alžirija

Tayeb Serradj  
Genius University Badji Mokhtar,  
Faculty of Science of the Ground  
BP 12, 23000 Annaba, Alžirija

---

## izvleček

*Pred vsakim projektom za izgradnjo tunela je treba zaradi visokih stroškov izdelati manjšo modelno študijo ter jo po potrebi matematično preveriti. S tem se pri realizaciji projekta izognemo nepredvidljivim posledicam. Slednje upošteva tudi predstavljen raziskava, pri kateri smo na fizikalnem modelu v razmerju 1:20 eksperimentalno preučili obnašanje avtocestnega tunela v Alžiru ter usipanje okoliških zemljin med izkopavanjem.*

---

## ključne besede

tunel, ustrezen material, fizikalni model, podpore, deformacije, prelom, oslABLJENE cone

# BEHAVIOUR OF THE SUBWAY TUNNEL IN ALGIERS: PHYSICAL MODEL EXPERIMENTAL STUDY

ABDELBAKI SERIANI, Y. KISMOUNE THÉSARD and TAYEB SERRADJ

## About the authors

Abdelbaki Seriani  
Genius University Badji Mokhtar,  
Faculty of Science of the Ground  
BP 12, 23000 Annaba, Algeria  
E-mail: seriani7@yahoo.fr

Y. Kismoune Thésard  
Genius University Badji Mokhtar,  
Faculty of Science of the Ground  
BP 12, 23000 Annaba, Algeria

Tayeb Serradj  
Genius University Badji Mokhtar,  
Faculty of Science of the Ground  
BP 12, 23000 Annaba, Algier

## Abstract

*Tunnel construction projects are too expensive to be approached directly without a preliminary small-scale model study and subsequent verification with a mathematical model, if needed. These studies enable to avoid unforeseen consequences which emerge at the time of the project realization. It is within this framework that we carried out our investigations. The behaviour of a subway tunnel in Algiers and the state of transition of the surrounding ground during digging are studied from an experimental point of view via a 1/20 physical model scale.*

## Keywords

tunnel, equivalent material, physical modelling, supports, deformations, rupture, loosened zone

## 1 GOALS OF THE INVESTIGATIONS

The lack of experimental data on the tunnel in Algiers (Batch 5) deprive us of a comparison base between measurements and observations carried out in situ and the results obtained by the physical model used within the framework of this research. Nevertheless, the work that we present will be highly useful, being the first approximation of the prospects of the subway tunnel in Algiers. The below methods and the reasons were considered in the investigation:

- the use of artificial rock medium corresponding perfectly to in situ conditions;
- the technology of tunnel construction proposed by the project which will be completely respected during the realization of the tunnel model;
- the digging will be carried out under the load which corresponds to actual weight of artificial material.

This method of investigation (technology and construction of the tunnel model under constant load) provides a better simulation model, much closer to the in situ conditions.

## 2 THE TASK TO BE SOLVED

This work is aimed at reporting about the aptitude of physical modelling in tunnel projects considering tender ground conditions. To achieve this, the following is considered:

- Measurement of convergence after each stage of construction.
- Observation of the ground movement around the tunnel after each phase, owing to the numerous reference marks placed in artificial material. These marks allow us to measure relative displacements and thus to calculate deformations and specify the state of material around the tunnel model.

- Qualitative verification of combining the supporting systems used.
- Conception of a physical model to carry out the observations and measurements. A mixture of industrial powder is used as artificial rock material.

### 3 PHYSICAL MODELLING

#### 3.1 CHOICE OF THE PHYSICAL MODEL

To simulate the subway tunnel in Algiers (Batch 5), a physical model was used (Fig. 1), which has two essential advantages:

- Economic advantage from the point of view of construction, and
- Simplicity from the point of view of uses and operation.

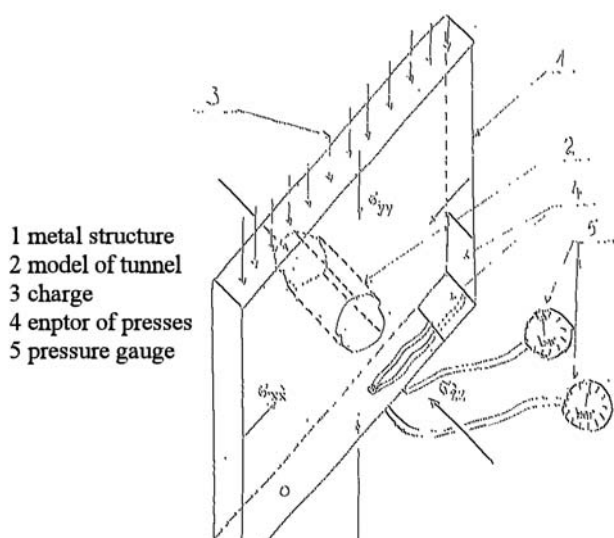


Figure 1. Physical model.

#### 3.2 CHOICE OF THE SCALES OF SIMULATION

We think that it is preferable to choose geometrical scales and scales of equal constraints to avoid complicating the choice of the material equivalent or to have additional loads applied in order to compensate for high values of the voluminal mass in the case of a high scale constraint compared to the 1 : 20 geometrical scale selected. With this scale the width of the tunnel model (50 cm) does not exceed 1/3 of the width of the model (180 cm), as recommended from experience (in order to avoid the influence of borders on the test results).

The calculation of the scales is shown in Table 1 (see next page).

Physical simulation won large applications since an international symposium in Italy on the physical modelling in geomechanics. Certain researchers approached the physical simulation in tunnelling by using different equivalent materials for the rocks and the systems of supports. Thus, for modelling the behaviour of a tunnel, equivalent materials such as: solids (bentonite, mica baryte, ground cork) and binders (paraffin oil, silicon oil) are used (Sauer, 1979). In order to simulate a tunnel in tender rock a mortar of water, cement, bentonite, and sand is used. Another mixture composed by cement, lime quick, sand, and water (Gajàry, 1990) was used for studying experimentally the stability of a roadway.

The simulation of the tunnel supports in appropriate conditions with different equivalent materials is summarized below.

Authors	Type of supports	Equivalent material
Tazawa.Y	Rock bolts	Cooper screws of variable length located at convenient relative distances
	Lining	Mortar of cement with a resistance to compression $\sigma_c = 20-30$ MPa
Adachi .T. & al.	Rock bolts and lining	Kint paper of variable thickness and resistance

In the light of these and other studies (Stimpson, 1968), and based on the criteria listed below (Baron and Larocque; 1960):

- the facility of fabrication of the proposed model,
- relative expenses for the material and the equipment, and
- environmental and security criteria will be observed too.

The author introduces new equivalent materials, such as industrial talk mixed with water.

Industrial talk mixed with water possesses plastic properties similar to in situ conditions (clay-marly soil). The mixture in question is simple (talk + % water), which renders this material recoverable, hence reusable, and therefore cheap.

Physical and mechanical properties of equivalent materials of the rock and of supporting are presented in table 2 on page 28 (Seriani, 1993).

**Table 1.** Scales of constraints compared to the geometrical scales.

Geometrical scale		Scale of stresses													
Insitu		Model	Insitu			Models									
Dimensions			Dimensions												
Names	Values	Value according to the scale	Names	Symbol	Units	1/40	1/30	1/25	1/20	1/15	1/4	1/3	1/2	1/1.5	
L/m Length	1	L	Stress	$\sigma$	N/m <sup>2</sup>										
			Force	F	NR										
H/m Depth	20	H	Unit weight	$\gamma$	Kg/dm <sup>3</sup>										
			Accel. gravity	G	Kg.m/s <sup>2</sup>	Model N°1	Model N°2	Model N°3	Model N°4	Model N°5	Model N°6	Model N°7	Model N°8	Model N°9	
W/m Width	10	W	Young modulus	E	N/m <sup>2</sup>										
			Poisson coef.	$\nu$	-										
b/m Height	11	b	Friction angle	$\phi$	degree										
			Cohesion	C	N/m <sup>2</sup>										
		1/40		$\sigma$		1/40	1/30	1/25	1/20	1/15	1/4	1/3	1/2	1/1.5	
				F		1:6400	1:480	1:40000	1:32000	1:24000	1:6400	1:4800	1:3200	1:2400	
		0.5		$\gamma$		1:1	1,33:1	2:1	2:1	2,66:1	10:1	13,3:1	20:1	26,6:1	
				G		1:1	1:1	1:1	1:1	1:1	1:1	1:1	1:1	1:1	
		0.25		E		1:40	1:30	1:25	1:20	1:15	1:4	1:33	1:2	1:1,5	
				$\nu$		1:1	1:1	1:1	1:1	1:1	1:1	1:1	1:1	1:1	
		0.25		$\phi$		1:1	1:1	1:1	1:1	1:1	1:1	1:1	1:1	1:1	
				C		1:40	1:30	1:25	1:20	1:15	1:4	1:3	1:2	1:1,5	
		1/30				1:36000	1:27000	1:25500	1:18000	1:1350	1:3600	1:2700	1:1800	1:1350	
						1:1,33	1:1	1,2:1	1,5:1	2:1	7,5:1	10:1	15:1	20:1	
		0.66				1:1	1:1	1:1	1:1	1:1	1:1	1:1	1:1	1:1	
						1:40	1:30	1:25	1:20	1:15	1:4	1:3	1:2	1:1,5	
		0.33				1:1	1:1	1:1	1:1	1:1	1:1	1:1	1:1	1:1	
						1:1	1:1	1:1	1:1	1:1	1:1	1:1	1:1	1:1	
		0.35				1:40	1:20	1:25	1:20	1:15	1:4	1:3	1:2	1:1,5	
		1/25				1:2500	1:18750	1:15625	1:12500	1:9735	1:2500	1:1875	1:1250	1:937,5	
						0,625:1	0,833:1	1:1	1,253:1	1,66:1	6,25:1	8,3:1	12,5:1	16,6:1	
		0.8				1:1	1:1	1:1	1:1	1:1	1:1	1:1	1:1	1:1	
						1:1	1:1	1:1	1:1	1:1	1:1	1:1	1:1	1:1	
		0.4				1:40	1:30	1:25	1:20	1:15	1:4	1:3	1:2	1:1,5	
						1:1	1:1	1:1	1:1	1:1	1:1	1:1	1:1	1:1	
		0.44				1:1	1:1	1:1	1:1	1:1	1:1	1:1	1:1	1:1	
						1:40	1:30	1:25	1:20	1:15	1:4	1:3	1:2	1:1,5	
		1/20				1:16000	1:12000	1:1000	1:8000	1:6000	1:1600	1:1200	1:800	1:600	
						1:2	1:1,5	0,8:1	1:1	1,33:1	15:1	6,66:1	10:1	13,3:1	
		1				1:1	1:1	1:1	1:1	1:1	1:1	1:1	1:1	1:1	
						1:40	1:30	1:25	1:20	1:15	1:4	1:3	1:2	1:1,5	
		0.5				1:1	1:1	1:1	1:1	1:1	1:1	1:1	1:1	1:1	
						1:1	1:1	1:1	1:1	1:1	1:1	1:1	1:1	1:1	
		0.55				1:40	1:30	1:25	1:20	1:15	1:4	1:3	1:2	1:1,5	
		1/15				1:9000	1:6750	1:5625	1:4500	1:3375	1:900	1:675	1:450	1:337,5	
						1:2,66	1:2	0,6:1	1:1,33	1:1	3,75:1	5:1	7,5:1	10:1	
		1.33				1:1	1:1	1:1	1:1	1:1	1:1	1:1	1:1	1:1	
						1:40	1:30	1:25	1:20	1:15	1:4	1:3	1:2	1:1,5	
		0.66				1:1	1:1	1:1	1:1	1:1	1:1	1:1	1:1	1:1	
						1:1	1:1	1:1	1:1	1:1	1:1	1:1	1:1	1:1	
		0.73				1:40	1:30	1:25	1:20	1:15	1:4	1:3	1:2	1:1,5	

**Table 2.** Mechanical properties of the mixture.

Geomechanical parameters	Symbols	Units	In situ values of marly clay	Laboratory tests results	Values required by scale (1/20)
Compressive strength	$\sigma$	kPa	270.0-600.0	30.0-50.0	13.5 30.0
Young's modulus	E	kPpa	9000-40000	368.0-520.0	450-2000
Internal friction angle	$\Phi$	degree	18-30	29.6	30
Cohesion	C	kPa	100-110	56.8	50-55
Weight unit mass	$\gamma$	kg/m <sup>3</sup>	1.6	1.6	1.6
Poisson's coefficient	$\nu$	-	0.45	0.40-0.45	0.45

**Table 3.** Mechanical properties of a support model (scale 1/20).

Kind of support	Mechanical and geometrical parameters	In situ values	Laboratory test results	Values required by scale
Bolting (soldering wire)	Tensile strength	275 MPa	21.49 MPa	13.75 MPa
	Length	3- 4 m		0.15 – 0.20 m
	Acting air	1.4 m <sup>2</sup>		0.0035 m <sup>2</sup>
Shotcrete (mixture of gypsum, quick lime, water and inert material [according to A.M.Kozuna 1957])	Compressive strength	21.0 MPa	1.05 MPa	1.05 MPa
Steel arches (very fine aluminium strips transformed in segments with a transversal U section)	Moment	108750 N.m	1.36N.m	1.36 N.m
	Transversal section width	180 mm		9.0 mm
	Distance between two successive steel arches	1.2 m		0.06 m

The materials for the simulation of different types of supports described above are not convenient for the artificial rocks used in our conditions owing to construction technology of the tunnel model (construction under a constant load, in extremely wet conditions, hence in very soft artificial rocks.)

The equivalent materials for simulating tunnel supports used in our case and their mechanical properties are shown in Table 3.

### 3.3 EXPERIMENTAL METHODOLOGY

The compacted equivalent material is placed in the model with the following dimensions:

- height: 110 cm
- extent: 180 cm, and
- thickness: 20 cm.

Black reference marks are established horizontally in the artificial material, white reference marks are stuck on Plexiglas just above the black reference marks. The

black reference marks are mobile and react to artificial rock displacement, while the white reference marks are fixed. These reference marks are photographed after each phase of construction (after it has undergone displacements). After consolidation, the model of tunnel is excavated to the thickness of 7cm representing the distance between the steel arches. The execution time of pickling and installation of the supporting systems is approximately three hours. The nomenclature of different tunnel cutting phases is as follows:

- Phase I: Cutting a working place in the excavation roof to a depth equal to rib spacings.
- Phase II: Installing rock bolts and a superior rib arch
- Phase III: Concrete projection
- Phase IV: Cutting a work place in the lower part of the excavation to a depth equal to rib spacings.
- Phase V: Installing the inferior rib arch
- Phase VI: Concrete projection on the lower part of the excavation.

In the model, the various phases of the superior section are represented successively in Figs. 2-7.





**Figure 2.** Cutting the first slice of the superior section.



**Figure 3.** Appearance of deformation.

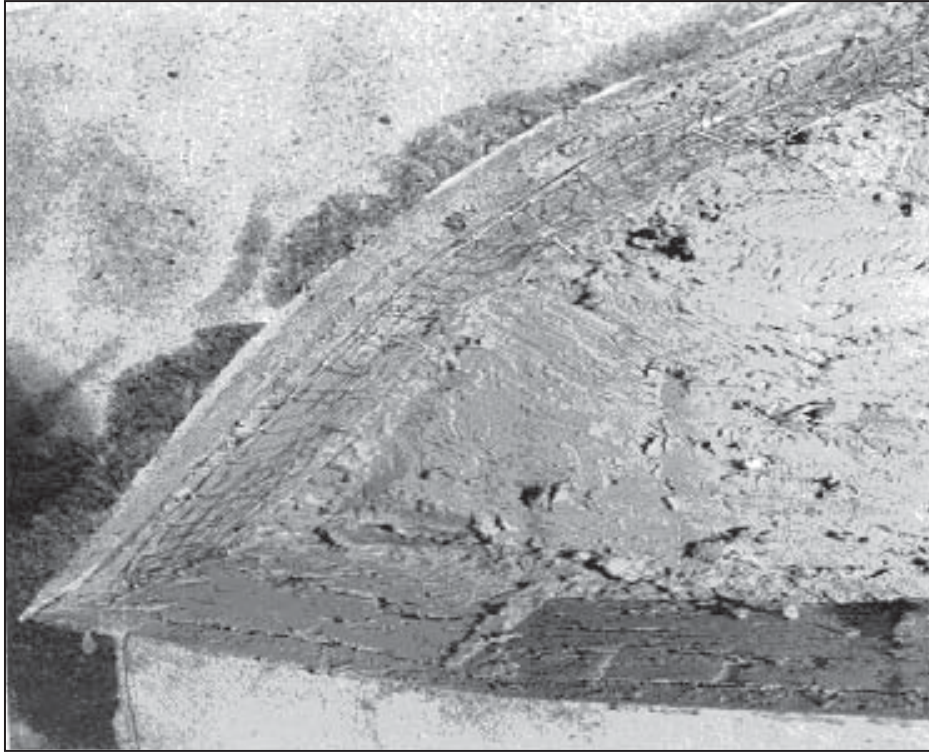


Figure 4. Installation of bolts and steel fabrics.



Figure 5. Installation of steel arches.



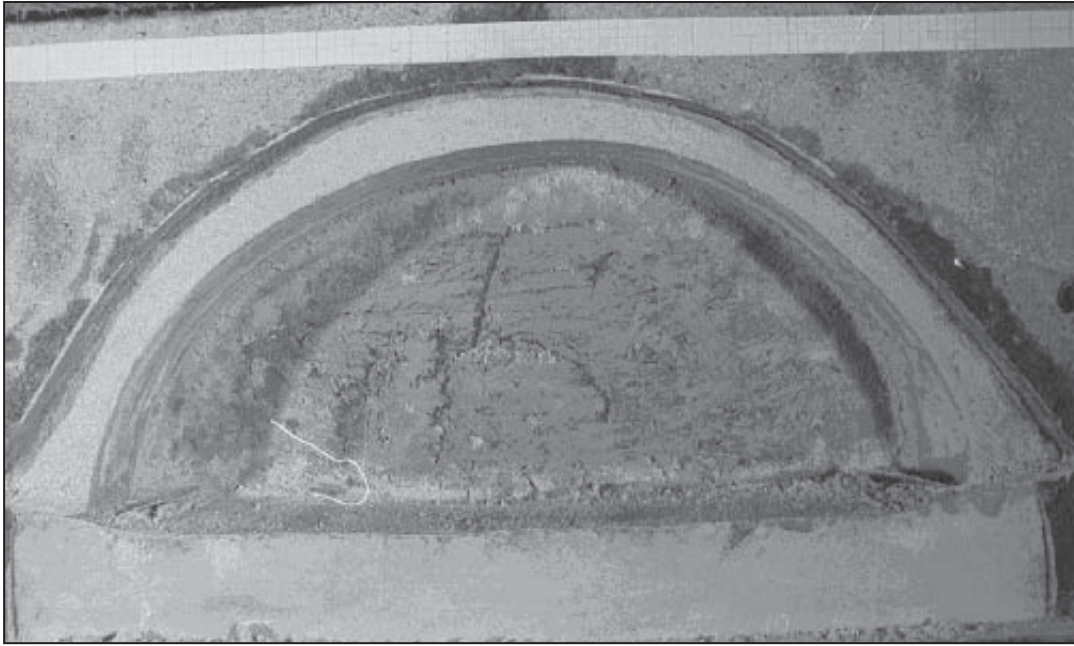


Figure 6. Projection of shotcrete.

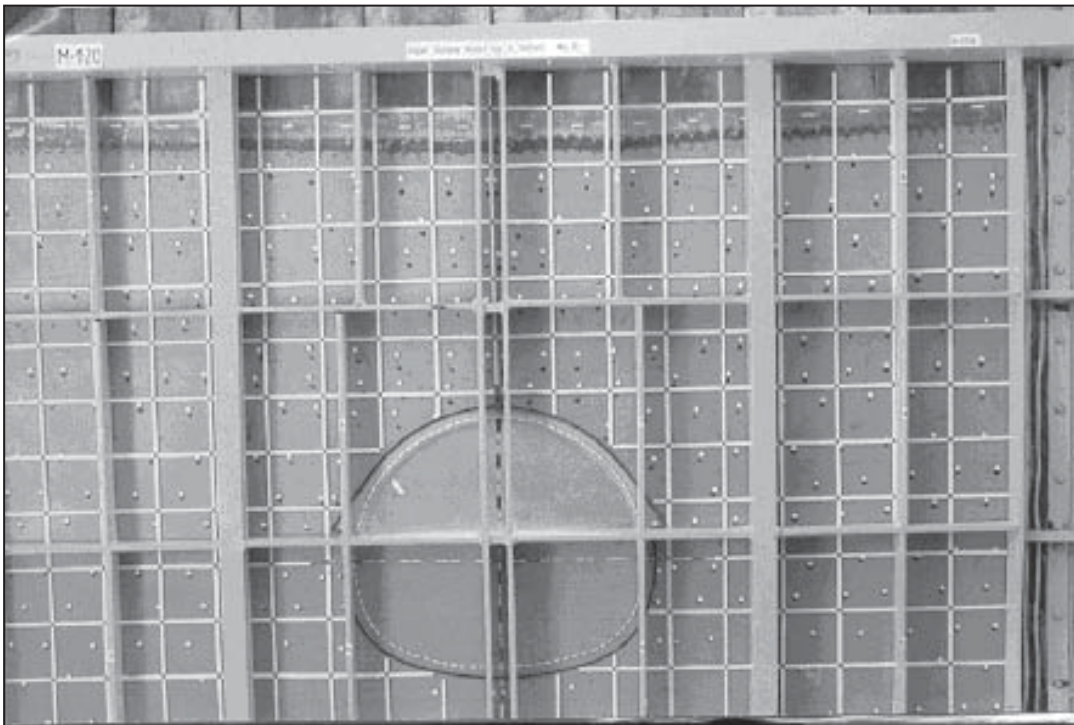


Figure 7. Completion of the higher section.

Deformations after each construction phase of the first section are illustrated in Fig. 8.

All these construction operations are repeated during the digging of other sections. However, it should be noted that a crack appeared in the shotcrete of the first section after the completion of the second section

digging. This crack was prolonged after concreting the third section which presupposed the formation of a disturbed zone on the roof of the tunnel model (Fig. 9).

Various construction stages in successive diggings of the lower section are presented in Figs. 10–13.

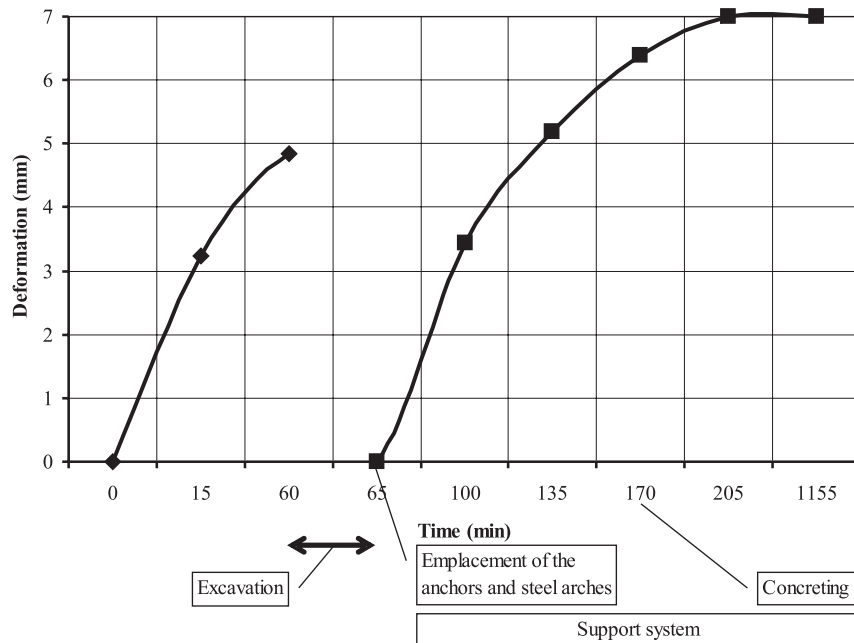


Figure 8. Evolution of the deformation at the end of the first section.

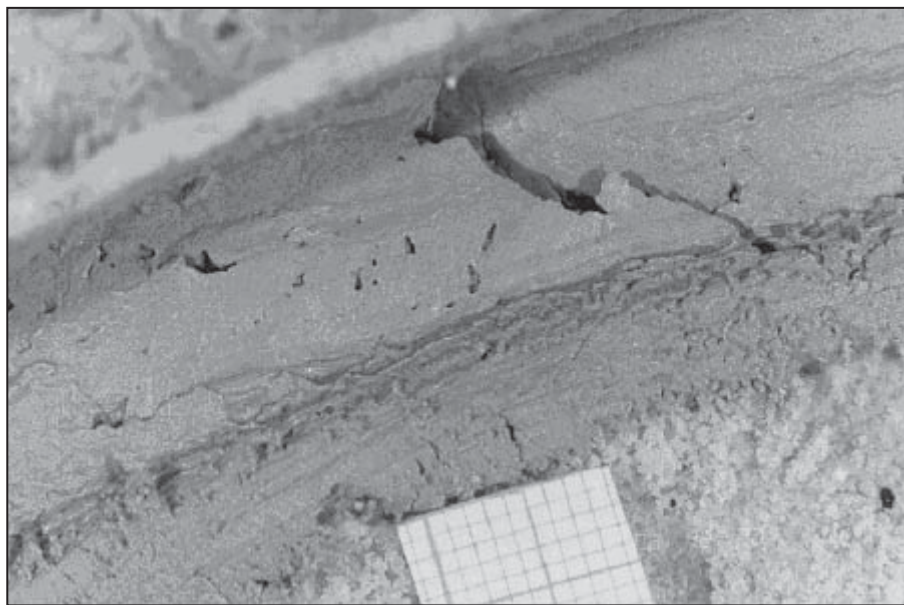
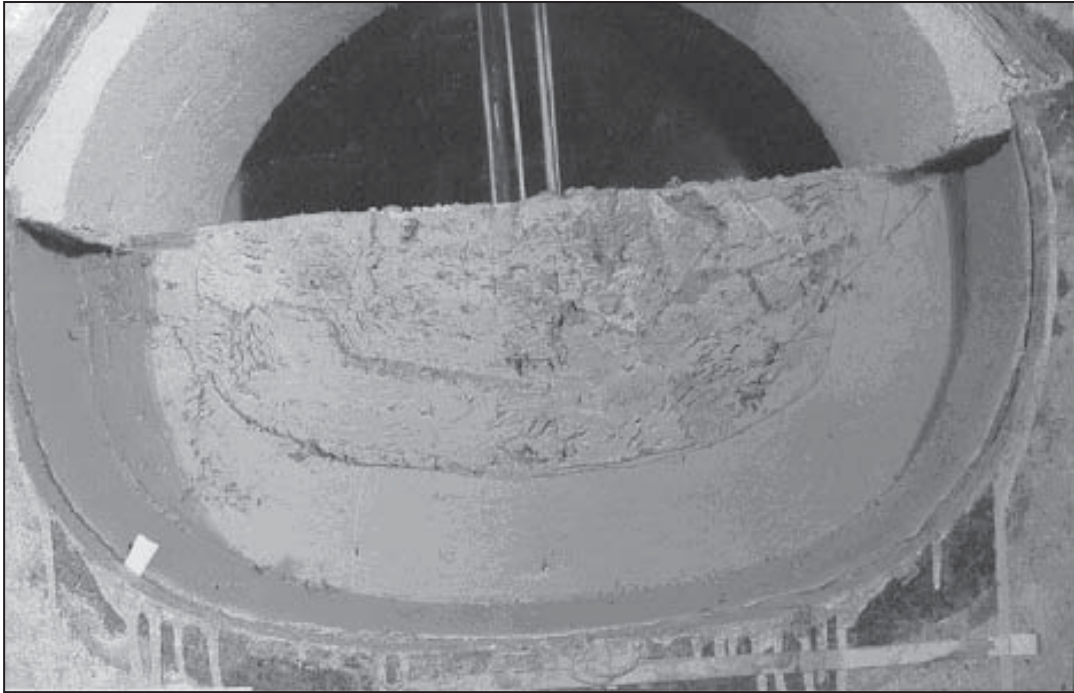


Figure 9. Appearance of a disturbed zone on the roof of the model.



**Figure 10.** Cutting of the first slice of the inferior section.



**Figure 11.** Installation of steel fabrics and steel arches.



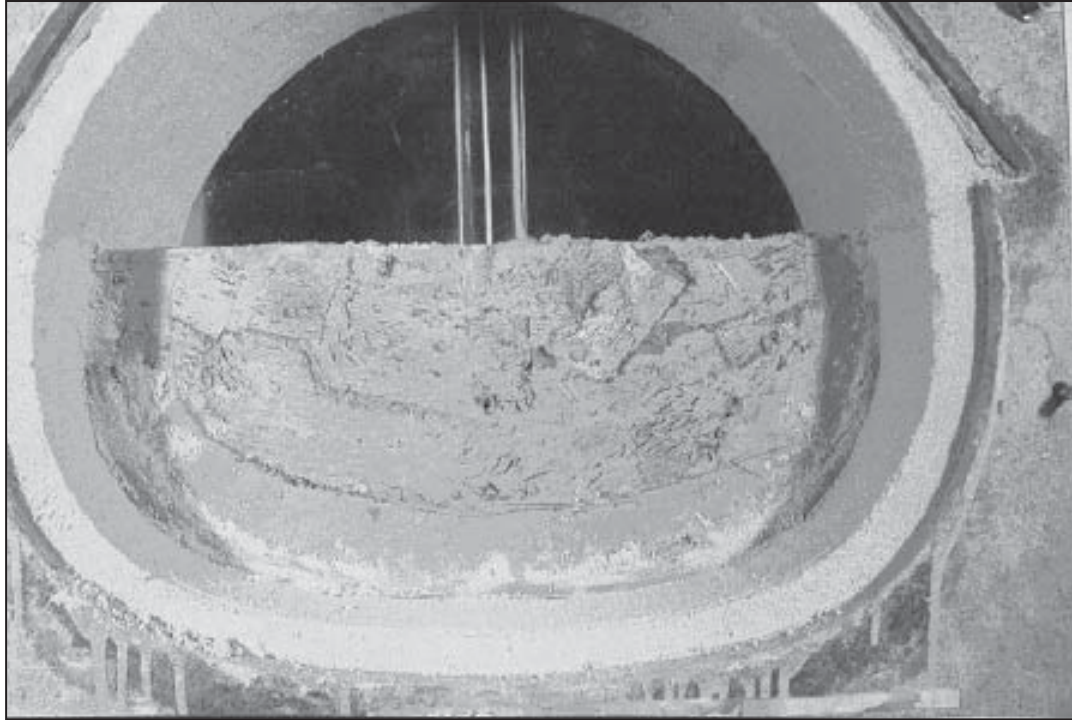


**Figure 12.** Concreting the first slice of the inferior section.

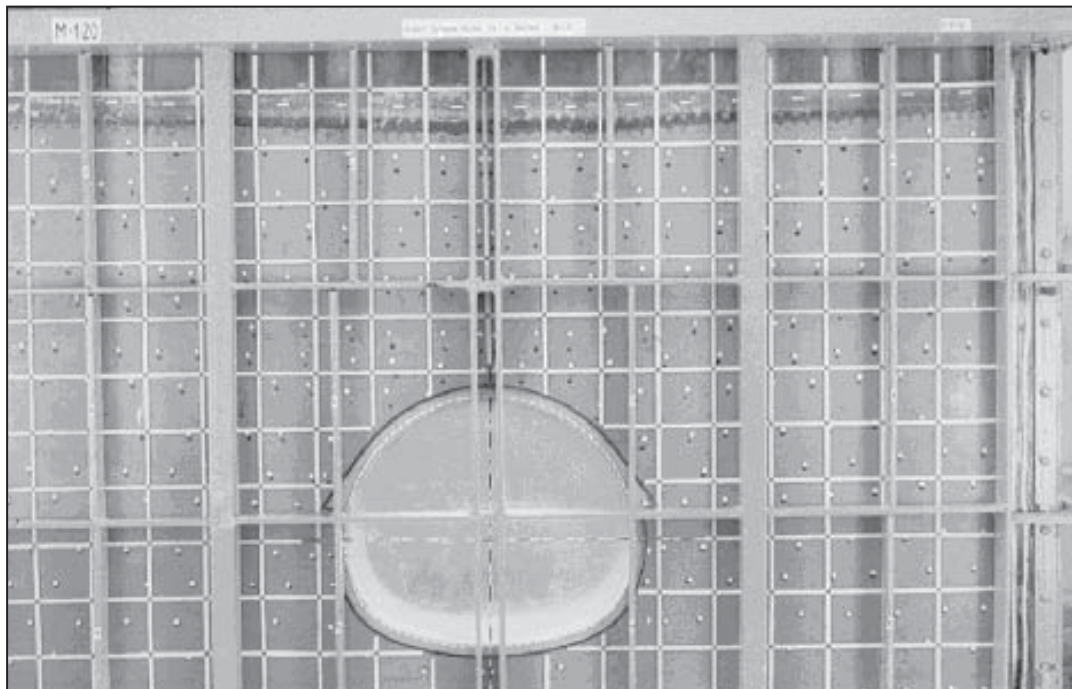


**Figure 13.** Final construction of the model.

Time evolution of the deformations is shown in Fig. 14.

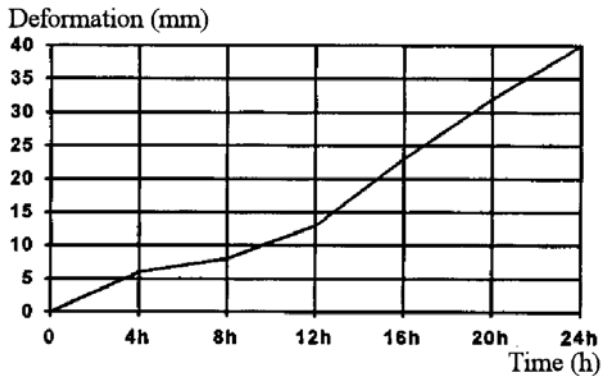


Figure 14. Convergence of the model according to time.

The measurement method of displacements is an optical method leading to misreadings of those reference marks especially which are far away from the centre of the model as shown in Fig. 15.

The coefficient of correction is calculated as follows:

A mesh of white squares on the model has a width of 10cm, which is 2cm on the photograph. This dimension corresponds to an opening of 19 units on the optical glass objective. These 19 units measure 1.9mm on the photograph, so the scale between the model and the photo is of 1:5 and the scale between the photo and

the optical glass is of 10:1. The measurement scale thus becomes of 10:5, therefore 2:1, from which 14 units correspond to 10.5mm. The correction coefficients are presented in Table 4.

Table 4. Correction coefficients of measured displacements.

Coordinate X	Correction	Coordinate Y	Correction
0	-3.6	0	2.4
10	-3.2	10	2.0
20	-2.8	20	1.6
30	-2.4	30	1.2
40	-2.0	40	0.8
50	-1.6	50	0.4
60	-1.2	60	0.0
70	-0.8	70	-0.4
80	-0.4	80	-0.8
90	0.0	90	-1.2
100	0.4	100	-1.6
110	1.2	110	-2.0
120	1.6	120	-2.4
130	2.0		
140	2.4		
150	2.8		
160	3.2		
170	3.6		

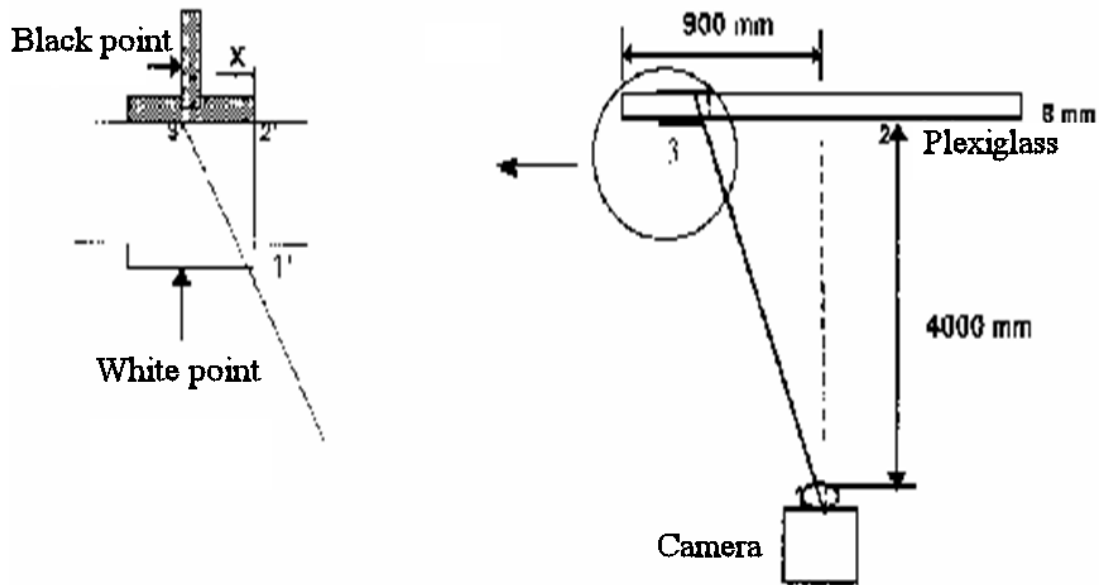


Figure 15. Concreting the first slice of the inferior section.

#### 4 CALCULATION OF THE VOLUMETRIC AND ANGULAR DEFORMATIONS

Many significant problems require constraints and elongations in the x-y plan although the constraints  $\sigma_{zz}$  can exist;  $\sigma_{xz}$  and  $\sigma_{yz}$  have been neglected in our case. If it is supposed that our model is one elastic unit yet sufficiently subjected to constraints which prevent sound movement, no particle displacements are possible inside the model without the model deformation.

Small displacements of the model particles are usually presented by the components  $u$  and  $v$  for a problem of plane deformation. These represent the displacements of the reference marks established in the model. Their measurement method is described later on. Elongations for such a problem are:

$$\varepsilon_{xx} = \frac{\partial u}{\partial x} \quad (1)$$

$$\varepsilon_{yy} = \frac{\partial v}{\partial y} \quad (2)$$

$$\theta_v = \varepsilon_{xx} + \varepsilon_{yy} \quad (3)$$

$$\gamma_{xy} = \frac{\partial u}{\partial y} + \frac{\partial v}{\partial x} \quad (4)$$

$$\gamma_{xy}^{\max} = \sqrt{(\varepsilon_x - \varepsilon_y)^2 + \gamma_{xy}^2} \quad (5)$$

The pictures show the isolines of expansion after digging and supporting each section.

The negative sign indicates the areas of extension while the positive sign indicates the areas of compression. That is how two compression zones of low intensity are formed at the end of the first slice in laterally anchored areas. Their value is of 1%. An extension zone starts to appear on the crown of the tunnel (Fig. 16).

Fig. 16 reflects the state of material when the higher section of the tunnel is completed. It is evident from Fig. 16 that the zones of high compression located in the previously quoted areas have moved to lower un-anchored areas. In turn, the inside of the stress is compressed. The extension area is amplified to reach a value of 3%. Laterally anchored areas have undergone a compression of 6% just above the crown. The area compressed earlier has slackened and has given rise to a disturbed zone. On the level of stress, compression reached 4% (Fig. 17 on next page).

Fig. 18 (on next page) shows a value of a maximum distortion which almost equals the one in the model of an intensity of 6°.

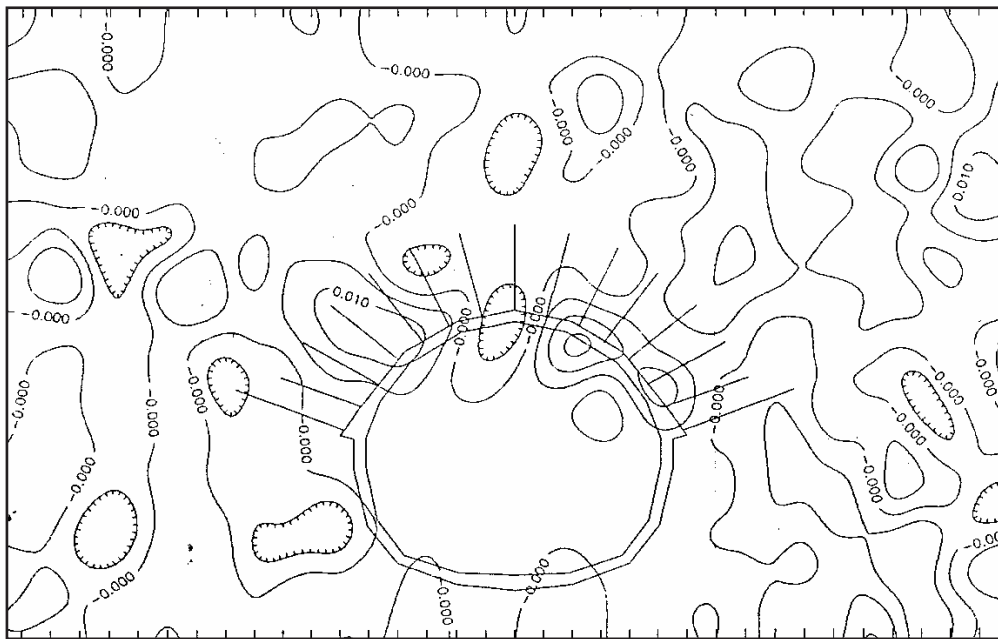


Figure 16. State of elongations at the end of the first slice.

Fig. 19 (on page 38) shows a maximum distortion of  $4^\circ$  at the end of the third slice. The distortion concerning this training course is much larger, it is  $4^\circ$ . On the crown of the tunnel model it is  $3^\circ$ . The rocks with the same distortion are similar to concentric boxing rings around the centre of the higher section floor of the tunnel model.

The excavation and the supporting of the tunnel model are finished with the completion of the sixth slice. Fig. 19 shows the state of the material around the tunnel model; below the stross, on its walls and at the anchoring level, the material is in a compression state. Above the crown, the extension is always of the same intensity, hence a permanent existence of a disturbed zone (Fig. 20, page 38).

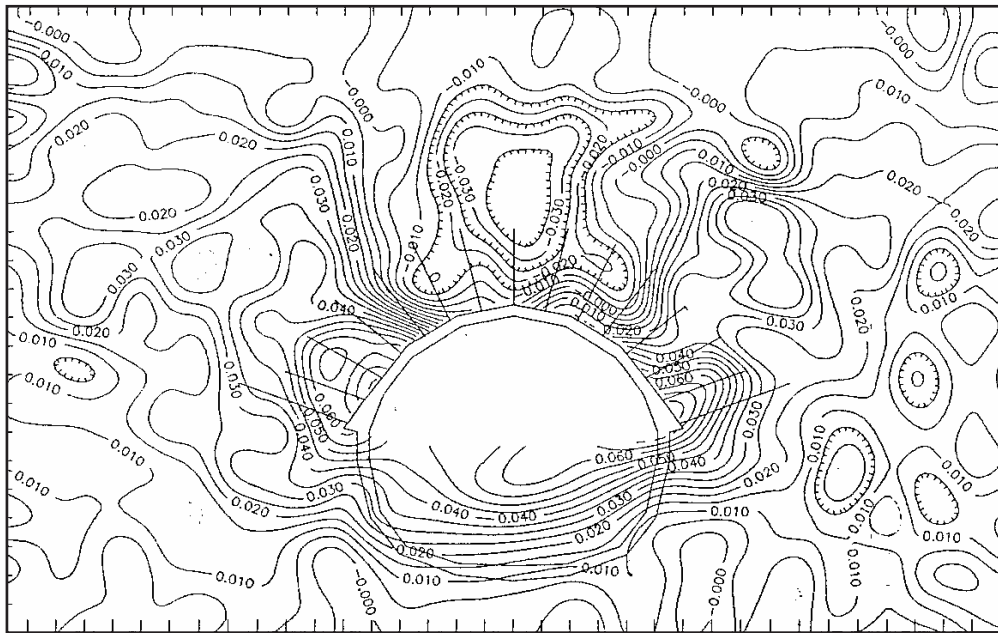


Figure 17. State of elongations at the end of the third slice.

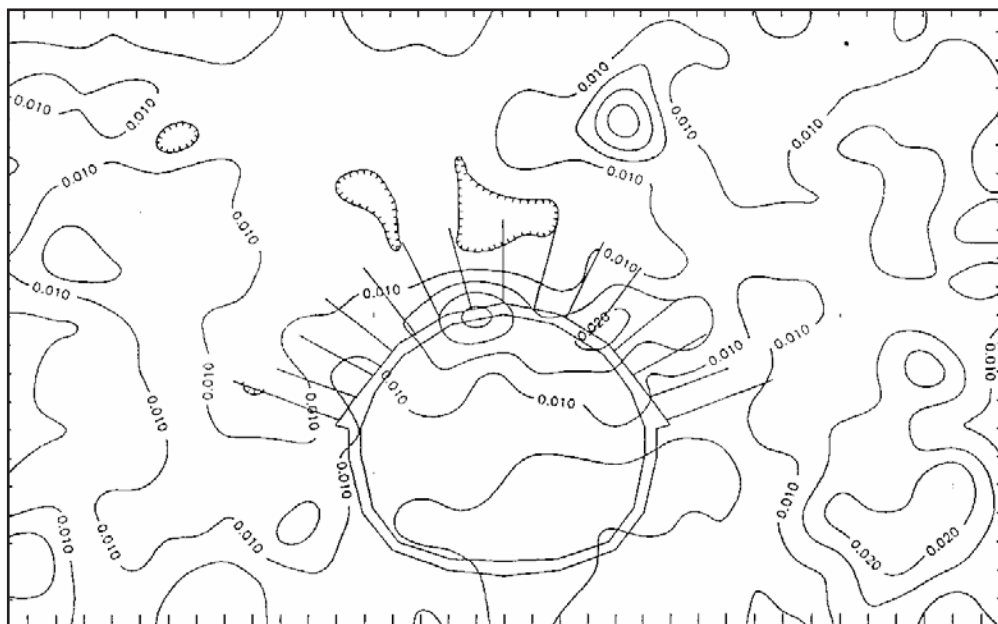


Figure 18. State of distortions at the end of the first slice.



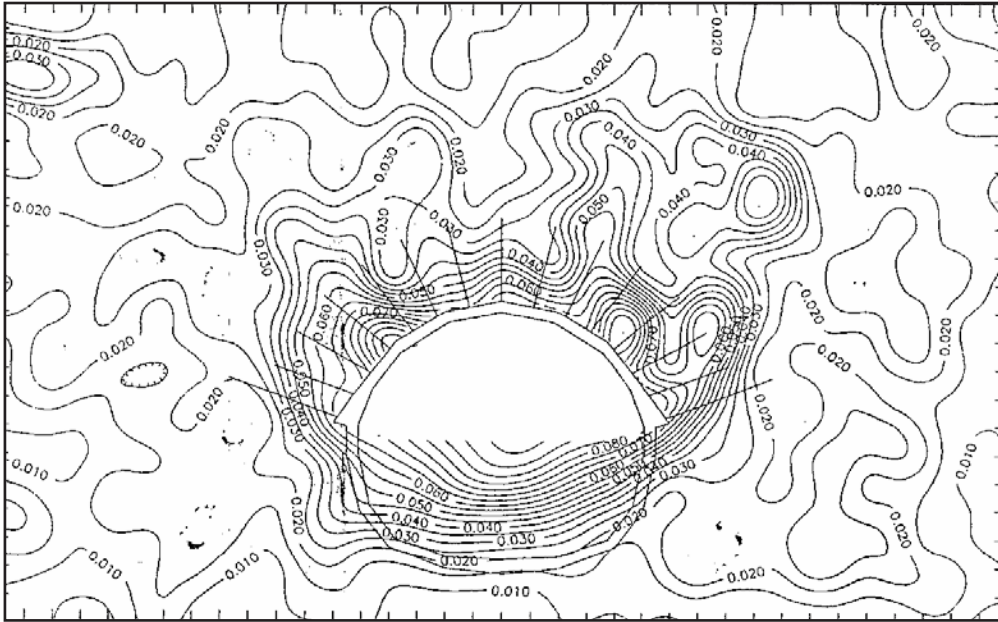


Figure 19. State of distortions at the end of the third slice.

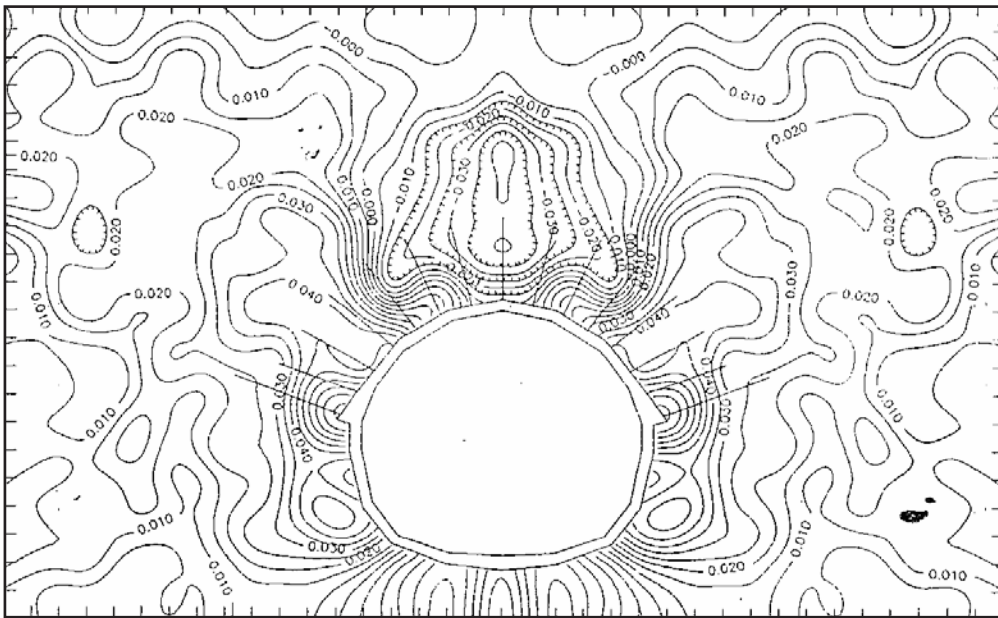


Figure 20. State of elongations at the end of the sixth slice.

Fig. 20 represents the state of distortions when the tunnel model is fully completed. Laterally anchored areas of the higher section remain subjected to a distur-

tion equal to  $3.43^\circ$ , while the value of  $\gamma$  max does not exceed  $3^\circ$  on the crown level and it is even lower around the stress (Fig. 21, next page).



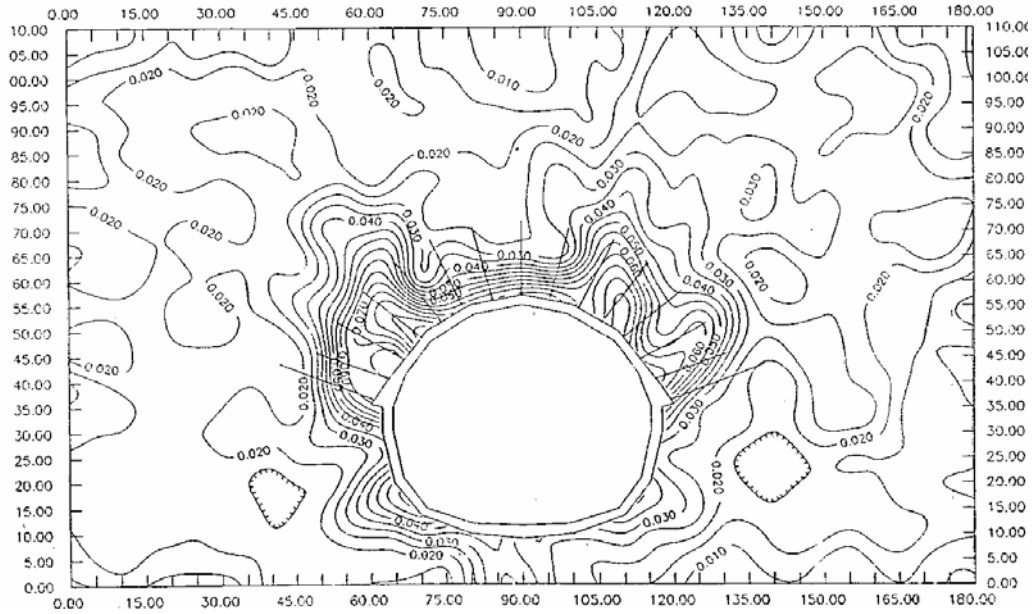


Figure 21. State of distortions at the end of the sixth slice.

## 5 EVALUATION OF THE PLASTIC ZONE

The fundamental equations are taken from Sakurai S. (1985).

From Hook's law

$$\varepsilon_1 \cdot E = \sigma_1 - \nu \cdot \sigma_3 \quad \varepsilon_3 \cdot E = \sigma_3 - \nu \cdot \sigma_1 \quad (6)$$

we obtain the deviatoric of the deformation

$$\varepsilon_1 - \varepsilon_3 = \frac{1 + \nu}{E} (\sigma_1 - \sigma_3) \quad (7)$$

and the volumetric elongation

$$\varepsilon_1 + \varepsilon_3 = \frac{1 + \nu}{E} (\sigma_1 + \sigma_3) \quad (8)$$

According to the Mohr-Coulomb criterion:

$$\varepsilon_1 - \varepsilon_3 = (\sigma_1 + \sigma_3) \cdot \sin \phi + 2 \cdot c \cdot \cos \phi \quad (9)$$

a maximum distortion of the elastoplastic border is expressed as:

$$D_{cr} = \frac{1 + \nu}{1 - \nu} \cdot \sin \phi + 2 \cdot c \cdot \frac{1 + \nu}{E} \cdot \cos \phi \quad (10)$$

with the below material equivalent constants (Table 5).

Table 5. Geomechanical parameters.

Parameters	Units	Values
$EP_{LP}$	Centimetre	2.5
$\nu_{LP}$	-	0.22
$E_{LP}$	MPa	15000
$\sigma_{cbp}$	MPa	1.04
$\sigma_{tbp}$	MPa	0.66

From Eq. (7) and Fig. 22 we obtain:

$$D_{cr} = \theta_v \cdot 1.3021 + 0.0447 \quad (11)$$

The values of the volumetric elongations are taken directly from fixed reference marks on the anchorages in Fig. 20 and are expressed by Eq. (11). If the results obtained are superior to  $\gamma_{max}$  and read on the same signs in Fig. 21, the latter belongs to a plastic zone located on the elasto-plastic deformation border shown in Fig. 23 (see next page). In the opposite case, it is to be found under the same zone and it belongs to an elastic zone. Maximum distortion signs belonging to a plastic zone are connected to mark the border of the plastic zone.

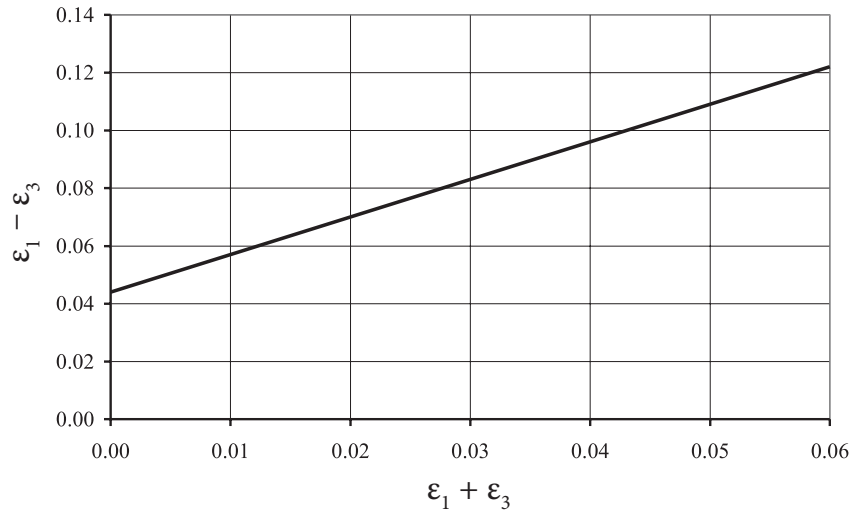


Figure 22. Criterion of the equivalent material rupture.

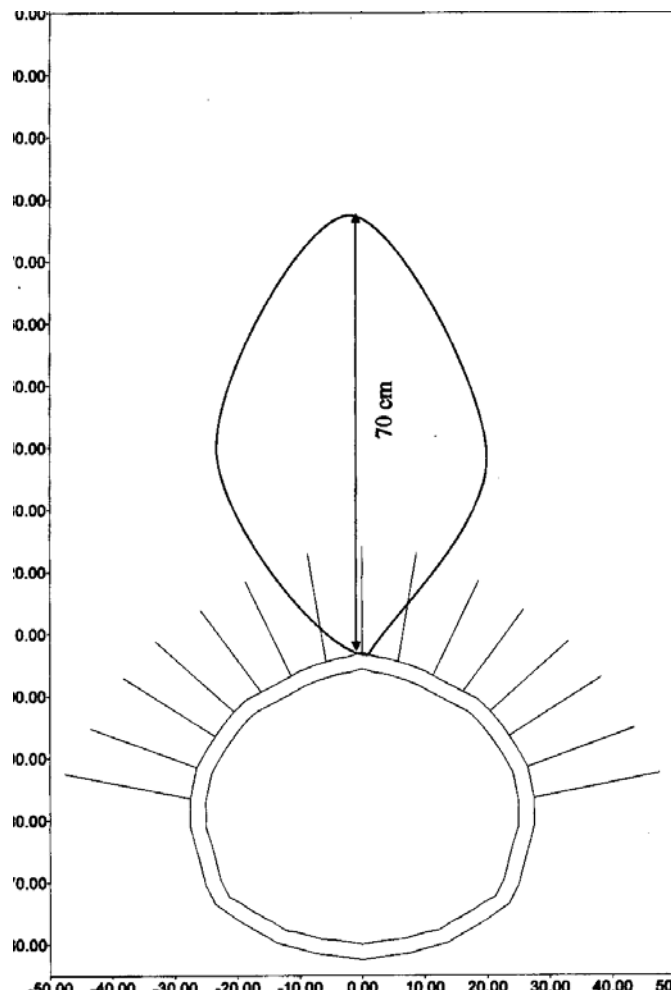


Figure 23. Extension of the plastic zone.

---

## CONCLUSION

The physical model can be directly gauged according to the results of measurements and in situ inspections. The capacity of simulation is based on the capacity of the model equipment to create three- and a two-dimensional field elongations. The investigation confirmed that physical simulations of the rock excavation and supporting systems are effective tools to conceive a proper excavation plan and supporting method of line tunnels.

This research method is able to provide general visual information on the state of the transition process from the excavation of rocks to the supporting systems. It gives a quantitative image of the deformation field and ruptures in each stage of tunnel construction. In this way, a broad deformation was observed at the time of this study which would surely damage the tunnel surface. This broad deformation appeared during the digging stress because of a simultaneous rupture of the injected concrete.

---

## REFERENCES

- Adachi, T. and Shinkawa, MR.(1982). Experimental and Analytical study on tunnel support system. *Proc. of the 'HT conf. on num. methods in geomech*, Edmonton, Canada.
- Adachi, T. (1985). Some supporting methods for tunneling in Japan and to their studies. *Rock mechanics suppl.*, Verlag.
- Baron, K. and Larocque, G. E. (1960). Development of a mine structure. *Wabama report N° 7*, Ottawa, Canada.
- Gajari, GY. (1990). Roadway stability investigations by physical and mathematical modelling. *Veszprém Coal Mines*, H-8201 Veszprém, Budapesti u.2, Hungary.
- Gerhard S'Mauro F. (1979). Technics and materials for modelling a tunnel drawing operation at moderate depth. *International colloquium on physical geomechanical models*, Bergamo, Italy.
- Kozuna, A.M. (1957). Technika modelitovanja ekvalent-nuni materialiani. Ugletehizdat Moskva, Russia.
- Sakurai,S. (1985). Evaluation of plastic zone around underground opening by means of displacement measurements. *Num. Meth. in geomech*. Nagoya, AA. Balkama Rotterdam, Boston.
- Seriani, A. (1993). Seek on equivalent materials for the simulation of tunnel of the subway of Algiers. *Acta Geod. Mount. Hung. Vol. 8*, Academy sciences Hungarian.
- Tazawa Y. (1979). Model tests on the effect of rock bolt and thin linings on tunnel supports in soft rock. *Annual report of Kajma institute of construction technology*, Japan.

---

# UPORABA BREZMREŽNIH METOD (RADIALNIH BAZNIH FUNKCIJ) ZA MODELIRANJE MIGRACIJE RADIO-NUKLIDOV IN PROBLEMOV S PREMIKAJOČO SE MEJO

---

LEOPOLD VRANKAR, FRANC RUNOVČ IN GORAN TURK

---

## o avtorjih

Leopold Vrankar  
Uprava Republike Slovenije za jedrsko varnost  
Železna cesta 16, 1001 Ljubljana, Slovenija  
E-pošta: leopold.vrankar@uni-mb.si

Franc Runovc  
Univerza v Ljubljani,  
Naravoslovnotehniška fakulteta  
Aškerčeva cesta 12, 1000 Ljubljana, Slovenija  
E-pošta: franc.runovc@ntf.uni-lj.si

Goran Turk  
Univerza v Ljubljani,  
Fakulteta za gradbeništvo in geodezijo  
Jamova cesta 2, 1000 Ljubljana, Slovenija  
E-pošta: gturk@fgg.uni-lj.si

---

## izvleček

Zadnje čase se, kot novejša računske metode, v znanstveni in inženirski skupnosti pojavljajo brez mrežne metode (radialne bazne funkcije). Numerično reševanje parcialnih diferencialnih enačb običajno poteka s pomočjo metode končnih diferenc, metode končnih elementov in metode robnih elementov. Te metode imajo še vedno nekaj pomanjkljivosti, in sicer npr. konstrukcija mreže v dveh ali treh prostorskih dimenzijah ni enostaven problem. Reševanje parcialnih diferencialnih enačb z uporabo radialne bazne kolokacije je primerna alternativa tradicionalnim numeričnim metodam, ker ne zahteva obsežnega generiranja mreže. Rezultati se bodo primerjali z rezultati dobljenimi s pomočjo metode končnih diferenc in analitičnih rešitev.

Predstavili bomo nekaj primerov: najprej uporabo radialnih baznih funkcij v geostatistični analizi modeliranja migracije radionuklidov. Migracija radionuklidov se bo simulirala s pomočjo adveksijske-disperzijske enačbe, in sicer v Eulerjevi in Lagrangeovi obliki. V nadaljevanju bodo predstavljeni tudi Stefanovi problemi oz. problem primikajočih se meja (površin). Položaje primikajoče meje bomo simulirali s pomočjo metode primikajočih se centrov in nivojne metode.

---

## ključne besede

brez mrežne metode, radialne bazne funkcije, metoda končnih diferenc, metoda končnih elementov, metoda robnih elementov, geostatistika, Euler, Lagrange, nivojna metoda

---

# THE USE OF THE MESH FREE METHODS (RADIAL BASIS FUNCTIONS) IN THE MODELING OF RADIONUCLIDE MIGRATION AND MOVING BOUNDARY VALUE PROBLEMS

---

LEOPOLD VRANKAR, FRANCO RUNOVČ and GORAN TURK

---

## about the authors

Leopold Vrankar  
Slovenian Nuclear Safety Administration  
Železna cesta 16, 1001 Ljubljana, Slovenia  
E-mail: leopold.vrankar@uni-mb.si

Franc Runovc  
University of Ljubljana,  
Faculty of Natural Sciences and Engineering  
Aškerčeva cesta 12, 1000 Ljubljana, Slovenia  
E-mail: franc.runovc@ntf.uni-lj.si

Goran Turk  
University of Ljubljana,  
Faculty of Civil and Geodetic Engineering  
Jamova cesta 2, 1000 Ljubljana, Slovenia  
E-mail: gturk@fgg.uni-lj.si

---

## abstract

*Recently, the mesh free methods (radial basis functions-RBFs) have emerged as a novel computing method in the scientific and engineering computing community. The numerical solution of partial differential equations (PDEs) has been usually obtained by finite difference methods (FDM), finite element methods (FEM) and boundary elements methods (BEM). These conventional numerical methods still have some drawbacks. For example, the construction of the mesh in two or more dimensions is a nontrivial problem. Solving PDEs using radial basis function (RBF) collocations is an attractive alternative to these traditional methods because no tedious mesh generation is required. We compare the mesh free method, which uses radial basis functions, with the traditional finite difference scheme and analytical solutions.*

*We will present some examples of using RBFs in geostatistical analysis of radionuclide migration modeling. The advection-dispersion equation will be used in the Eulerian and Lagrangian forms. Stefan's or moving boundary value problems will also be presented. The position of the moving boundary will be simulated by the moving data centers method and level set method.*

---

## keywords

mesh free methods, radial basis functions, finite difference methods, finite element methods, boundary elements methods, geostatistics, Eulerian method, Lagrangian method, level set method

---

## 1 INTRODUCTION

In recent years, the mesh free methods have emerged as a novel computing method in the scientific and engineering computing community. Traditionally, the most popular methods have been the finite element methods (FEM), the finite difference methods (FDM), and the boundary element method (BEM). In spite of their great success in solving scientific and engineering problems over the past four decades, these conventional numerical methods still have some drawbacks that impair their computational efficiency and even limit their applicability to more practical problems, particularly in a three-dimensional space.

The term mesh free method refers to the ability of the method to solve the given differential equations from a set of unstructured nodes, i.e. without any pre-defined connection or relationship among the nodes. Instead of generating a mesh, mesh free methods use scattered nodes, which can be randomly distributed or patterned through the computational domain.

During the past decade, increasing attention has been given to the development of mesh free methods using RBFs for the numerical solution of PDEs. There are two major developments in this direction. The first is the method of fundamental solutions (MFS) coupled with the dual reciprocity method (DRM), which evolved from the dual reciprocity boundary element method (DRBEM). More details about MFS can be found in review papers [1] and [2]. RBFs played a key role in the theoretical establishment and applications in the development of the DRM. With the combined features of the MFS and DRM, a mesh free numerical scheme for solving PDEs has been achieved.

The second mesh free method using RBFs is the Kansa method [3-4], where the RBFs are directly implemented for the approximation of the solution of PDEs introducing the concept of solving PDEs, using radial basic functions for hyperbolic, parabolic and elliptic PDEs. A key feature of the RBF method is that it does not need a grid. In contrast to the MFS-DRM boundary method, the Kansa method is considered to be a domain type method, which has many features similar to the finite element method.

In our case, we use the Kansa method which uses radial basis functions. We compare the results with a traditional finite difference scheme and analytical solutions.

We will present two examples: some previous work results of using RBFs in geostatistical analysis of transport modeling of the radionuclide migration and moving boundary value problems.

## 2 RADIAL BASIS FUNCTIONS METHOD

The base of this approach is its employment of high-order interpolating functions to approximate solutions of differential equations. All RBFs possess the property that their values are only determined by distance and have nothing to do with directions. Kansa [4] introduced multiquadric functions to solve hyperbolic, parabolic and elliptic differential equations with collocation methods. This method is an asymmetric collocation set-up in which boundary conditions are treated separately from the interior problem. One of the most powerful RBF methods is based on multiquadric basis functions (MQ), first used by R. L. Hardy [5]. It is important to mention that the MQ was until now efficiently used in transport modeling [6].

A radial basis function is a function  $\varphi(\mathbf{x}) = \varphi(\|\mathbf{x} - \mathbf{x}_j\|)$ , which depends only on the distance between  $\mathbf{x} \in \mathbf{R}^d$  and a fixed point  $\mathbf{x}_j \in \mathbf{R}^d$ . Here,  $\varphi$  is continuous and bounded on any bounded sub-domain  $\Omega \subseteq \mathbf{R}^d$ . Let  $r$  denote the Euclidean distance between any pair of points in the domain  $\Omega$ . The commonly used radial basis functions are: linear ( $\varphi(r) = r$ ), cubic ( $\varphi(r) = r^3$ ), thin-plate spline ( $\varphi(r) = r^2 \log r$ ), Gaussian ( $\varphi(r) = e^{-\alpha^2 r}$ ) and multiquadric (MQ) ( $\varphi(r) = (r^2 + c^2)^\beta$ ). Commonly used values for  $\beta$  are -1/2 and 1/2. The parameter  $c > 0$  is a shape parameter controlling the fitting of a smoothing surface to the data. We usually use MQ or inverse MQ RBFs.

To introduce RBF collocation methods, we consider a PDE in the form of

$$Lu(\mathbf{x}) = f(\mathbf{x}), \quad \text{in } \Omega \subset \mathbf{R}^d, \quad (1)$$

$$Bu(\mathbf{x}) = g(\mathbf{x}), \quad \text{on } \partial\Omega, \quad (2)$$

where  $u$  is the concentration,  $d$  denotes the dimension,  $\partial\Omega$  is the boundary of the domain  $\Omega$ ,  $L$  is the differential operator on the interior, and  $B$  is the operator that specifies the boundary conditions of the Dirichlet, Neumann or mixed type.

Using Kansa's asymmetric multiquadric collocation method, the unknown PDE solution  $u$  is approximated by RBFs in the form:

$$u \approx U(\mathbf{x}) = \sum_{j=1}^N \alpha_j \varphi_j(\mathbf{x}) + \sum_{l=1}^M \gamma_l p_l(\mathbf{x}), \quad (3)$$

where  $\varphi$  can be any of above mentioned radial basis function,  $p_1, \dots, p_M \in \Pi_m^d$ , is a polynomial of degree  $m$  or less. Let  $(\mathbf{x}_j)_{j=1}^N$  be the  $N$  collocation points in  $\Omega \cup \partial\Omega$ . We assume the collocation points are arranged in such a way that the first  $N_I$  points are in  $\Omega$ , whereas the last  $N_B$  points are on  $\partial\Omega$ . To evaluate  $N+M$  unknown coefficients,  $N+M$  linearly independent equations are needed. Ensuring that  $U(\mathbf{x})$  satisfies (1) and (2) at the collocation points results in a good approximation of the solution  $u$ . The first  $N$  equations are given by

$$\sum_{j=1}^N \alpha_j L\varphi_j(\mathbf{x}_i) + \sum_{l=1}^M \gamma_l Lp_l(\mathbf{x}) = f(\mathbf{x}_i), \quad \text{for } i = 1, \dots, N_I, \quad (4)$$

$$\sum_{j=1}^N \alpha_j B\varphi_j(\mathbf{x}_i) + \sum_{l=1}^M \gamma_l Bp_l(\mathbf{x}) = g(\mathbf{x}_i), \quad \text{for } i = N_I + 1, \dots, N_I + N_B. \quad (5)$$

The last  $M$  equations could be obtained by imposing some extra condition on  $v(\cdot)$ :

$$\sum_{j=1}^N \alpha_j p_k(\mathbf{x}_j) = 0, \quad k = 1, \dots, M. \quad (6)$$

The choice of a basis function is another flexible feature of RBF methods. RBFs can be globally supported, infinitely differentiable, and contain a free parameter,  $c$ . This leads to a full coefficient matrix or a dense interpolation matrix. The shape parameter  $c$  affects both the accuracy of the approximation and the conditioning of the interpolation matrix. The optimal shape parameter  $c$  is still an open question. In our case we used an iterative mode by monitoring the spatial distribution of the residual errors



in  $\Omega$  and  $\partial\Omega$  as a function of  $c$ . The iterations are terminated when errors are smaller than a specified bound. This map is then used to guide the search of the optimal shape parameter  $c$  that gives the best approximation of the solution.

### 3 THE MODELING OF RADIONUCLIDE MIGRATION

Assessment of the release and the transport of long-lived radioactive nuclides from a repository to the biological environment is an important part of the safety analysis of repository concepts. In this assessment, mathematical models describing the mechanisms involved in the nuclide transport from the repository to the biosphere are essential tools. For example, the groundwater models are mathematical representations of the flow of water and the transport of solutes in the subsurface. Models are used to compute the hydraulic head, velocity, concentration, etc., from hydrologic and mass inputs, hydro geologic and mass-transfer parameters, and conditions at the boundary of the domain.

#### 3.1 GEOSTATISTICS

Many processes are inherently uncertain, and this uncertainty is handled through the use of stochastic realizations. The goal of stochastic simulation is to reproduce geological texture in a set of equiprobable simulated realizations. In mathematical terms, the most convenient method for simulation is sequential Gaussian simulation, because all successive conditional distributions from which simulated values are drawn are Gaussian with parameters determined by the solution of a simple kriging system.

##### 3.1.1 simulation of hydraulic conductivity

The hydraulic conductivity was generated at different points based on different input data. The hydraulic conductivity at 8 different points is given (values are: 66.00, 71.00, 73.00, 75.00, 76.52, 77.02, 79.74, 83.41 [m/y]).

The distribution of hydraulic conductivity for one specific simulation is shown in Fig. 1 (the numbers on the axes in Fig. 1 are distances in metres).

The coordinates of these values are also presented in Fig. 1 and marked with +. The following variogram parameters are chosen: positive variance contribution

or sill is equal to 0.8 and the nugget effect is 0.2. Simple kriging is chosen as the type of kriging. A spherical model is chosen as a type of a variogram structure.

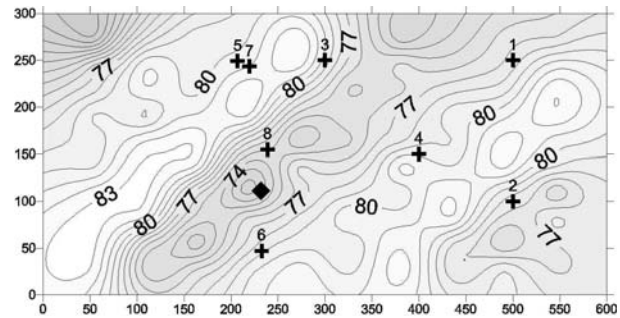


Figure 1. Distribution of hydraulic conductivity.

#### 3.2 SIMULATION OF DARCY VELOCITY

For the calculation of velocity in principal directions, Darcy's law is used. The velocities were determined from the pressure of the fluid  $p$  by solving the Laplace differential equation. Homogeneous and anisotropic porous media and incompressible fluid are assumed. The equation has the following form:

$$K_x \frac{\partial^2 p}{\partial x^2} + K_y \frac{\partial^2 p}{\partial y^2} = 0, \quad (7)$$

where  $K_x$  and  $K_y$  are the components of a hydraulic conductivity tensor. The corresponding Neumann and Dirichlet boundary conditions, defined along the boundary, are presented in Fig. 2.

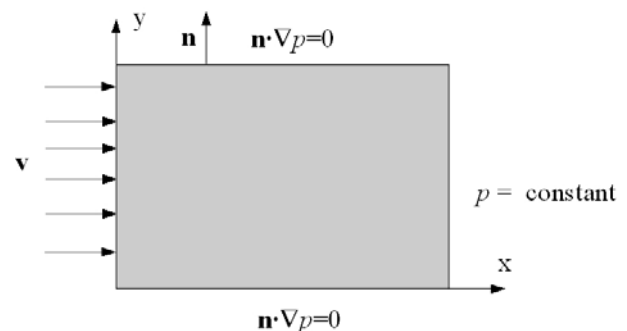


Figure 2. Boundary conditions.

For the calculation of velocity in principal directions we use Darcy's law:

$$v_x = -\frac{K_x}{\omega \rho a} \frac{\partial p}{\partial x}, \quad v_y = -\frac{K_y}{\omega \rho a} \frac{\partial p}{\partial y}, \quad (8)$$

where  $\rho$  is the density of the fluid and  $a$  is the gravitational acceleration. The Laplace equation was solved by using direct collocation [7]. Fig. 3 presents the velocity vector. In our case we considered anisotropic porous media, thus we obtained the velocity vectors of different size which depends on porosity and permeability.

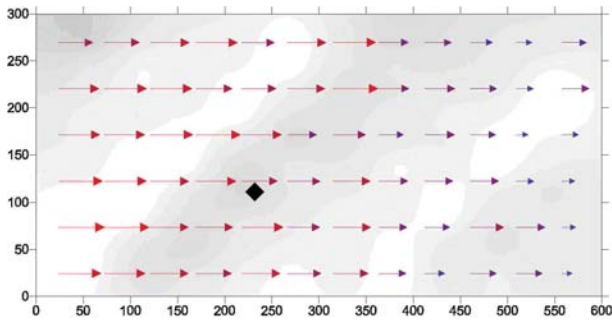


Figure 3. Calculated Darcy's velocity.

### 3.3 SIMULATION OF THE CONTAMINANT CONCENTRATIONS WITH ADVECTION-DISPERSION EQUATION (AD)

#### 3.3.1 The eulerian form of the AD

The velocities obtained from Laplace equation are used in the advection-dispersion equation. The AD equation for transport through the saturated porous media zone at a macroscopic level with retardation and decay is

$$R \frac{\partial u}{\partial t} = \frac{D_x}{\omega} \frac{\partial^2 u}{\partial x^2} + \frac{D_y}{\omega} \frac{\partial^2 u}{\partial y^2} - v_x \frac{\partial u}{\partial x} - R \cdot u,$$

$$(x, y) \in \Omega, \quad 0 \leq t \leq T, \tag{9}$$

$$u|_{(x,y) \in \partial\Omega} = g(x, y, t) \quad 0 \leq t \leq T,$$

$$u|_{t=0} = h(x, y), \quad (x, y) \in \Omega,$$

where  $x$  is the Eulerian groundwater flow axis and  $y$  is the Eulerian transverse axis in the 2D problem,  $u$  is the concentration of contaminant in the groundwater [Bqm<sup>3</sup>],  $D_x$  and  $D_y$  are the components of dispersion tensor [m<sup>2</sup>/y] in saturated zone,  $\omega$  is porosity of the saturated zone [-],  $R$  is the retardation factor in the saturated zone [-] and  $\lambda = \ln 2 / t_0$  is the radioactive decay constant [1/y].  $t_0$  is a half-life. In these cases “y” means years.

For the parabolic problem, we consider the implicit scheme [8] and radial basis functions formulation is presented in [9].

The simulation was implemented for a rectangular area which was 600 m long and 300 m wide. The source (initial condition) was Thorium (Th-230) with the activity of 1 MBq. The location of the radioactive source is presented in Fig. 3 with the symbol  $\blacklozenge$ .

The longitudinal dispersivity  $a_x$  is 200 m and the transversal dispersivity  $a_y$  is 20 m. For the porosity  $\omega$  we used values between 0.25 and 0.26. The retardation constant  $R$  is 800. The average contaminant concentrations distribution for the radial basis function method is shown in Fig. 4 (the axes in Fig. 4 present distances in metres).

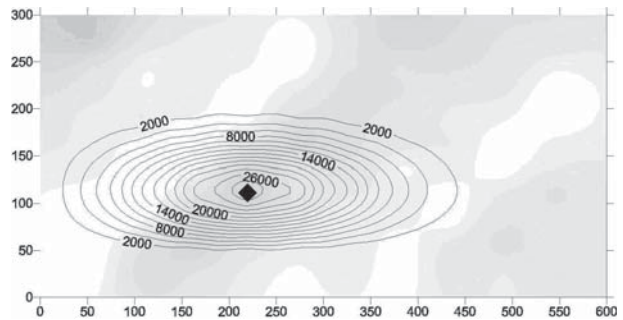


Figure 4. Distribution of average of contaminant concentrations (Radial basis function).

The traditional finite difference scheme was used for solving the Laplace and advection-dispersion equation. For the approximation of the second derivatives we used the central difference with respect to  $x$  and  $y$ . The average contaminant concentrations distribution for the finite difference method is shown in Fig. 5 (the axes in Fig. 5 present distances in metres).

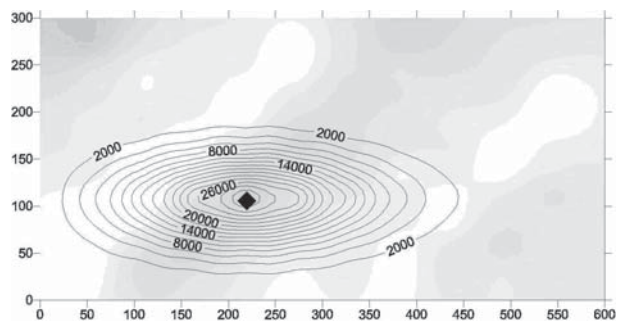


Figure 5. Distribution of average of contaminant concentrations (FDM).

### 3.3.2 The Lagrangian form of the AD

In this case the time-derivative term and the advection term of Eq. (9) are expressed as a material derivative:

$$\frac{du}{dt} \equiv \frac{\partial u}{\partial t} + \mathbf{v} \cdot \nabla u. \quad (10)$$

After including the material derivative into the advection-dispersion equation (9), we have:

$$\frac{du}{dt} + \lambda u = \left( \frac{D_x}{R\omega} \frac{\partial^2 u}{\partial x^2} + \frac{D_y}{R\omega} \frac{\partial^2 u}{\partial y^2} \right). \quad (11)$$

The solution of non-homogeneous ordinary differential equations (ODEs) can be found as a superposition of homogeneous and particular solutions. The particular solution of ODEs was found by the method of constant modification. In our case it was assumed that  $\lambda$  is constant in each time step [9].

The calculation of radioactive concentrations in partly heterogeneous porous media was also carried out. The results of radioactive concentrations for one particular simulation in partly heterogeneous porous media for the Eulerian and Lagrangian method are presented in Figs. 6 and 7. The partly heterogeneous porous media means in our case the area which was split into three regions. In the central region we prescribed the conductivity of porous media with the value of 320 [m/y], and elsewhere the prescribed conductivity was 50 [m/y].

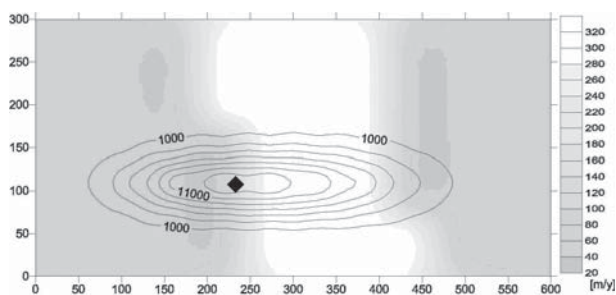


**Figure 6.** Concentrations and conductivity in partly heterogeneous porous media size 50 and 320 [m/y] (Eulerian method).

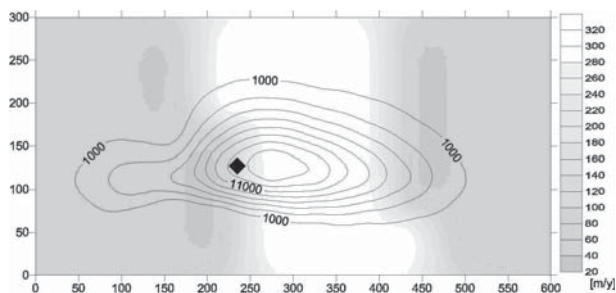


**Figure 7.** Concentrations and conductivity in partly heterogeneous porous media size 50 and 320 [m/y] (Lagrangian method).

## 4 MOVING BOUNDARY VALUE PROBLEMS

### 4.1 PROBLEM DEFINITION AND MOVING DATA CENTERS METHOD

Many physical processes involve heat conduction and materials undergoing a change of phase. Examples include the safety studies of nuclear reactors (the molten corium concrete interaction), casting of metals, geophysics and industrial applications involving metals, oil, and plastics. The molten core discharged to the containment cavity will interact with the concrete basement if it is not, or cannot be, cooled below the solidus temperature of the concrete. The molten core concrete interaction results in decomposition and melting of very large quantities of carbon dioxide and steam.

Several numerical methods have been developed to solve various Stefan's problems. Crank [10] provides a good introduction to the Stefan's problems and presents an elaborate collection of numerical methods for these problems. According to Crank the numerical methods for moving boundary problems can be classified in three categories: front-tracking methods, front-capturing methods and hybrid methods. We follow front-tracking methods (moving data centers method) which use an explicit representation of the interface, given by a set of points lying on the interface location, which must be updated at each time step.

Heat treatment of metals is often used to optimize mechanical properties. During heat treatment, the metallurgical state of the alloy changes. This change can involve the phase present at a given location or the morphology of the various phases. One of these processes, which is both of large industrial and scientific interest and amenable to modeling, is the dissolution of the second-phase particles in a matrix with a uniform initial composition. The position of the moving boundary will be simulated by moving data centers method.

#### 4.1.1 The physical model

We consider the solid state phase transformation problem in binary metallic alloys which is described in [11]. In this problem a volume of constant composition is surrounded by a diffusive phase. In the interface between the particle and the diffusive phase a constant concentration is assumed, and the gradient of the concentration causes the movement of the interface.

### 4.1.2 The mathematical model

We studied the domain  $\Omega$  containing a diffusive phase  $\Omega_{dp}$  and the part where the material characteristic  $\Omega_{part}$  remains of constant composition  $c_{part}$ . The particle dissolves due to Fickian diffusion in the diffusive phase. The concentration at the interface  $\Gamma$ , separating  $\Omega_{part}$  and  $\Omega_{dp}$ , is assumed to be given by the constant value  $c_{sol}$ . The concentration gradient on the side of  $\Omega_{dp}$  at  $\Gamma$  causes its displacement. The governing equations and boundary conditions of this problem are:

$$\frac{\partial u}{\partial t}(\mathbf{x}, t) = D \Delta u(\mathbf{x}, t), \quad x \in \Omega_{dp}(t), t > 0, \quad (12)$$

$$u(\mathbf{x}, t) = u^{part}, \quad x \in \Omega_{part}(t), t \geq 0, \quad (13)$$

$$u(\mathbf{x}, t) = u^{sol}, \quad x \in \Gamma(t), t \geq 0, \quad (14)$$

$$(u^{part} - u^{sol})v_n(\mathbf{x}, t) = D \frac{\partial u}{\partial \mathbf{n}}(\mathbf{x}, t), \quad x \in \Gamma(t), t > 0, \quad (15)$$

$$\frac{\partial u}{\partial \mathbf{n}}(\mathbf{x}, t) = 0, \quad x \in \partial\Omega_{dp}(t) \setminus \Gamma(t), t > 0, \quad (16)$$

where  $\mathbf{x}$  is the coordinate vector of a point in  $\Omega$ ,  $D$  means the diffusivity constant,  $\mathbf{n}$  is the unit normal vector on the interface pointing outward with respect to  $\Omega_{part(t)}$  and  $v_n$  is the normal component of the velocity of the interface. The initial concentration  $u(\mathbf{x}, 0)$  inside the diffusive phase is given.

### 4.1.3 The numerical solution method

Our interest is to give an accurate discretization of the moving boundary conditions. Here we present an interpolative moving data centers method by which the data centers are computed for each time step and the solution is interpolated from the old data centers to the new ones. The equations are solved with the collocation method using RBFs. An outline of the algorithm is:

- I. Compute the concentrations profiles solving Eqs. (12-14) and (16).
- II. Predict the position of the boundary  $s_1$  at the new time-step:  $s_1(t + \Delta t)$  using Eq. (15).
- III. Once the boundary is moved, the concentration  $u$  can be computed in the new region using Eq. (12). The solution is interpolated from the old point location to the new one.

## 4.2 THE LEVEL SET METHOD

The level set method has gained much popularity for solving moving boundary problems. It was firstly introduced by Osher and Sethian [13]. The level set function captures the interface position as its zero level set, and it is advected by introduction of a hyperbolic equation into the governing set of equations.

### 4.2.1 The level set formulation

In the level set formulation of the moving interface, the interfaces, denoted by  $\Gamma$ , are represented implicitly through a level set function  $\phi(\mathbf{x}, t)$ , where  $\mathbf{x}$  is a position of the interface,  $t$  is a point of time. Usually, the  $\phi$  is defined as a signed distance function to the interface. The moving interface is then captured in all times by locating the set of  $\Gamma(t)$  for which  $\phi$  vanishes. The level set function is advected with time by a transport equation which is known as the level set equation:

$$\frac{\partial \phi}{\partial t} + v_n |\nabla \phi| = 0, \quad \phi(\mathbf{x}, 0) = \phi_0(\mathbf{x}) \quad (17)$$

where  $\phi_0(\mathbf{x})$  embeds the initial position of the interface and  $v_n$  is the normal component of the velocity of the interface:

$$v_n = v \cdot \frac{\nabla \phi}{|\nabla \phi|}. \quad (18)$$

where  $\nabla \phi / |\nabla \phi|$  is the unit normal to the surface  $N$ .

If we take into account a continuous extension of the interface velocity  $v$ , the evolution of the level set function can be done by the hyperbolic equation for the level set equation:

$$\frac{\partial \phi}{\partial t} + v \cdot \nabla \phi = 0, \quad \phi(\mathbf{x}, 0) = \phi_0(\mathbf{x}) \quad (19)$$

In our case the continuous extension of the velocity  $v$  is taken as the (steady) solution of the following evolution equation [14]:

$$\frac{\partial v}{\partial \tau} \pm \frac{\partial v}{\partial \mathbf{x}} \cdot \mathbf{N} = 0, \quad (20)$$

where  $\tau$  denotes a fictitious time step not related to the main time step and the sign is determined from the normal direction of the level set function.

The RBFs are incorporated into level set methods to construct a more efficient approach. At the initial time,

all the time dependent variables should be specified over entire domain. The initial value problem (17) can be considered equivalent to an interpolation problem, and hence the starting point of the use of RBFs to solve partial differential equations is the interpolation problem. Further, the spatial portion is approximated by the RBFs and the temporal variations are approximated by the time dependent expansion coefficients.

### 4.2.2 RBF implicit modeling of the level set function

#### interpolation of the level set function

In the present implicit modeling, the MQ RBFs is used to interpolate the scalar implicit level set functions  $\phi(x)$  with  $N$  points by using  $N$  MQs centered at these points. The resulting RBF interpolant of the implicit function can be written as

$$\phi(\mathbf{x}) = \sum_{j=1}^N \alpha_j \varphi_j(\mathbf{x}) + \sum_{l=1}^M \gamma_l p_l(\mathbf{x}), \quad (21)$$

Because of the introduction of this polynomial, the RBF interpolant of  $\phi(x)$  in Eq. (21) must be subject to the side constraints (6).

If the interpolation data values  $f_1, \dots, f_N \in \mathfrak{R}$  at the point locations  $\mathbf{x}_1, \dots, \mathbf{x}_N \in \mathfrak{R} \subset \mathfrak{R}^d$  are given, the RBF interpolant of  $\phi(x)$  in Eq. (21) can be obtained by solving the system of  $N+2$  linear equations for  $N+2$  unknown generalized expansion coefficients:

$$\begin{aligned} \phi(\mathbf{x}_i) &= f_i, \quad i = 1, \dots, N, \\ \sum_i \alpha_i &= 0, \quad \sum_i \alpha_i x_i = 0, \quad \sum_i \alpha_i y_i = 0, \end{aligned} \quad (22)$$

which can be re-written in a matrix form as

$$\mathbf{H}\alpha = \mathbf{f}, \quad (23)$$

where

$$\mathbf{H} = \begin{bmatrix} \mathbf{A} & \mathbf{P} \\ \mathbf{P}^T & \mathbf{0} \end{bmatrix} \in \mathfrak{R}^{(N+3) \times (N+3)}, \quad (24)$$

$$\mathbf{A} = \begin{bmatrix} \varphi_1(\mathbf{x}_1) & \dots & \varphi_N(\mathbf{x}_1) \\ \vdots & \ddots & \vdots \\ \varphi_1(\mathbf{x}_N) & \dots & \varphi_N(\mathbf{x}_N) \end{bmatrix} \in \mathfrak{R}^{N \times N}, \quad (25)$$

$$\mathbf{P} = \begin{bmatrix} 1 & x_1 & y_1 \\ \vdots & \vdots & \vdots \\ 1 & x_N & y_N \end{bmatrix} \in \mathfrak{R}^{N \times 3}, \quad (26)$$

$$\alpha = [\alpha_1 \quad \dots \quad \alpha_N \quad p_0 \quad p_1 \quad p_2]^T \in \mathfrak{R}^{N \times 3}, \quad (27)$$

$$\mathbf{f} = [f_1 \quad \dots \quad f_N \quad 0 \quad 0 \quad 0]^T \in \mathfrak{R}^{N \times 3}, \quad (28)$$

The generalized expansion coefficients  $\alpha$  can be obtained by

$$\alpha = \mathbf{H}^{-1}\mathbf{f}, \quad (29)$$

The resulting RBF interpolant of the implicit function in Eq. (21) can be re-written compactly as

$$\phi(\mathbf{x}) = \Psi^T(\mathbf{x})\alpha, \quad (30)$$

where

$$\Psi(\mathbf{x}) = [\varphi_1(\mathbf{x}) \quad \dots \quad \varphi_N(\mathbf{x}) \quad 1 \quad x \quad y]^T \in \mathfrak{R}^{(N+3) \times 1}, \quad (31)$$

#### equation of motion

Since the Hamilton-Jacobi PDE (17) is time dependent, it is further assumed that all knots are fixed in space and the space and time are separable, and therefore the RBF interpolant of the implicit function in Eq. (30) becomes time dependent as

$$\phi(\mathbf{x}, t) = \Psi^T(\mathbf{x})\alpha(t), \quad (32)$$

Substituting Eq. (32) in (17) yields

$$\Psi^T \frac{d\alpha}{dt} + v_n |(\nabla \Psi)^T \alpha| = 0, \quad (33)$$

where

$$|(\nabla \Psi)^T \alpha| = \left[ (\mathbf{G}_{,1}^T \alpha)^2 + (\mathbf{G}_{,2}^T \alpha)^2 \right]^{1/2}, \quad (34)$$

$$\begin{aligned} \mathbf{G}_{,1} &= \begin{bmatrix} \frac{\partial \varphi_1}{\partial x} & \dots & \frac{\partial \varphi_N}{\partial x} & 0 & 1 & 0 \end{bmatrix}^T \in \mathfrak{R}^{(N+3) \times 1}, \\ \mathbf{G}_{,2} &= \begin{bmatrix} \frac{\partial \varphi_1}{\partial y} & \dots & \frac{\partial \varphi_N}{\partial y} & 0 & 0 & 1 \end{bmatrix}^T \in \mathfrak{R}^{(N+3) \times 1}, \end{aligned} \quad (35)$$



The initial value problem can be considered equivalent to the interpolation problem since the expansion coefficients at the initial time are found as a solution of the interpolation problem [15]. Therefore the preliminary starting point of the use of RBFs to solve PDEs is the interpolation problem that is equivalent to solving the initial value problem. The original equation (17) is thus converted into a time-dependent interpolation problem for the initial values of expansion coefficients and the propagation of the front is governed by the time dependent equation (33).

For time advance the initial values of  $\alpha$  in Eq. (33) we used a collocation formulation of the method of lines. The governing equation of motion of the front (33) is extended to the whole domain  $\Omega$  and the normal velocities  $v_n$  at the front are thus replaced by the extension velocities in  $\Omega$ . All nodes of domain are taken as fixed nodes of RBF interpolation. We also take into consideration constraints which must be introduced to guarantee that the generalized coefficients  $\alpha$  can be solved.

Using the present collocation method for  $N$  points and above mentioned constraints, a set of resulting ODEs can be compactly written as:

$$\mathbf{H} \frac{d\alpha}{dt} + \mathbf{B}(\alpha) = 0, \quad (36)$$

where

$$\mathbf{B} = \begin{bmatrix} v_n^e(\mathbf{x}_1) |(\nabla \Psi^T(\mathbf{x}_1))\alpha| \\ \vdots \\ v_n^e(\mathbf{x}_1) |(\nabla \Psi^T(\mathbf{x}_1))\alpha| \\ 0 \\ 0 \\ 0 \end{bmatrix} \in \mathbb{R}^{(N \times 3) \times 1}, \quad (37)$$

The set of ODEs can be solved by several ODE solvers such as the first-order forward Euler's method and higher-order Runge-Kutta, Runge-Kutta-Fehlberg, Adams-Bashforth, or Adams-Moulten methods [16].

We used

- a) the first-order forward Euler's method, an approximate solution to Eq. (36) is the following:

$$\alpha(t^{n+1}) = \alpha(t^n) - dt \mathbf{H}^{-1} \mathbf{B}(\alpha(t^n)), \quad (38)$$

where  $dt$  is the time step, and

- b) the exact explicit time integration. The first order homogeneous ODE of the form

$$\frac{d\alpha}{dt} + \mathbf{E}\alpha = 0, \quad (39)$$

where

$$\mathbf{E} = \mathbf{H}^{-1}(v_1 \mathbf{G}_{,1} + v_2 \mathbf{G}_{,2}), \quad (40)$$

has the solution:

$$\alpha(t + dt) = \mathbf{expm}(-\mathbf{E}dt)\alpha(t - dt). \quad (41)$$

The expression  $\mathbf{expm}(-\mathbf{E}dt)$  is a MATLAB exponential matrix function represents the series expansion or a rational fraction:

$$\mathbf{expm}(-\mathbf{E}dt) = \mathbf{I} - \mathbf{E}dt + (dt^2/2!)\mathbf{E}^2 - (dt^3/3!)\mathbf{E}^3 \mp \dots \quad (42)$$

$\mathbf{E}$  is the coefficient matrix resulting from the application of the Eq. (35).

### 4.2.3 numerical example

For the simulation we used data from [11]: the concentration inside the part where the material characteristics remain constant  $u^{part} = 0.53$ , the concentration on the interface  $u^{sol} = 0$ , the initial concentration of the diffusive phase  $u^0 = 0.1$ , the diffusivity constant  $D = 1$ , the domain length  $l = 1$  and the initial position of the interface  $s_0 = 0.2$ . Let  $N$  be total number of points,  $r$  the number of points that lie inside a constant composition and  $N - r$  the number of points that lie inside the diffusive phase. Due to the movement of the interface, the point locations are adapted at each time step. The MQ exponent  $\beta$  had the values 0.5 and 1.5. In Fig. 8 the movement of the interface positions calculated with a different MQ exponent,  $\beta$  is presented. In the numerical experiments we compared our numerical solutions with the analytical solutions that exist for the problem presented in Chapter 4. (See [12]). The results are presented in Fig. 8 (see next page).

The next example is the rotation of the solid body.

Consider the rotation of a circular bubble of the radius  $r = 0.25$  centered at  $(0.5, 0.15)$  in a vortex flow with the velocity field  $(v_1, v_2) = (-y, x)$ . A half cycle of rotation is presented in Fig. 9.



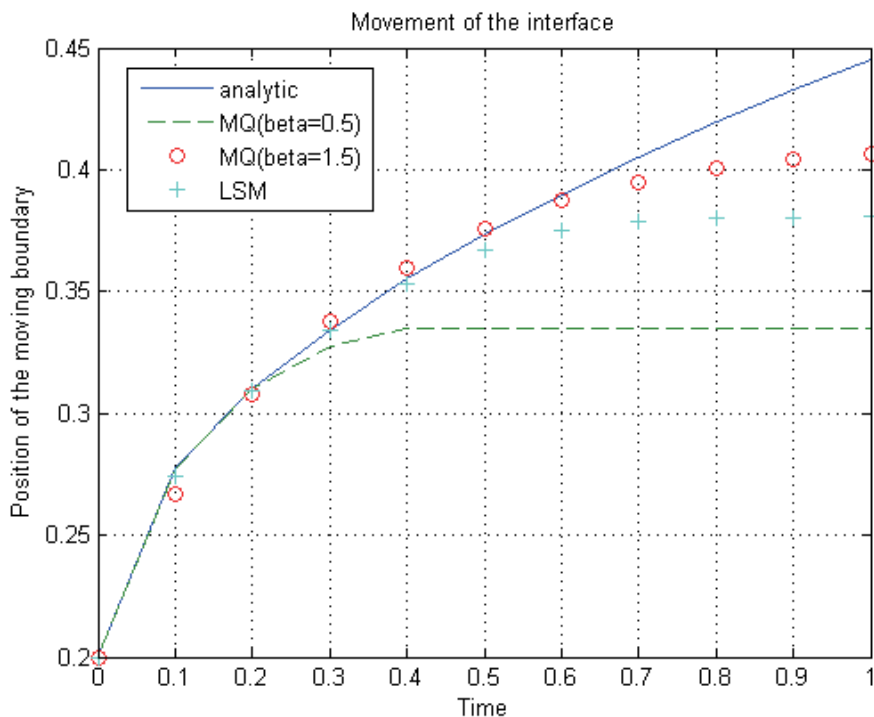


Figure 8. Interface position vs. time.

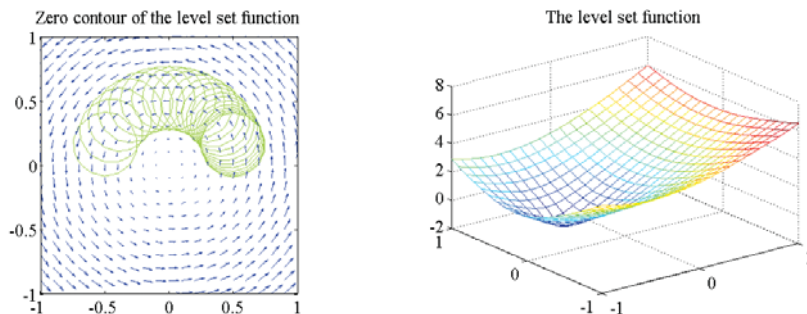


Figure 9. Zero contour of the level set function at different points and time during the rotation of a circle.

## 5 DISCUSSION AND CONCLUSION

In the case of the radionuclide migration (see also [6], [9] and [12]), two evaluation steps were performed. In the first step the velocities in principal directions were determined from the pressure of the fluid obtained from the Laplace differential equation. In the second step the advection-dispersion equation was solved to find the concentration of the contaminant. In this case the method of evaluation was verified by comparing results with those obtained from the finite difference method.

The traditional finite difference scheme was also used for solving the Laplace and advection-dispersion equation. For the approximation of the first derivative second-order central difference or one-sided difference were used. But for the approximation of the second derivatives we used the second-order central second difference. The time dependent part was implemented with the implicit scheme. The discretization grid has actually 12x12 points.

Te results show that differences exist between both numerical schemes (Figs. 4 and 5). Different sets of input data yield differences between the schemes. In the simulation, a very large scatter caused by different given values of hydraulic conductivity was observed. Another reason for differences could result from the kriging method applied in the sequential Gaussian methods.

The comparison of concentrations calculated with the Eulerian and Lagrangian methods in partly heterogeneous porous (Figs. 6 and 7) media shows that the Lagrangian methods provide a wider concentration cloud in the area of high conductivity. It seems that it shows the influence of non-smooth change between low and high conductivity.

In general, the Eulerian approach is more convenient and more frequently used. But if it is important to study sharp changes (in our case between areas of low and high conductivity) of the solutions where important chemistry and physics take place, it is better to use the Lagrangian RBF scheme.

The comparison of the moving boundary positions calculated with the moving data centers method and MQ ( $\beta=0.5$ ) and MQ ( $\beta=1.5$ ) (Fig. 8) shows that MQ ( $\beta=1.5$ ) determines the position of the interfaces much more accurately than MQ ( $\beta=0.5$ ). The simulations have also shown that the value of the shape parameter  $c$  which was computed by the residual error procedure was in the range between 0.01 and 0.09. This confirms the fact that for a fixed number of centers  $N$ , smaller shape parameters produce more accurate approximations.

The comparison of the moving boundary positions calculated with the moving data centers method (MQ ( $\beta=1.5$ )) and the level set method (Fig. 8) also shows that the moving data centers method gives better results in this case. To achieve better accuracy, the resultant system of the RBF-PDE problem usually becomes badly conditioned. Several different strategies [17] have been somewhat successful in reducing the ill-conditioning problem when using RBF methods in PDE problems. These strategies include: variable shape parameters, domain decomposition, preconditioning of the interpolation matrix, and optimizing the center locations.

From chapter 4.2 we can see that RBFs (MQ) can be easily included in the level set formulation. Fig. 9 shows that we can get logical results using MQ in a 2-dimensional example.

We can conclude that the Kansa method is a valid alternative to the FDM because of its simple implementation and its easy use in the level set formulations. The only

geometric properties that are used in the RBF approximation are the pair-wise distances between points. Figs. 4 and 5 show that the RBF solution has far less diffusion than the finite difference method with the included upwinding.

In the future work we will use the Gershgorin circle theorem that could be useful a tool for choosing appropriate RBFs. For each value of the shape parameter, eigenvalues and their distribution can be studied to obtain knowledge concerning properties of an approximation matrix and their role being played in finding a better approximation of computed data to the equation solution. The solutions can be improved by using an affine space decomposition that decouples the influence between the interior and boundary collocations.

---

## REFERENCES

- [1] G. Fairweather, A. and Karageorghis (1998). The method of fundamental solutions for elliptic boundary value problems. *Adv. Comput. Math.*, 9(1/2), 69-95.
- [2] Golberg, M.A. and Chen, C. S. (1998). The method of fundamental solutions for potential, Helmholtz and diffusion problems, in *Boundary Integral Methods-Numerical and Mathematical Aspects*, M. A. Golberg (Ed.). *Computational Mechanics Publications*, 103-176.
- [3] Kansa, E. J. (1990). Multiquadrics - A scattered data approximation scheme with applications to computational fluid dynamics - I. Surface approximations and partial derivative estimates. *Computers Math. Applic.* 19 (8/9), 127-145.
- [4] Kansa, E. J. (1990). Multiquadrics - A Scattered data approximation scheme with applications to computational fluid dynamics - II. Solutions to parabolic, hyperbolic and elliptic partial differential equations. *Computers Math. Applic.* 19 (8/9), 147-161.
- [5] Hardy, R. L. (1971). Multiquadric equation of topography and other irregular surfaces. *J. Geophys. Res.* Vol. 176, 1905-1915.
- [6] Vrankar, L., Turk, G. and Runovc, F. (2004). Modelling of radionuclide migration through the geosphere with radial basis function method and geostatistics. *Journal of the Chinese Institute of Engineers*, Vol. 27, No. 4, 455-462.
- [7] Fedoseyev, A. I, Friedman, M. J. and Kansa, E. J. (2002). Improved multiquadric method for elliptic

- partial differential equations via PDE collocation on the boundary. *Computers Math. Applic.* Vol. 43, 439-455.
- [8] Smith, G. D. (1978). Numerical solution of partial differential equations: Finite difference methods. *Oxford Applied Mathematics and Computing Science Series*, Oxford University Press.
- [9] Vrankar, L., Turk, G. and Runovc, F. (2004). Combining the radial basis function Eulerian and Lagrangian schemes with geostatistics for modelling of radionuclide migration through the Geosphere. *Computers. Math. Applic.*, Vol. 48, No. 10-11, 1517-1529.
- [10] Crank, J. (1984). *Free and Moving Boundary Problems*, Clarendon Press, Oxford.
- [11] Javierre, E., Vuik, C., Vermolen, F. J. and Van der Zwaag, S. (2005). A comparison of numerical models for one-dimensional Stefan problems, *Reports of the Delft Institute of Applied Mathematics*, Netherlands.
- [12] Vrankar, L., Turk, G., Runovc, F. and Kansa, E. J. (2006). Solving one-dimensional phase change problems with moving grid method and mesh free radial basis functions. *International Conference Nuclear Energy for New Europe*, Portoroz. 1005.1.-1005.8.
- [13] Osher, S. and Sethian, J. A. (1988). Front propagating with curvature dependent speed: algorithms based on Hamilton-Jacobi formulations. *Journal of Computational Physics*. Vol. 78, 12--49.
- [14] Li, Z. and Ito, K. (2006). *The Immersed Interface Method - Numerical Solutions of PDEs Involving Interfaces and Irregular Domains*. Society for Industrial and Applied Mathematics, Philadelphia, USA.
- [15] Wang, S. Y., Lim, K. M., Khoo, B. C. and Wang, M. Y. (2007). An extended level set method for shape and topology optimization. *Journal of Computational Physics*. Vol. 221, 395-421.
- [16] Greenberg, M. D. (1988). *Advanced Engineering Mathematics*, 2<sup>nd</sup> ed., Prentice-Hall International Inc., Upper Saddle River, NJ, USA.
- [17] Kansa, E. J. and Hon, Y. C. (2000). Circumventing the Ill - Conditioning problem with multiquadric radial basis functions: Applications to elliptic partial differential equations, *Computers Math. Applic.*, Vol. 39, No. 7-8, 123-137.

# NAVODILA AVTORJEM

Članki so objavljeni v angleškem jeziku s prevodom izvlečka v slovenski jezik.

## VSEBINA ČLANKA

Članek naj bo napisan v naslednji obliki:

- Naslov, ki primerno opisuje vsebino članka in ne presega 80 znakov.
- Izvleček, ki naj bo skrajšana oblika članka in naj ne presega 250 besed. Izvleček mora vsebovati osnove, jedro in cilje raziskave, uporabljeno metodologijo dela, povzetek izidov in osnovne sklepe.
- Uvod, v katerem naj bo pregled novejšega stanja in zadostne informacije za razumevanje ter pregled izidov dela, predstavljenih v članku.
- Teorija.
- Eksperimentalni del, ki naj vsebuje podatke o postavitvi preiskusa in metode, uporabljene pri pridobitvi izidov.
- Izidi, ki naj bodo jasno prikazani, po potrebi v obliki slik in preglednic.
- Razprava, v kateri naj bodo prikazane povezave in posplošitve, uporabljene za pridobitev izidov. Prikazana naj bo tudi pomembnost izidov in primerjava s poprej objavljenimi deli.
- Sklepi, v katerih naj bo prikazan en ali več sklepov, ki izhajajo iz izidov in razprave.
- Literatura, ki mora biti v besedilu oštevilčena zaporedno in označena z oglatimi oklepaji [1] ter na koncu članka zbrana v seznamu literature.

## OBLIKA ČLANKA

Besedilo naj bo pisano na listih formata A4, z dvojnimi presledki med vrstami in s 3.0 cm širokim robom, da je dovolj prostora za popravke lektorjev. Najbolje je, da pripravite besedilo v urejevalniku Microsoft Word. Hkrati dostavite odtis članka na papirju, vključno z vsemi slikami in preglednicami ter identično kopijo v elektronski obliki.

Enačbe naj bodo v besedilu postavljene v ločene vrstice in na desnem robu označene s tekočo številko v okroglih oklepajih.

## ENOTE IN OKRAJŠAVE

V besedilu, preglednicah in slikah uporabljajte le standardne označbe in okrajšave SI. Simbole fizikalnih

veličin v besedilu pišite poševno (npr.  $v$ ,  $T$  itn.). Simbole enot, ki sestojijo iz črk, pa pokončno (npr. Pa, m itn.).

Vse okrajšave naj bodo, ko se prvič pojavijo, izpisane v celoti.

## SLIKE

Slike morajo biti zaporedno oštevilčene in označene, v besedilu in podnaslovu, kot sl. 1, sl. 2 itn. Posnete naj bodo v kateremkoli od razširjenih formatov, npr. BMP, JPG, GIF. Za pripravo diagramov in risb priporočamo CDR format (CorelDraw), saj so slike v njem vektorske in jih lahko pri končni obdelavi preprosto povečujemo ali pomanjšujemo.

Pri označevanju osi v diagramih, kadar je le mogoče, uporabite označbe veličin (npr.  $v$ ,  $T$ ). V diagramih z več krivuljami mora biti vsaka krivulja označena. Pomen oznake mora biti razložen v podnapisu slike.

Za vse slike po fotografskih posnetkih je treba priložiti izvorne fotografije ali kakovostno narejen posnetek.

## PREGLEDNICE

Preglednice morajo biti zaporedno oštevilčene in označene, v besedilu in podnaslovu, kot preglednica 1, preglednica 2 itn. V preglednicah ne uporabljajte izpisanih imen veličin, ampak samo ustrezne simbole. K fizikalnim količinam, npr.  $t$  (pisano poševno), pripišite enote (pisano pokončno) v novo vrsto brez oklepajev.

Vse opombe naj bodo označene z uporabo dvignjene številke<sup>1</sup>.

## SEZNAM LITERATURE

Vsa literatura mora biti navedena v seznamu na koncu članka v prikazani obliki po vrsti za revije, zbornike in knjige:

- [1] Feng, T. W. (2000). Fall-cone penetration and water content relationship of clays. *Geotechnique* 50, No. 2, 181-187.
- [2] Ortolan, Ž. and Mihalinec, Z. (1998). Plasticity index-Indicator of shear strength and a major axis of geotechnical modelling. *Proceedings of the Elev-*

*enth Danube-European conference on soil mechanics and geotechnical engineering*, Poreč, 25 –29 May 1998.

- [3] Toporišič, J. (1994). *Slovenski pravopis*. 2nd.ed., DZS, Ljubljana.

## PODATKI O AVTORJIH

Članku priložite tudi podatke o avtorjih: imena, nazive, popolne poštne naslove, številke telefona in faksa, naslove elektronske pošte. Navedite kontaktno osebo.

## SPREJEM ČLANKOV IN AVTORSKE PRAVICE

Uredništvo si pridržuje pravico do odločanja o sprejemu članka za objavo, strokovno oceno mednarodnih recenzentov in morebitnem predlogu za krajšanje ali izpopolnitev ter terminološke in jezikovne korekture.

Avtor mora predložiti pisno izjavo, da je besedilo njegovo izvirno delo in ni bilo v dani obliki še nikjer objavljeno. Z objavo preidejo avtorske pravice na revijo ACTA GEOTECHNICA SLOVENICA. Pri morebitnih kasnejših objavah mora biti AGS navedena kot vir.

Rokopisi člankov ostanejo v arhivu AGS.

Vsa nadaljnja pojasnila daje:

Uredništvo  
ACTA GEOTECHNICA SLOVENICA  
Univerza v Mariboru  
Fakulteta za gradbeništvo  
Smetanova ulica 17  
2000 Maribor  
Slovenija  
E-pošta: ags@uni-mb.si

# INSTRUCTIONS FOR AUTHORS

The papers are published in English with a translation of the abstract into Slovene.

## FORMAT OF THE PAPER

The paper should have the following structure:

- A Title that adequately describes the content of the paper and should not exceed 80 characters;
- An Abstract, which should be viewed as a mini version of the paper and should not exceed 250 words. The Abstract should state the principal objectives and the scope of the investigation and the methodology employed, it should also summarise the results and state the principal conclusions;
- An Introduction, which should provide a review of recent literature and sufficient background information to allow the results of the paper to be understood and evaluated;
- A Theoretical section;
- An Experimental section, which should provide details of the experimental set-up and the methods used for obtaining the results;
- A Results section, which should clearly and concisely present the data using figures and tables where appropriate;
- A Discussion section, which should describe the relationships shown and the generalisations made

possible by the results and discuss the significance of the results, making comparisons with previously published work;

- Conclusions, which should present one or more conclusions that have been drawn from the results and subsequent discussion;
- References, which must be numbered consecutively in the text using square brackets [1] and collected together in a reference list at the end of the paper.

## LAYOUT OF THE TEXT

The text should be written in A4 format, with double spacing and margins of 3 cm, to provide editors with space to write in their corrections. Microsoft Word for Windows is the preferred format for submission. One hard copy, including all figures, tables and illustrations and an identical electronic version of the manuscript must be submitted simultaneously.

Equations should be on a separate line in the main body of the text and marked on the right-hand side of the page with numbers in round brackets.

## UNITS AND ABBREVIATIONS

Only standard SI symbols and abbreviations should be used in the text, tables and figures. Symbols for physical

quantities in the text should be written in *Italics* (e.g.  $v$ ,  $T$ , etc.). Symbols for units that consist of letters should be in plain text (e.g. Pa, m, etc.).

All abbreviations should be spelt out in full on first appearance.

## FIGURES

Figures must be cited in consecutive numerical order in the text and referred to in both the text and the caption as Fig. 1, Fig. 2, etc. Figures may be saved in any common format, e.g. BMP, JPG, GIF. However, the use of CDR format (CorelDraw) is recommended for graphs and line drawings, since vector images can be easily reduced or enlarged during final processing of the paper.

When labelling axes, physical quantities (e.g.  $v$ ,  $T$ ) should be used whenever possible. Multi-curve graphs should have individual curves marked with a symbol; the meaning of the symbol should be explained in the figure caption.

Good quality black-and-white photographs or scanned images should be supplied for illustrations.

## TABLES

Tables must be cited in consecutive numerical order in the text and referred to in both the text and the caption as Table 1, Table 2, etc. The use of names for quantities in tables should be avoided if possible: corresponding symbols are preferred. In addition to the physical quantity, e.g.  $t$  (in *Italics*), units (normal text), should be added on a new line without brackets.

Any footnotes should be indicated by the use of the superscript<sup>1</sup>.

## LIST OF REFERENCES

References should be collected at the end of the paper in the following styles for journals, proceedings and books, respectively:

- [1] Feng, T. W. (2000). Fall-cone penetration and water content relationship of clays. *Geotechnique* 50, No. 2, 181-187.
- [2] Ortolan, Ž. and Mihalinec, Z. (1998). Plasticity index-Indicator of shear strength and a major axis of geotechnical modelling. *Proceedings of the Eleventh Danube-European conference on soil mechanics and geotechnical engineering*, Poreč, 25 –29 May 1998.

- [3] Toporišič, J. (1994). *Slovenski pravopis*. 2nd.ed., DZS, Ljubljana.

## AUTHOR INFORMATION

The following information about the authors should be enclosed with the paper: names, complete postal addresses, telephone and fax numbers and E-mail addresses. Indicate the corresponding person.

## ACCEPTANCE OF PAPERS AND COPYRIGHT

The Editorial Committee of the Slovenian Geotechnical Review reserves the right to decide whether a paper is acceptable for publication, to obtain peer reviews for submitted papers, and if necessary, to require changes in the content, length or language.

Authors must also enclose a written statement that the paper is original unpublished work, and not under consideration for publication elsewhere. On publication, copyright for the paper shall pass to the ACTA GEOTECHNICA SLOVENICA. The AGS must be stated as a source in all later publication.

Papers will be kept in the archives of the AGS.

For further information contact:

Editorial Board  
 ACTA GEOTECHNICA SLOVENICA  
 University of Maribor  
 Faculty of Civil Engineering  
 Smetanova ulica 17  
 2000 Maribor  
 Slovenia  
 E-mail: ags@uni-mb.si



## **NAMEN REVIJE**

Namen revije ACTA GEOTECHNICA SLOVENICA je objavljavanje kakovostnih teoretičnih člankov z novih pomembnih področij geomehanike in geotehnike, ki bodo dolgoročno vplivali na temeljne in praktične vidike teh področij.

ACTA GEOTECHNICA SLOVENICA objavlja članke s področij: mehanika zemljin in kamnin, inženirska geologija, okoljska geotehnika, geosintetika, geotehnične konstrukcije, numerične in analitične metode, računalniško modeliranje, optimizacija geotehničnih konstrukcij, terenske in laboratorijske preiskave.

Revija redno izhaja dvakrat letno.

## **AVTORSKE PRAVICE**

Ko uredništvo prejme članek v objavo, prosi avtorja(je), da prenese(jo) avtorske pravice za članek na izdajatelja, da bi zagotovili kar se da obsežno razširjanje informacij. Naša revija in posamezni prispevki so zaščiteni z avtorskimi pravicami izdajatelja in zanje veljajo naslednji pogoji:

### **fotokopiranje**

V skladu z našimi zakoni o zaščiti avtorskih pravic je dovoljeno narediti eno kopijo posameznega članka za osebno uporabo. Za naslednje fotokopije, vključno z večkratnim fotokopiranjem, sistematičnim fotokopiranjem, kopiranjem za reklamne ali predstavitvene namene, nadaljnjo prodajo in vsemi oblikami nedobičkonosne uporabe je treba pridobiti dovoljenje izdajatelja in plačati določen znesek.

Naročniki revije smejo kopirati kazalo z vsebino revije ali pripraviti seznam člankov z izvlečki za rabo v svojih ustanovah.

### **elektronsko shranjevanje**

Za elektronsko shranjevanje vsakršnega gradiva iz revije, vključno z vsemi članki ali deli članka, je potrebno dovoljenje izdajatelja.

## **ODGOVORNOST**

Revija ne prevzame nobene odgovornosti za poškodbe in/ali škodo na osebah in na lastnini na podlagi odgovornosti za izdelke, zaradi malomarnosti ali drugače, ali zaradi uporabe kakršnekoli metode, izdelka, navodil ali zamisli, ki so opisani v njej.

## **AIMS AND SCOPE**

ACTA GEOTECHNICA SLOVENICA aims to play an important role in publishing high-quality, theoretical papers from important and emerging areas that will have a lasting impact on fundamental and practical aspects of geomechanics and geotechnical engineering.

ACTA GEOTECHNICA SLOVENICA publishes papers from the following areas: soil and rock mechanics, engineering geology, environmental geotechnics, geosynthetic, geotechnical structures, numerical and analytical methods, computer modelling, optimization of geotechnical structures, field and laboratory testing.

The journal is published twice a year.

## **COPYRIGHT**

Upon acceptance of an article by the Editorial Board, the author(s) will be asked to transfer copyright for the article to the publisher. This transfer will ensure the widest possible dissemination of information. This review and the individual contributions contained in it are protected by publisher's copyright, and the following terms and conditions apply to their use:

### **photocopying**

Single photocopies of single articles may be made for personal use, as allowed by national copyright laws. Permission of the publisher and payment of a fee are required for all other photocopying, including multiple or systematic copying, copying for advertising or promotional purposes, resale, and all forms of document delivery.

Subscribers may reproduce tables of contents or prepare lists of papers, including abstracts for internal circulation, within their institutions.

### **electronic storage**

Permission of the publisher is required to store electronically any material contained in this review, including any paper or part of the paper.

## **RESPONSIBILITY**

No responsibility is assumed by the publisher for any injury and/or damage to persons or property as a matter of product liability, negligence or otherwise, or from any use or operation of any methods, products, instructions or ideas contained in the material herein.